

**Exploring the effects of aperture size, aperture variability and matrix properties on
biocolloid transport and retention in a single saturated fracture**

**Exploring the effects of aperture size, aperture variability and matrix properties on
biocolloid transport and retention in a single saturated fracture**

By

MAGGIE BURKE, B. Eng

A Thesis

Submitted to the School of Graduate Studies

In Partial Fulfillment of the Requirements

For the Degree

Master of Applied Science

McMaster University

© Copyright by Maggie Burke, February 2012

MASTER OF APPLIED SCIENCE (2012)

McMaster University

(Civil Engineering)

Hamilton, Ontario

TITLE: Exploring the effects of aperture size, aperture variability and matrix properties on biocolloid transport and retention in a single saturated fracture

AUTHOR: Maggie Burke (McMaster University)

SUPERVISOR: Dr. Sarah E. Dickson

NUMBER OF PAGES: ix, 98

ABSTRACT

To increase the understanding of contaminant transport, specifically biocolloid transport in fractured media, a series of experiments were conducted on single saturated fractures. Hydraulic and solute tracer tests were used to characterize three separate fractures: one natural fracture and two synthetic fractures. Zeta potentials are reported showing the high negative electric charge of the synthetic fractures relative to the natural fractures in the phosphate buffer solution (PBS) used during the biocolloid tracer tests.

E. coli RS2-GFP tracer tests were conducted on all three fractures at specific discharges of 5 m/d, 10 m/d and 30 m/d. Lower *E. coli* recovery was consistently observed in the natural fracture, due to 1) attachment because of the lower negative charge of the natural fracture relative to the synthetic fracture; and 2) the presence of dead end fractures within the fracture matrix. In the synthetic fractures, where surface charges were equal, in the larger, more variable fracture aperture, lower recoveries were found when compared to the smaller, less variable fracture aperture, which was not expected. This indicates that aperture variability plays a larger role than fracture aperture size in the retention of biocolloids in fractures.

Differential transport was consistently observed in all three fractures, but was more prominent in the synthetic fractures. This indicates that charge exclusion plays a more dominant role in the differential transport of colloids than size exclusion, though size exclusion cannot be eliminated as a retention mechanism based on these experiments. Differential transport was also heavily influenced by specific discharge as the difference in arrival times between the bromide and *E. coli* increased in all three fractures as the specific discharge decreased.

Visualization tests were completed on the synthetic fractures showing the location of multiple preferential flow paths, as well as areas with low flow.

ACKNOWLEDGEMENT

I would like to take this opportunity to express my thanks to the people who have supported me throughout this program. First and foremost, my supervisor, Dr. Sarah E. Dickson. Your guidance and input has always been appreciated and has helped me overcome more than a few barriers over the term of my degree. It has been a wonderful opportunity to work with someone so passionate and full of contagious enthusiasm.

The laboratory technicians, Anna Robertson and Peter Koudys. You're patient help and expertise saved me countless hours in the laboratory. Thank you.

The McMaster Civil Engineering administrative staff. Your assistance has been greatly appreciated, particularly, Carol Robinson. Thank you, for keeping me organized and meeting deadlines without me even realizing it.

Sandrina Rodrigues. More than just a sensible friend. Time spent in the lab was always much more enjoyable when you were there. I appreciate your constant help and lessons in the lab (and in life). Your friendship, support and guidance are much appreciated.

Mike Schutten. Thank you for providing me with results from Fracture 1. Also, thank you for your help in the lab, your friendship and your general cheerfulness. I doubt you have ever turned down lending a helping hand to anyone. I could not imagine starting my degree with anyone else.

The rest of my research group and office mates. Thank you for your wonderful company and for your valuable insight. You're patient and thoughtful answers to my constant questions were untiring and enlightening.

My wonderful family and my amazing friends. You are an invaluable part of my life.

Table of Contents

ABSTRACT	iv
ACKNOWLEDGEMENT	v
Chapter 1: Introduction	1
1.1 Background.....	1
1.2 Objective.....	2
1.3 Scope	3
Chapter 2: Literature Review	4
2.1 Colloid Transport within Fractured Media	5
2.1.1 Advection and Dispersion.....	6
2.1.2 Diffusion.....	10
2.1.3 Size and Charge Exclusion.....	12
2.2 Retention Mechanisms.....	16
2.2.1 Attachment due to Sedimentation or Diffusion.....	17
2.2.2 Straining.....	20
2.3 Biological Mechanisms	20
2.3.1 Growth and Decay	21
2.3.2 Active Adhesion and Detachment	22
2.3.3 Chemotaxis	22
2.3.4 Biofilm Development and Bioclogging	23
2.4 <i>E. Coli</i> Characteristics and Previous Studies.....	24
Chapter 3: Methods and Experimental Setup	26
3.1 Fracture Collection and Preparation	26
3.2 Epoxy Replicas	33
3.3 Experimental Setup	37
3.4 Aperture Field Characterization	40
3.4.1 Hydraulic Tests.....	40
3.4.2 Solute Tracer Tests	41

3.5 *E. Coli* Tracer Tests..... 42

 3.5.1 *E. coli* Stock Preparation 44

 3.5.2 *E. coli* RS2G Enumeration 45

 3.5.2 Visualization..... 45

3.6 Reagent List..... 47

Chapter 4..... 49

 4.1 Aperture Field Characterization 49

 4.1.1 Hydraulic Tests..... 49

 4.1.2 Solute Tracer Tests 57

 4.2 *E. coli* RS2G Tracer Tests..... 62

 4.2.1 Visualization..... 74

Chapter 5..... 79

 5.1 Conclusions..... 79

 5.1 Recommendations 81

References 82

Appendix A 86

Appendix B 90

Appendix C 94

Appendix D..... 98

List of Figures

Figure 2 - 1 : Parallel Plate Velocity Profile..... 7

Figure 2 - 2 : Obtained from Tsang, 1987. Showing dispersion due to aperture variations. (a) Approximate relative aperture field, darker being smaller apertures. (b) Approximate flow paths..... 10

Figure 2 - 3 : Showing Size Exclusion; Colloids and particulates stay in larger aperture regions..... 13

Figure 2 - 4 : Showing Size Exclusion. The colloid stays in the middle of the channel, experiencing high velocities..... 14

Figure 2 - 5 : Showing the Electric Double Layer surrounding a particle..... 15

Figure 2 - 6 : Showing filtration mechanisms within a fracture. (A) Sedimentation, (B) Diffusion, (C) Straining	17
Figure 3 - 1: Location of the DoLime Quarry in Guelph, ON	26
Figure 3 - 2: Dimensions of a dolomite sample	27
Figure 3 - 3: The Guelph and Eramosa formations visible at the DoLime Quarry (source: Ontario Geological Survey, 2010)	28
Figure 3 - 4 Stylolites in a) the Guelph Formation and b) the Eramosa Formation.....	28
Figure 3 - 5: A sample coated in FRP and banded, prepared to undergo uniaxial loading.	29
Figure 3 - 6: Inducing a fracture along the stylolite. a) Theoretical setup b) The actual fracture undergoing uniaxial compression	30
Figure 3 - 7: illustrates the compression forces added by the uniaxial loading machine and the resulting tension forces, b) is a photograph of a prepared sample in the uniaxial lading machine, and c) is a close-up of the fracture induced.....	30
Figure 3 - 8: Shows a photo of a) one wall of Fracture 1, which is from the Eramosa formation, with b) a black organic deposit, c) a porous area with crystal formation, d) a vug and e) Fracture 2 -crystallization feature and the prominent organic deposits.....	32
Figure 3 - 9: Schematic showing the process used to create mould the original fracture into an epoxy replica. Silicone was applied to the original fracture in order to create a negative mould and then a clear epoxy was used to create the final replica of the rock	33
Figure 3 - 10: A comparison of the vugs in a) the natural dolomite fracture wall and b) the epoxy replica.....	35
Figure 3 - 11: Showing the larger chips that occurred during the fracturing process.....	36
Figure 3 - 12: Experimental set-up a) section view, and b) three-dimensional view	38
Figure 3 - 13: Flow cell during a mixing experiment.....	39
Figure 3 - 14: Showing theoretical setup for visualization tests. The E. coli become excited by blue light and emit green wavelengths and the camera lens filters out all light except for green.....	46
Figure 4 - 1: Hydraulic Test Results for Replica 1.....	52
Figure 4 - 2 : Hydraulic Test Results for Replica 2.....	54
Figure 4 - 3: Mass balance approach used to back calculate the actual concentration exiting the fracture	58
Figure 4 - 4: Typical Solute Breakthrough Curve: Replica 1, 30 m/d. Error bars represent the standard error based on the calibration curve.	61
Figure 4 - 5: E. coli breakthrough curve from Replica 1, 30 m/d. Error bars represent the average percent deviation.	63

Figure 4 - 6: Comparing the bromide tracer test results of Fracture 1 and Replica 1. The error represents the average standard error	69
Figure 4 - 7: Percent recovery vs. specific discharge for each fracture	72
Figure 4 - 8: Comparing the <i>E. coli</i> tracer test results of Fracture 1 and Replica 1. The error represents the average percent deviation.	73
Figure 4 - 9: Visualization results at a) 0.25 Pore Volume Flushes b) 0.5 Pore Volume Flushes c) 0.75 Pore Volume Flushes d) 2.0 Pore Volume Flushes.....	77

List of Tables

Table 1: Showing the initial concentration of <i>E. coli</i> in the influent flow cell for each <i>E. coli</i> tracer test performed.....	44
Table 2: List of tracer tests performed on Replica 1 at varying hydraulic apertures	52
Table 3: Hydraulic aperture comparison between Replica 1 and Fracture 1 for each tracer test (*averaged)	55
Table 4: Summary of aperture characterization tests and results for Replica 1 and Replica 2.....	56
Table 5: Summary of aperture characterization tests and results for Replica 1 and Fracture 1	56
Table 6: Flow Cell Mixing Times.....	57
Table 7: Summary of bromide tracer test results.....	62
Table 8: Summary of <i>E. coli</i> tracer test results	64
Table 9: Showing the differences in mean residence time of Bromide and <i>E. coli</i> (*averaged).....	65
Table 10: Zeta Potential of Dolostone, Epoxy and <i>E. coli</i> (*grown in nutrient rich media. (Soni <i>et al.</i> , (2008))).....	67
Table 11: Summary of Bromide Tracer Tests comparing Replica 1 and Fracture 1	70
Table 12: Summary of <i>E. coli</i> Tracer Tests comparing Replica 1 and Fracture 1 (*manually estimated from the tracer curves).....	70
Table 13: Comparing the arrival times of bromide and <i>E. coli</i> in both Fracture 1 and Replica 1 (* averaged).....	74

Chapter 1: Introduction

1.1 Background

Groundwater is a vital drinking water source for many people around the world, and for many Canadians. In Canada alone, approximately 30% of the water used is groundwater, either supplied by a municipal system or a private well (Environment Canada, 2000).

Groundwater is not only a drinking water source but it is also used for agriculture and industry. It is vital that communities have access to clean water but this is becoming a significant challenge. The United Nations (World Water Report 3, 2009) predicts that the world population will increase by 2 billion by 2050, and states that many cities, particularly in developing countries, cannot meet the current water needs. Clean drinking water is not only essential to maintain the health of those who drink it, but also for the economic well-being of a country. The UN (2009) estimates that the overall economic loss in Africa alone due to poor sanitation and water supply is approximately 28.4 billion dollars per year. These losses are due to increased health care costs, deaths, and children being unable to attend school due to either poor health or too much time spent transporting clean water for their families. The combination of these issues

demonstrates the necessity to develop plans to better understand and protect the world's already stressed water resources.

Although fractured media is a common aquifer material, it is an under-investigated area within the study of groundwater aquifers (Berkowitz, 2002). It has the ability to transport contaminants over longer distances in less time than porous media.

Furthermore, colloids display unique transport characteristics in comparison to dissolved constituents, including the fact that they typically exhibit earlier initial arrival times. Of particular concern to human health are pathogenic microorganisms, which often originate from fecal contamination. *Escherichia coli* (*E. coli*) is a common indicator for fecal contamination; some strains are pathogenic, causing acute illness, and sometimes death, in humans. A mechanistic understanding of the transport and retention of colloids, and particularly biotic colloids in fractured media, is important towards developing groundwater remediation and protection strategies for fracture rock aquifers.

1.2 Objective

The city of Guelph is entirely dependent on groundwater and relies on an aquifer that is mostly made up of fractured materials (City of Guelph, 2010). The city of Guelph is also surrounded by farmland and the Guelph Region has a “high” level, 3.35 – 4 cases per 10 000 persons, of reported Verocytotoxigenic *E. coli* cases per year (Michel *et al.*, 1999).

Due to the vulnerability of Guelph's bedrock aquifer to contamination, the City of Guelph is collaborating with the Ontario Research Fund (ORF) and a team of researchers

(Principal Investigator: Dr. Beth Parker) with the overall goal of securing the City of Guelph's bedrock aquifer as a long term drinking water supply. The goal of the present research is a part of this larger project, and specifically addresses improving the mechanistic understanding of biocolloid (*E. coli* RS2 GFP) transport and retention in saturated fractures. Specifically, the influence of specific discharge and aperture field characteristics will be evaluated.

The knowledge gathered from this research will be relevant to particulate transport in saturated fractured media in many different applications. For example, understanding the transport and survival of pathogenic microorganisms is crucial for choosing a water supply well location, and is also fundamental in developing much needed policy and guidelines for protecting fractured rock aquifers from particulate contamination.

1.3 Scope

This thesis contains four additional chapters. Chapter 2 reviews the fundamental theory on flow and contaminant (dissolved and particulate) transport in fractured media and reviews relevant literature in this field. Chapter 3 contains the various experiments that were conducted and information detailing the experiments' setups and methodologies. Chapter 4 contains the results of the experiments and a comprehensive discussion of the results from each experiment. Chapter 5 provides the conclusions from this work and describes their implications, as well as some suggested recommendations for future research.

Chapter 2: Literature Review

The work presented in this section is a review of particulate transport and retention mechanisms within both fractured and porous media. Although the experimental work presented within this study focuses solely on particulate transport through a single saturated fracture, there has only been a fraction of the number of studies completed in fractured media relative to porous media. Since many of the basic concepts regarding particulate transport in porous media can be directly applied to fractured media, particularly at the micro-scale, it is instructive to review the porous media literature. Transport mechanisms for particulates drawn from the filtration theory will also be reviewed, and similarities and differences between solute and particulate transport will be distinguished. Due to the interdisciplinary nature of this topic, information will be drawn from many disciplines, including hydrogeology, water resources, chemistry and biology.

2.1 Colloid Transport within Fractured Media

Due to the infancy of the field particulate transport in fractured media, together with its multidisciplinary nature (Berkowitz, 2002), it is necessary to define certain terms prior to reviewing the literature. The term fractured media, unless specified, could refer to a single fracture plane or a fracture network that consists of multiple continuous and discontinuous fractures, fissures and cracks as well as fracture joints and nodes (Bonnet, et al., 2001). The scale of these networks and fractures depends on the study area. Single fractures have been found to range from microns to hundreds of kilometers in length (Berkowitz, 2002).

Particulate transport is affected by many of the same physiochemical factors as solutes; however, solutes and colloids also have very different transport and retention mechanisms, which will be explored in this chapter. Although the definition of colloid size varies between disciplines, colloids will be defined within this work as ranging between 10 nm and 10 μm (Myers, 1999). Colloids often have an electrical charge on their surface which influences many of their unique transport characteristics (Sen & Khilar, 2006). Sources of colloids within groundwater include inorganic and organic material, mineral precipitates, soil and rock fragments, and of particular importance to this study, biocolloids (Sen & Khilar, 2006). Biocolloids include but are not limited to bacteria, protozoa and viruses. Transportation and recovery rates of biocolloids differ from, and are more complex than, abiotic colloids due to the fact that they undergo biological processes in addition to physio-chemical interactions (Ginn, *et al.*, 2002).

Some of these include growth and decay, active adhesion, chemotaxis and biofilm development (with potential clogging) (Ginn, *et al.*, 2002).

2.1.1 Advection and Dispersion

Advection and dispersion are the most basic, and often the most influential, mechanisms in both colloid and solute transport. Advection is the movement of contamination with the flow of water (Fetter, 1999). It is particularly influential within fractured media due to the fact that water flow is generally limited to void space within the fracture plane itself, largely excluded from the rock matrix, as the permeability of the fracture aperture is significantly greater than that of the matrix (Berkowitz, 2002).

In the context of fractured media, advection describes the movement of a center of mass based on the mean velocity of water within that fracture or fracture network.

However, dispersion describes the spreading of mass mostly due to velocities greater and less than the average velocity (Fetter, 1999). At the fracture scale, hydrodynamic dispersion is the most influential form of dispersion, and is caused by the combination of the variations in velocity within a fracture and diffusion due to chemical potentials.

Within a fracture aperture, solutes are known to diffuse into areas of lower flow, whereas larger colloids are suspected to stay in the faster flowing aperture regions due to size exclusion (to be discussed further in section 2.1.3). This range of low and high fluid velocities distributed around the average velocity within a fracture were first described by Taylor (Taylor S. G., 1953), who conducted an experiment to show the parabolic nature of the velocity profile within a tube. The theory can be applied to

parallel plates, as shown in Figure 2-1. In 1956, Aris developed what is now known as the Taylor-Aris dispersion theory, in which dispersion is velocity dependent and has been demonstrated to be proportional to the average fluid velocity squared (Dronfield, *et al.* 1993). Moreover, a critical time exists when the constituent has experienced the full range of velocity variation, at which point it has experienced the maximum amount of dispersion (J. Bodin, 2003). The Taylor-Aris dispersion theory is valid only for laminar flow scenarios. (Aris, 1956)

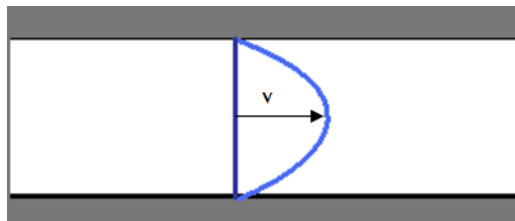


Figure 2 - 1 : Parallel Plate Velocity Profile

Although natural fractures are not made up of smooth parallel surfaces, the parallel plate concept is still instructive for approximating contaminant transport under certain flow conditions. Fracture walls are often rough and apertures are variable in nature, which increases the range of the velocity distribution, adding to the spreading of the contaminant. The advection-dispersion equation (ADE) describes concentration as a function of time and space as follows:

$$\frac{\delta C}{\delta t} = D_L \frac{\delta^2 C}{\delta x^2} - v_x \frac{\delta C}{\delta x} \quad (1)$$

where C (M/L^3) is the concentration, D_L (L^2/T) is the longitudinal dispersion coefficient and v_x (L/T) is the average linear velocity.

An examination of the equation for the longitudinal dispersion coefficient shows that it is a velocity dependant factor that also incorporates effective diffusion:

$$D_L = \alpha_L v_x + D^* \quad (2a)$$

where α_L (L) is the dispersivity in the direction of flow and D^* (L^2/T) is the effective diffusion coefficient. The effective diffusion coefficient is a function of the free solution diffusion coefficient, D_o (L^2/T), and the tortuosity of the flow pathway, τ , and is given by:

$$D^* = D_o \tau \quad (2b)$$

The ADE is very useful for predicting the transport of solutes, however there are many mechanisms, in addition to advection and dispersion, involved in colloidal transport. Therefore, the use of the ADE as it appears in (1) is inappropriate for predicting colloid transport. Some researchers have found it useful to add an additional term to the ADE that compensates for the number of colloids transferred from the aqueous phase to the solid phase (e.g., Torkzaban *et al.*, 2008; Johnson & Elimelech, 1995) as follows:

$$\frac{\delta C}{\delta t} = D_L \frac{\delta^2 C}{\delta x^2} - v_x \frac{\delta C}{\delta x} - r_d \quad (3)$$

where r_d ($M/L^3/T$) is an averaged mass transfer rate. The mass transfer rate considered within this equation includes both the number of colloids adsorbed onto the matrix as well as the number that are re-mobilized under steady flow conditions. Others have had more success separating the two variables, finding that the attachment and detachment rates were different, and both dependent on the aqueous phase concentration (Sirivithayapakorn & Keller, 2003). The separation of the two processes also becomes

important when biological processes are considered. Yates and Ouyang (1992) used two separate die off rates for attached viruses and viruses within the aqueous phase, thereby making it necessary to separate the attachment and detachment rates. It has also proven useful to separate the different mechanisms of colloid immobilization, or removal. Bradford *et al.* (2003) created a model for colloid removal within porous media, and separated the straining and attachment mechanisms (Bradford *et al.*, 2003).

It has been found that hydrodynamic dispersion is not sufficient to account for the total amount of dispersion found within fractured media (Ewing & Jaynes, 1995). Another form of dispersion that occurs within fractures is dispersion on the scale of the fracture plane itself, which is known as geometric dispersion or macro dispersion. The ideal parallel plate scenario does not exist within the natural environment. In natural fractures there is typically a great deal of aperture variability, which causes more variance about the mean fluid velocity (J. Bodin, 2003) than would be expected in a parallel plate. Aperture variability is the main cause of the formation of preferential pathways within a fracture, which is the phenomenon commonly known as channeling (Tsang & Tsang, Channel model of flow through fractured media, 1987). Channeling creates a large amount of spreading both longitudinally and transversely (Tsang & Tsang, Channel model of flow through fractured media, 1987). Figure 2-2, from a study by Tsang and Tsang (1987), shows an example of preferential pathways within a fracture. It is apparent that the aperture field and flow pathways are very related; if super imposed the flow paths in Figure 2-2b) would line up with the larger aperture regions shown on Figure 2-2a).

These flow directing mechanisms are partially responsible for the spreading of the plume in all directions and what cause geometric dispersion. High connectivity between these flow channels can result in either unusually fast arrival times when the flow is concentrated in high velocity pathways, or pronounced tailing when the flow is directed through low velocity pathways (Bodin 2003).

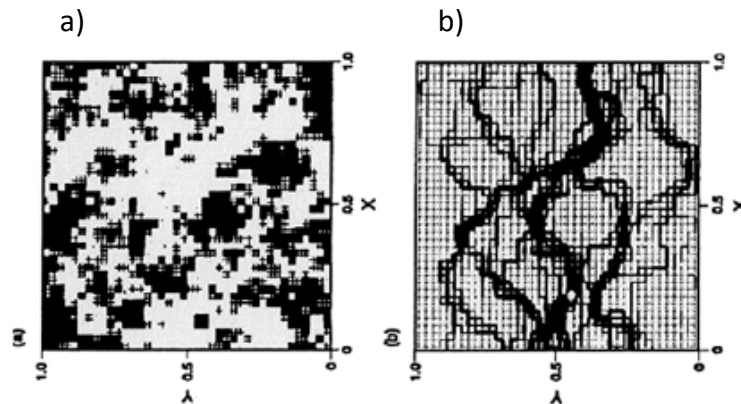


Figure 2 - 2 : Source: Tsang&Tsang, 1987. Showing dispersion due to aperture variations. (a) Approximate relative aperture field, darker being smaller apertures. (b) Approximate flow paths

Dispersion caused by aperture field variability is highly dependent on mixing zones, size of the fracture plane, and the correlation length of the aperture. Dispersion will decrease with increasing opportunities for mixing, increasing aerial extent of the fracture plane, and decreasing correlation length (Ewing & Jaynes, 1995). Aperture field variability dispersion is also dependent on the variance of the mean aperture (Tsang & Tsang, Channel model of flow through fractured media, 1987). As the variance from the mean decreases, so does the flow directing strength, or channeling.

2.1.2 Diffusion

Diffusion can play a role in mass transport, but it is only influential under certain flow conditions. Like dispersion, there are multiple different types of diffusion. Molecular

diffusion is caused by a chemical potential, and is controlled by Fick's First Law as follows:

$$F = -D_d \frac{dC}{dx} \quad (4)$$

where F (M/T/L³) is the mass flux, D_d (L²/T) is the diffusion coefficient, and dC/dx (M/L³/L) is the chemical potential. Although diffusion is always present, it is often neglected as advection and dispersion are orders of magnitude larger when flow rates are large enough, rendering diffusion negligible.

Several studies have been conducted to determine when diffusion is one of the dominant transport mechanisms for solutes within fracture media (e.g., Detwiler *et al.*, 2000; Roux *et al.*, 1998). Diffusion is considered to be a dominant transport mechanism when the Peclet Number (equation 5) is equal to or less than one. The Peclet Number has been used in many studies with some success (Zvikelsky & Weisbrod, 2006). Unlike looking solely effects of velocity on dispersion, the Peclet Number is based around the geometry of the fracture and distinguishes between the different dispersion mechanisms by analyzing the statistics of the fracture aperture plane (Detwiler *et al.*, 2000).

$$Pe = \frac{v_x(b)}{D_d} \quad (5)$$

where Pe (-) is the Peclet Number, and b (L) is the equivalent hydraulic aperture.

Solute diffusion out of the fracture and into the matrix is a different issue. Although the majority of the mass flows through the fracture, it has been demonstrated that matrix

diffusion is often not negligible (e.g., Grisak & Pickens, 1980; Jardine *et al.*, 1999; Maloszewski & Zuber, 1993). Even small colloids have been found to diffuse into the matrix (McKay & Driesse, 2004). Retention caused by diffusion or attachment onto the matrix will be discussed further in the retention mechanisms section.

2.1.3 Size and Charge Exclusion

Size and charge exclusion is an extremely important mechanism of colloid transport. Early arrival times of colloids relative to solutes, also known as differential transport, have been attributed to both size and charge exclusion (e.g., Cumbie & McKay, 1998; Torkzaban *et al.*, 2008; Sen & Khilar, 2006; McKay *et al.*, 2000; Litton & Olsen, 1996). It must be noted here, however, that the term “size exclusion” has been used to describe two separate processes within the literature, both of which will be discussed and differentiated in the following paragraphs.

One definition of size exclusion, which will be referred to as pore size exclusion in this paper, occurs when a colloid is unable to move into a pore space or fracture aperture region due to the size of the colloid relative to that of the aperture (Sirivithayapakorn & Keller, 2003). This results in colloids being transported in larger aperture regions, which have a high likelihood of being preferential pathways and therefore subject to higher velocities. It is thought that the early arrival time of colloids is partially due to continual pore size exclusion, meaning that the colloid continually chooses the fastest route and therefore spends the majority of its transport time in preferential flow pathways (e.g., Cumbie & McKay, 1998; Sen & Khilar, 2006). Sirivithayapakorn and Keller (2003) tested

size exclusion within porous media using a range of colloid sizes and observed that the smallest ratio of pore throat to colloid diameter (T/C Ratio) that did not promote exclusion was 1.5. They also recorded colloid arrival times 4-5 times higher than the average pore water velocity. Figure 2-3 shows an example of size exclusion within a fracture. Researchers such as Chrysikopoulos and Abdel-Salam (1997) used a literature-based T/C ratio of 12 in the development of when creating a mathematical model that attempted to show the effects of size exclusion. They compared the transport of a $1\ \mu\text{m}$ colloid and a $0.1\ \mu\text{m}$ colloid through a variable aperture field and found earlier arrival times and higher relative concentrations from the $1\ \mu\text{m}$ colloid. This was expected because as the colloid size gets smaller, the number of areas within an aperture less than 12 times the colloid size increases.

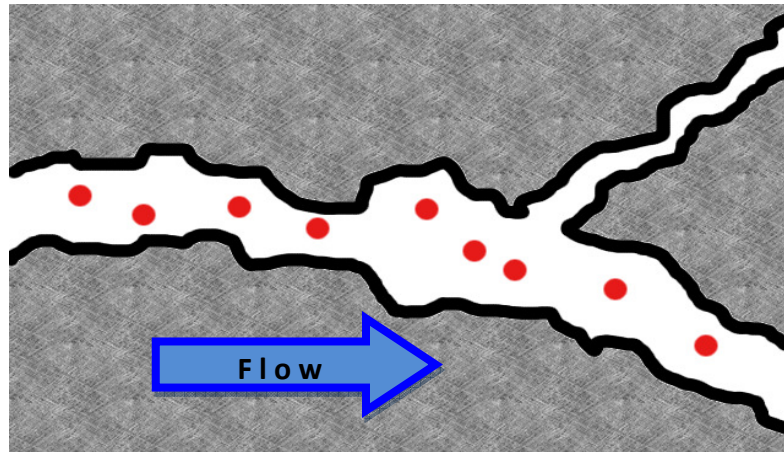


Figure 2 - 3 : Showing Size Exclusion; Colloids and particulates stay in larger aperture regions

The second type of size exclusion defined in the literature is caused by the inability of a colloid's centroid to diffuse into the lower velocity regions, adjacent to the fracture walls due to its size, as shown in Figure 2-4a. This results in the colloid spending the

majority of its travel time at higher- than- average velocities. James and Chrysikopoulos (2003) noted that size exclusion not only increased the effective velocity of the colloid, but it also decreased the hydrodynamic dispersion coefficient of the colloids. Figure 2-4b shows an example of a pulse of soluble tracer that diffuses in and out of the higher and lower velocity regions which causes conservative, soluble tracers to arrive more or less at the time predicted by the average velocity.

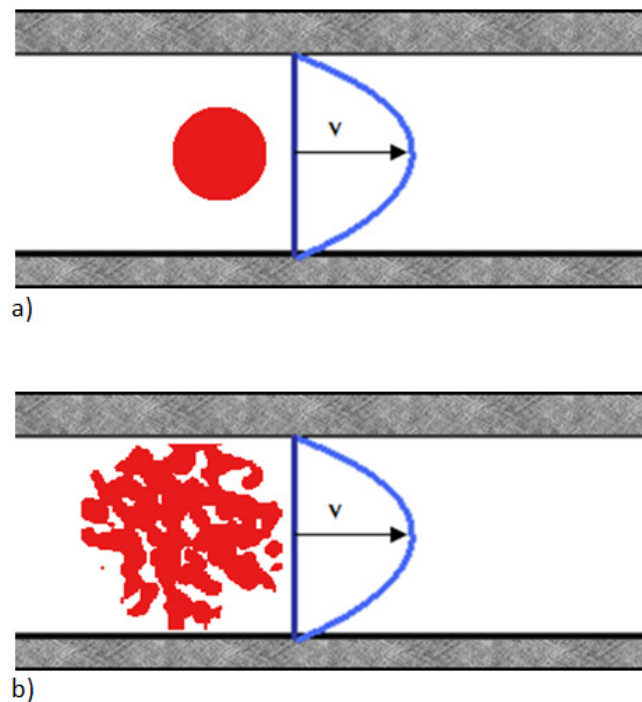


Figure 2 - 4 : Showing Size Exclusion. The colloid stays in the middle of the channel, experiencing high velocities

Colloids have an electric charge, which is dependent on their structure, size, source and material. This charge attracts ions of the opposite charge, which form a fixed layer around the particle, known as the Stern layer. The ions in the Stern layer in turn attract

more ions of the opposite charge, resulting in the formation of a second, more diffuse, layer around the particle. Together, these layers are known as the electric double layer (EDL) (Myers, 1999). The thickness of these layers depends on the ionic strength of the solution, and the electric potential of the particle itself.

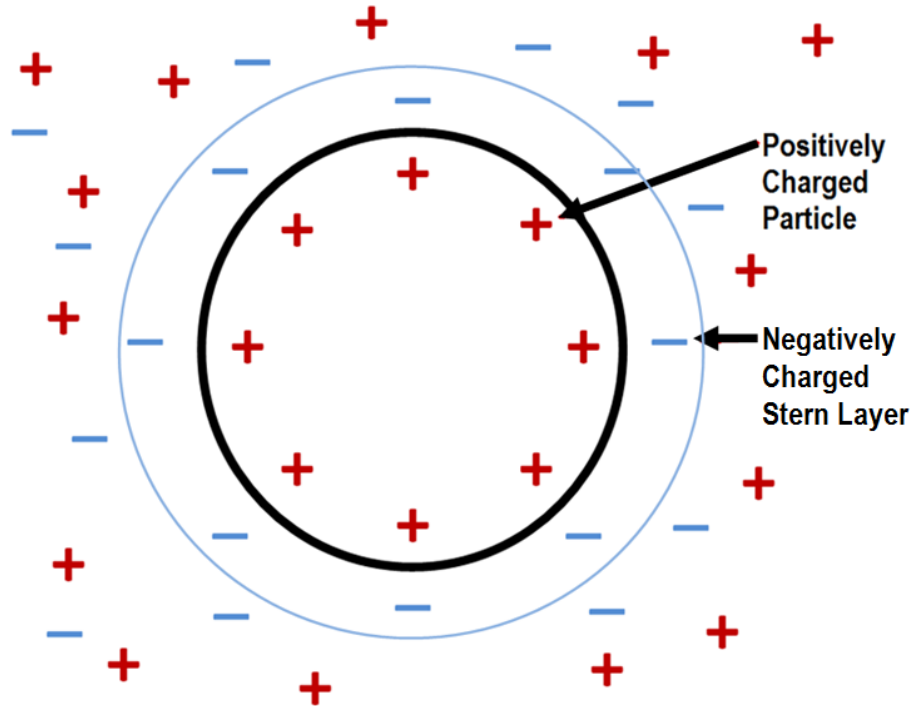


Figure 2 - 5 : Showing the Electric Double Layer surrounding a particle

Charge exclusion occurs due to a repulsive force between the colloid and the media. In the scenario where both the colloid and the media possess the same charge, the resulting interaction force is repulsive, and the colloid is repelled from both fracture walls. This causes the colloid to remain near the center of the fracture aperture, away from the low velocity zones along the fracture wall, resulting in a similar effect as size exclusion.

In a column study through fractured shale conducted by McCarthy, McKay and Bruner (2002), colloids ranging in size from $0.1\mu\text{m}$ – $2.1\mu\text{m}$, and possessing different intensities of negative electric charges, were used to evaluate the importance of the ionic strength of the aqueous solution. Various concentrations of monovalent (Na^+) and divalent (Ca^+) cation solutions were used for each experiment. It was found that as the concentration of the solutions increased, the percent recovery of colloids decreased. This was expected due to the fact that the EDL of the colloids was suppressed with increasing ionic strength, and therefore the repellent force between the colloid and the media walls decreased, enabling attachment. During the same study, the researchers found that the particle size that experienced the least amount of retention was $0.5\mu\text{m}$ and that solution chemistry played a much more significant role than colloid size in colloid transport, while the magnitude of the colloid charge played an even less significant role. What was not evaluated in this study was the effect of aperture size and variability. It can be expected that number of each colloid size retained would change based upon the aperture characteristics due to effects such as size and charge exclusion (Zvikelsky & Weisbrod, 2006) .

2.2 Retention Mechanisms

Colloids display very unique retention mechanisms that are due to a variety of different factors, including: colloid density, ionic strength, colloid size, matrix properties, flow rates, and aperture variability, among others (Cumbie & McKay, 1998) (Johnson & Elimelech, 1995) (Sen & Khilar, 2006). The main mechanisms of colloid retention (originally determined from porous media in the filtration theory literature) are straining

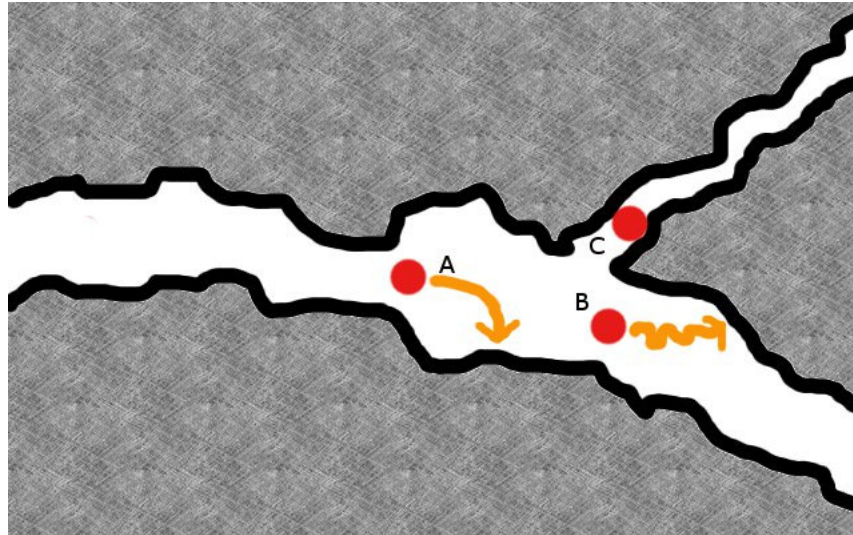


Figure 2 - 6 : Showing filtration mechanisms within a fracture. (A) Sedimentation, (B) Diffusion, (C) Straining

and attachment (Yao, Habibian, & O'Melia, 1971). These retention mechanisms have also been used to explain retention within fractured media environments (e.g. Cumbie & McKay, 1998, Torkzaban, et al, (2008). Figure 2-6 illustrates the retention mechanisms; sedimentation, diffusion and straining, within a fracture.

2.2.1 Attachment due to Sedimentation or Diffusion

Attachment of colloids onto fracture walls is a major retention mechanism within fractured media. Attachment onto the fracture walls occurs primarily from two key steps. First, a collision must occur between the colloid and the fracture wall due to sedimentation, Brownian motion or hydrodynamic forces and second, the colloid sticks or attaches to the wall. Certain forces prevent colloids from entering low velocity zones near the wall, such as size and charge exclusion, and therefore prevent the collision required for attachment to occur. . However, when the sum of the attractive forces (i.e. attractive electrostatic forces, gravity, hydrodynamics forces, dispersion forces, hydrophobicity) exceeds the sum of the repulsive forces (i.e., electrostatic forces,

hydrodynamic forces), a collision will occur, providing the colloid with an opportunity to attach to the surface with which it collided. Under ideal conditions, where the colloids are neutrally buoyant and neutrally charged, there are two main processes thought to cause collision with the fracture walls: sedimentation and diffusion (e.g., Cumbie & McKay, 1998; Chrysikopoulos & Abdel-Salam, 1997; Corapcioglu & Haridas, 1984; Sen & Khilar, 2006). Whether sedimentation or diffusion is the dominant process is greatly dependent on particle size. Studies have been performed in fractured media in attempt to find the ideal colloid size to minimize retention (e.g. Cumbie & McKay, 1998; Zvikelsky & Weisbrod, 2006); however the results of these studies are not consistent. Studies by McKay and Cumbie (1998) and McCarthy *et al.* (2002) found the least retained colloid size to be 0.5 μm . Zvikelsky and Weisbrod (2006), however, found that the optimum colloid size was not consistent between experiments and was dependent on the mean aperture size. Within an equivalent aperture of 380 μm , the optimal colloid size was found to be 1.0 μm with 0.2 μm experiencing slightly more retention. Conversely, in a core sample with an equivalent aperture of 183 μm , the 1.0 μm colloid experienced slightly more retention than the 0.2 μm colloid. Although further evidence is needed, these results imply that aperture size and variability play a major role in colloid transport and retention. It is generally agreed that increased retention of colloids larger than the optimal size is caused by sedimentation and subsequent attachment, while increased retention of colloids smaller than the optimal colloid size is generally attributed to Brownian motion and subsequent attachment. In reality, the situation is likely much more complicated than this, as the magnitude of the electrostatic and

hydrodynamic forces are dependent on aperture size, aperture variability, and colloid size.

Sedimentation becomes dominant when the effective velocity within the fracture is small, and the colloids are more dense than water and large enough for gravity to turn their trajectory downwards (Sen & Khilar, 2006). McKay and Cumbie (1998) defined settling velocity by using Stokes' law as follows:

$$v_t = \frac{2R^2}{9\mu} g (\rho - \rho_w) \quad (6)$$

where v_t (L/T) is the settling velocity of the colloid, R (L) is the radius of the colloid, μ (M/T/L) is the dynamic viscosity, g (L/T²) is the acceleration due to gravity and ρ and ρ_w (M/L³) are the densities of the colloid and water respectively.

Brownian motion, which is considered to be the main type of diffusion for colloids and particles, is inversely proportional to the colloid radius and becomes practically negligible at diameters greater than 1 μm (Sen & Khilar, 2006). It can be described as follows:

$$D = \frac{kT}{3\mu\pi d_p} \quad (7)$$

where D (L²/T) is the Stokes-Einstein diffusion coefficient, T is the water temperature (K), k is the Boltzmann Constant and d_p (L) is the particle diameter.

It should be noted that flow within the matrix and diffusion into the matrix are often neglected due to the fact that they are often negligible relative to flow through the

fracture and diffusion within the fracture. However, McKay and Cumbie (2004) experimented with a wide range of microsphere sizes in fractured shale, and found that microspheres ranging in size from 0.05-0.1 μm diffused up to 3-4 mm into the fracture matrix. Matrix diffusion was found to be negligible, however, for larger colloids.

2.2.2 Straining

Straining (sometimes referred to as mechanical filtration) occurs when the colloid size is physically too large to fit within a pore throat or aperture. In certain cases, as the colloids continue to flow through the media, straining increases and causes “clogging” in certain cases (Sen & Khilar, 2006). Straining increases as the pore size or aperture size decreases and the colloid size increases (Bradford S. A., et al., 2003). Straining differs from attachment due to settling or diffusion due to the fact that is often considered to be irreversibly retained (Bradford S. A., et al., 2003). In a study by Bradford, *et al.*, (2006) it was shown that straining could play a significant role in retention and that it could help fill in gaps within the filtration theory. Nonetheless, it is generally accepted that straining is not significant if the colloid diameter is less than 5% of the porous media grain diameter (Ginn, et al., 2002).

2.3 Biological Mechanisms

Microorganisms present in saturated media behave very similarly to abiotic colloids in terms of the physicochemical transport mechanisms (i.e. straining and attachment). However, microorganisms are also subject to biological processes, including growth and decay, active adhesion and detachment, chemotaxis and biofilm development (Ginn, et

al., 2002). Therefore, it is important to evaluate microbial transport using both physiochemical processes as well as biological mechanisms. However, to date, many studies completed neglect the biological mechanisms and focus on the physiochemical mechanisms (Ginn, Wood, Nelson, Scheibe, Murphy, & Clement, 2002).

2.3.1 Growth and Decay

It is important to consider growth and decay when investigating microbiological transport in the subsurface, especially in longer column tests and field-scale applications. The growth and decay of individual microbes is dependent on the concentration of microorganisms, nutrient availability, solution chemistry, age of a microorganisms, and properties of the microorganism itself. Bacteria and viruses have been found to be able to survive in the subsurface for 2-3 months (Gerba, Melnick, & Wallis, 1975). Once growth and decay have been evaluated for a certain microorganism, they can be added into the ADE as shown below (adapted from Corapcioglu & Haridas, 1984):

$$\frac{\delta C}{\delta t} = D_L \frac{\delta^2 C}{\delta x^2} - v_x \frac{\delta C}{\delta x} - r_d - R_D + R_G \quad (8)$$

where R_D (CFU/L³/T) is the number of microorganisms removed due to die-off and R_G (CFU/L³/T) is the number microorganisms added due to growth. Other researchers have found it beneficial to include multiple growth and dye-off rates to differentiate between microorganisms that are suspended in aqueous solution and those that are attached to the media wall. (Yates & Ouyang, 1992)

2.3.2 Active Adhesion and Detachment

Active adhesion and detachment is the attachment or detachment of a microorganism onto a solid surface driven by a biological process. An example of this may be the attachment of a microbe to a solid surface due to the presence of a food source (Ginn et al., 2002). Properties and growth stages of cells can make them more or less likely to adhere to a solid surface. In a study by Haznedaroglua *et al.*, (2008) two types of *E. coli* were starved for time periods of 6, 12 and 18 hours before performing column tests through packed sand. They found that the *E. coli* that underwent the least amount of starvation was the most adhesive and the *E. coli* that were starved for the longest period of time were the least adhesive. It was found that cells that been starved for 18 hours had developed Extracellular Polymeric Substance (EPS) on its surface in response to the starvation, which increased the hydrophobicity of the *E. coli* cells. Unlike abiotic colloids, adhesive properties are more likely to change over time or if the subsurface chemical conditions undergo a major change. Although more evidence is needed regarding the effect of starvation and other survival processes on transportation mechanisms, it is important to understand that the transport properties of microorganisms can change.

2.3.3 Chemotaxis

Water chemistry in natural aquifers is not homogenous and therefore concentration gradients will be present. Chemotaxis is the movement of microorganisms along a concentration gradient within an aqueous solution; the most obvious movement being from a low nutrient zone to a high nutrient zone (Corapcioglu & Haridas, 1984). This can

be an important factor affecting transport, especially during periods of recharge in an aquifer when a microorganism may be directed out of a low flow zone back into a preferential pathway due to incoming nutrients (Ginn *et al.*, 2002). However, chemotaxis will have little to no influence in a laboratory setting when solution chemistry is consistent and controlled.

2.3.4 Biofilm Development and Bioclogging

When microorganisms attach onto a solid media surface, whether porous or fractured, they may start to develop what is known as a biofilm on the surface, depending on the properties of the microbe, aqueous solution and solid material. Once attached, microorganisms can produce EPS, bringing them past the stage of initial attachment (removable attachment) to what is known as irreversible attachment (Ginn *et al.*, 2002). This type of attachment is often called polymer bridging (Ginn *et al.*, 2002). In order to produce such a layer, nutrients or an alternate form of microbial growth stimulation is needed (e.g., Ross *et al.*, 2001; Taylor & Jaffé; 1990). However, once stimulated biofilm growth starts, the conductive properties of the original media change quite drastically. In a study conducted by Taylor and Jaffé (1990), the permeability of a sand column due to biofilm stimulation and growth was found to decrease by 3 orders of magnitude. Similarly, Ross *et al.*, found that the hydraulic conductivity of a limestone fracture decreased by three orders of magnitude after stimulation and nutrient injection. Transport properties are significantly affected by the growth of biofilm. However, biofilm growth can be monitored by continually checking for hydraulic changes or changes in flow rate.

2.4 E. Coli Characteristics and Previous Studies

There are multiple strains of *Escherichia coli*, which all have unique properties that can affect transport properties (Yang *et al.*, 2006). For the purpose of this thesis, the general properties of *E. coli* will be presented together with the specific properties for the strain *E. coli* RS2G used in these experiments.

E. coli RS2G is a non-pathogenic strain, that is resistant to 2 types of antibiotics (Kanamycin and Rifampicin) and fluoresces green due to an attached green fluorescent protein (Passmore *et al.*, 2010). Like other strains of *E. coli*, RS2G is negatively charged and is cylindrical in shape. By using image analysis and dynamic light scattering, it was found that the average length is about 2.5 μm and the average diameter was 1.16 μm (Passmore *et al.*, 2010). *E. coli* also produce EPS, in the form of called lipopolysaccharides (LPS), that extend from their surface (Foppen & Schijven, 2006). These extended polymers are likely to influence adhesion. A study by Abu-Lail and Camesano (2003) compared the transport of an *E. coli* strain with the LPS attached and with LPS removed, and it was found that the *E. coli* with the LPS was indeed subject to more retention than the *E. coli* without.

Even the same strain of *E. coli* can have very different transport properties. A study by Haznedaroglua, *et al.*, (2008) shows that starvation can greatly affect the transport properties of *E. coli*, and that the properties depends on the degree of starvation. Also showing that the stage of development can have a large effect on the transport characteristics is a study by Yang, *et al.*, (2006), who isolated several types of *E. coli* from

a feedlot and then grew them under two separate conditions; intestinal growth and external growth. The same strain of *E. coli* were found to have different properties, which influenced their retention. The *E. coli* grown externally were found to have increased hydrophobicity as well as an increased ability to grow biofilm. However, strains grown within the intestines were found to have increased motility. The Zeta potential remained relatively consistent regardless of the growth conditions.

Bacteria, including *E. coli*, are subject to multiple different transport mechanisms. It is most important, however, that both physiochemical and biological processes be taken into consideration during transport studies that include biotic colloids. The knowledge surrounding colloid transport is lacking, and that surrounding biotic colloid transport is even more limited. Further studies are required in both fields to concretely address many of the remaining questions. As demand on fresh water increases, so will the demand on both surface and groundwater sources. In some cases, existing groundwater sources will have to be evaluated as a potable water source for a new or growing community. On a smaller scale, rural groundwater wells are used for both drinking and agriculture. Understanding the basic transport and retention mechanisms of biotic colloid transport will help in the development of evaluating and modeling biotic colloid transport on a large scale.

Chapter 3: Methods and Experimental Setup

3.1 Fracture Collection and Preparation

Dolomite rock samples were retrieved from the DoLime Quarry in Guelph, ON (Figure 3-1). Permission was obtained from the quarry manager to explore the quarry and retrieve appropriate samples. Samples were chosen based on several specifications, including size, native unit, presence of a stylolite, and features of interest (e.g. vugs).

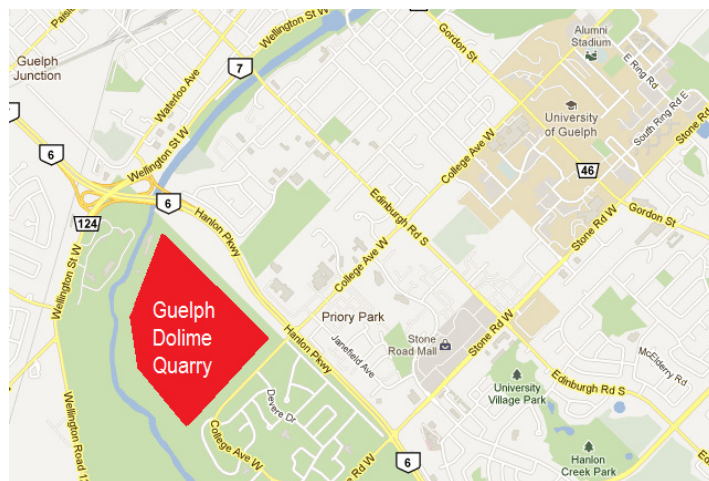


Figure 3 - 1: Location of the DoLime Quarry in Guelph, ON

The sample size is important for handling and mobility purposes, in that large rocks can be difficult to move and transfer in the lab. However, it was also important to increase

the flow region within the fracture. Ultimately, the goal was to minimize the dolomite sample thickness (h) and maximize the length (l) and width (w) (i.e. the plane in which the fracture lies) (Figure 3-2), thereby maximizing the aerial extent of the fracture while minimizing the weight for practicality.

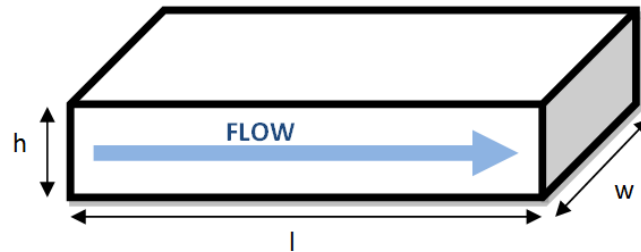


Figure 3 - 2: Dimensions of a dolomite sample

Two formations are accessible in the DoLime Quarry. The top layer is the Guelph Formation, and consists of a light in colour and visibly porous dolostone. The Guelph Formation is underlain by the Eramosa Formation, which is much darker and is visibly less porous in nature relative to the Guelph Formation, almost to the point of having a shale-like texture. Figure 3-3 shows a photograph from the Ontario Geological Survey (2011) of the exposed layers within the DoLime quarry. Based on the colour of the samples retrieved, it was determined that Fracture 1 is likely from the Guelph Formation, and Fracture 2 is from the upper portion of the Eramosa Formation. Samples from the lower portion of the Eramosa Formation were avoided, as they are similar in texture to shale (i.e. brittle and easily shattered) and therefore could not be subjected to a uniaxial load (as described below) without breaking.



Figure 3 - 3: The Guelph and Eramosa formations visible at the DoLime Quarry (source: Ontario Geological Survey, 2010)

Samples were selected based on the presence of a well-defined stylolite that extended horizontally through the entire sample. Figure 3-4 shows photographs of several stylolites, which are planes of weakness that occurred due to a number of possible factors including pressure or temperature variants, crystal formation, and water flow. Generally, well-defined stylolites were a water flow channel at some point in the past, and the increased definition is caused by the dissolution of minerals in the water (Middleton, 2003).

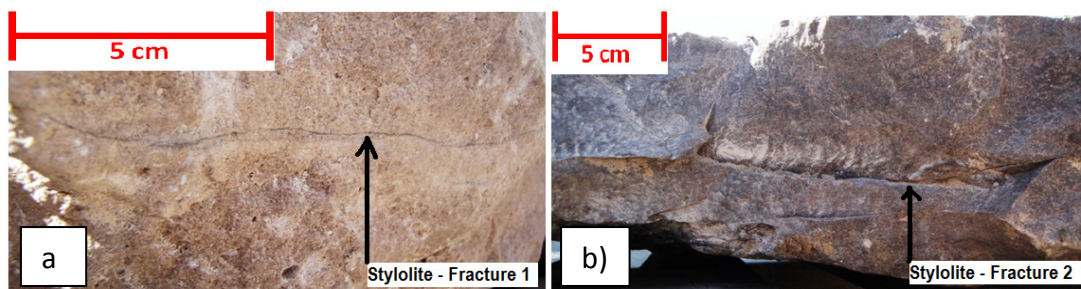


Figure 3 - 4 Stylolites in a) the Guelph Formation and b) the Eramosa Formation.

Once collected, the samples were prepared for fracturing under a uniaxial load. The preparation was accomplished through first cutting the fractures into rectangular prisms and then covering them with fibre re-enforced polymer (FRP) to re-enforce all planes except that of the stylolite. The FRP ensured that when the sample was subject to the uniaxial loading machine, a fracture would be induced along the stylolite only, and not in any other plane, which would have resulted in the sample shattering. Once the FRP was dry, banding was added and tightened to further reinforce the sample, and ensure that it would not open upon being fractured. Figure 3-5 shows a photograph of a sample coated in FRP and banded, fully prepared to undergo uniaxial loading.



Figure 3 - 5: A sample coated in FRP and banded, prepared to undergo uniaxial loading.

After the rocks were fully prepared they were placed into a uniaxial loading machine. Triangular bars were placed between the machine and the sample to concentrate the

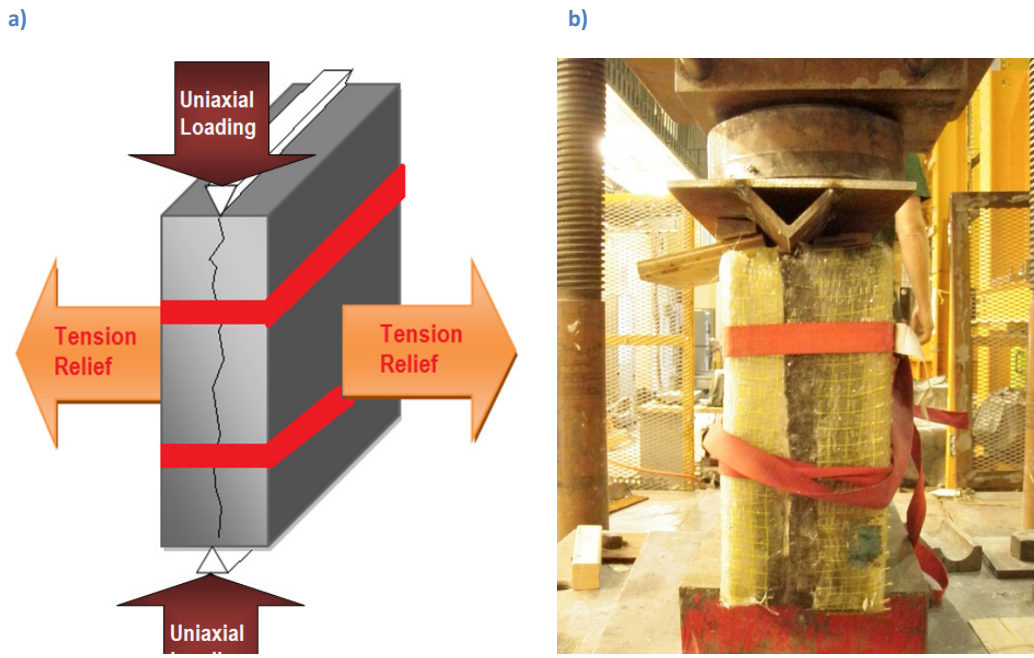


Figure 3 - 6: Inducing a fracture along the stylolite. a) Theoretical setup b) The actual fracture undergoing uniaxial compression

force along the plane of stylolite (Figure 3-6 a). This induced a tension fracture, similar to the mechanism under which unloading fractures occur in nature. Figure 3-6 b) shows a photograph of the fracture in the uniaxial compression machine. The loading is added longitudinally, along the stylolite, causing tension orthogonally to the stylolite so that the sample will fracture along the stylolite.



Figure 3 - 7: A close-up of the fracture induced.

Upon fracturing, the bands were cut, the fractures were opened, and interesting features on the fracture walls were observed. Figure 3-8 a) is a photograph of a wall of Fracture 1, and shows several dark grey areas that are likely organic deposits, which are characteristic of the rocks in both the Guelph and Eramosa Formations (Ontario Geological Survey, 2010). Figure 3-8 d) also shows a small porous area where some crystallization has occurred, and a larger hole that is also porous with crystal formation, called a vug.

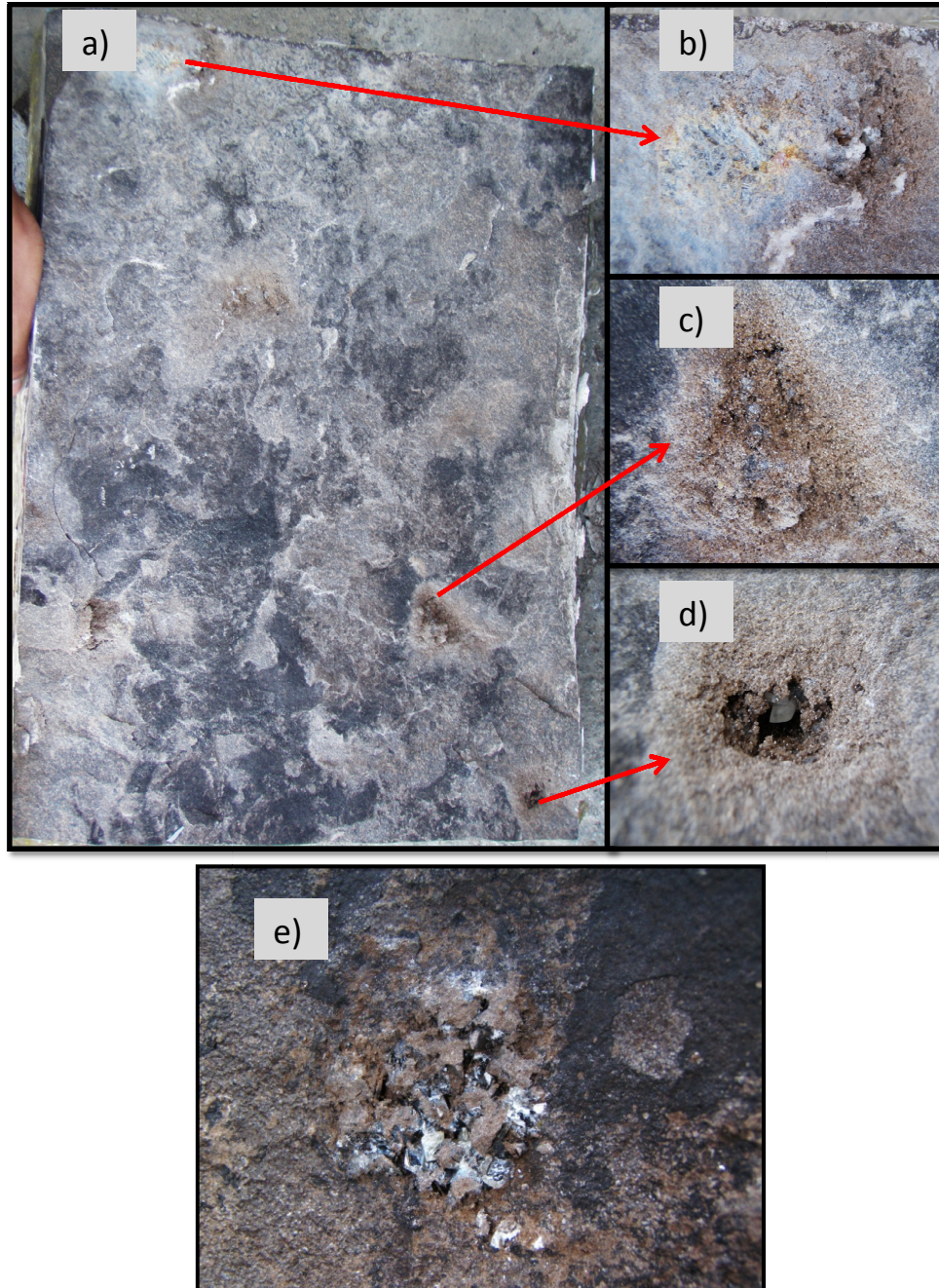


Figure 3 - 8: Shows a photo of a) one wall of Fracture 1, which is from the Eramosa formation, with b) a black organic deposit, c) a porous area with crystal formation, d) a vug and e) Fracture 2 -crystallization feature and the prominent organic deposits

Fracture 2 was different in nature from Fracture 1. While it also contained areas where small crystals had formed, they were not surrounded by porous areas. Figure 3-8 e) shows an example of the crystal formations observed within Fracture 2.

3.2 Epoxy Replicas

The dolostone fractures were cast in clear epoxy in order to observe *E. coli* transport through the fractures. Figure 3-9 shows the basic moulding steps for one side of the rock fracture.

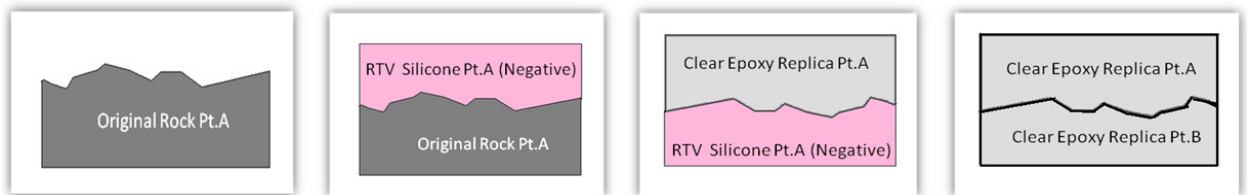


Figure 3 - 9: Schematic showing the process used to mould the original fracture using epoxy. Silicone was applied to the original fracture in order to create a negative mould and then a clear epoxy was used to create the final replica of the rock

The replicas were made by first fabricating a negative of each fracture wall using a two part silicone (RTV-4018 A and RTV-4018 B). To prepare the silicone, the parts were each measured out by weight and mixed together by hand until the silicone was a uniform colour. After mixing, the silicone was de-aired by vacuum for at least 20 minutes. After de-aeration, a small layer of silicone was poured over top of the rock and was rubbed into the surface of the rock using gloved hands to ensure no air bubbles were trapped at the surface. The remaining silicone was then poured on top of the rock. After the silicone spread out evenly on the rock, a rigid, flat piece of 0.5 inch plexiglass was pressed into the surface of the silicone and then set to dry. The rigid plexiglass was necessary so that the silicone would not deform when it is taken off the rock and

prepared for epoxy moulding. The silicone was removed from the rock once it was completely dry (approximately 24 hours later).

The material used to cast the positive of each fracture face was a two part epoxy (EP691F Clear Part A and B, Resinlab). An anti-foam agent (antifoam 88, Resinlab) was also added to the epoxy at 0.2% of the total weight of the epoxy to ensure that dissolved gases within the epoxy mixture would not emerge from the liquid and form on the replicated surface thereby compromising it. The epoxy and anti-foam must be weighed out according to manufacturer's standards and then mixed by hand until a uniform consistency is reached. The epoxy was then be de-aired by vacuum for at least 20 minutes. Following a similar protocol to the silicone, a small layer of epoxy was poured over the silicone negative and then rubbed onto the surface of the silicone, either by hand (gloves) or using an alternative aid. The remaining epoxy was then be poured onto the silicone mould. In order to remove air bubbles entrained in the epoxy, the surface tension on the exposed layer of the epoxy was reduced through using, a 10% solution of isopropyl alcohol. The surface of the epoxy temporarily turned cloudy due to small bubbles surfacing and popping. The antifoam caused the epoxy mixture to turn somewhat cloudy and the epoxy dried slightly cloudy. This technique resulted in excellent replicas with intricate surface details. Figure 3-10 shows a comparison of the vug within the rock fracture and the vug within the epoxy mould.

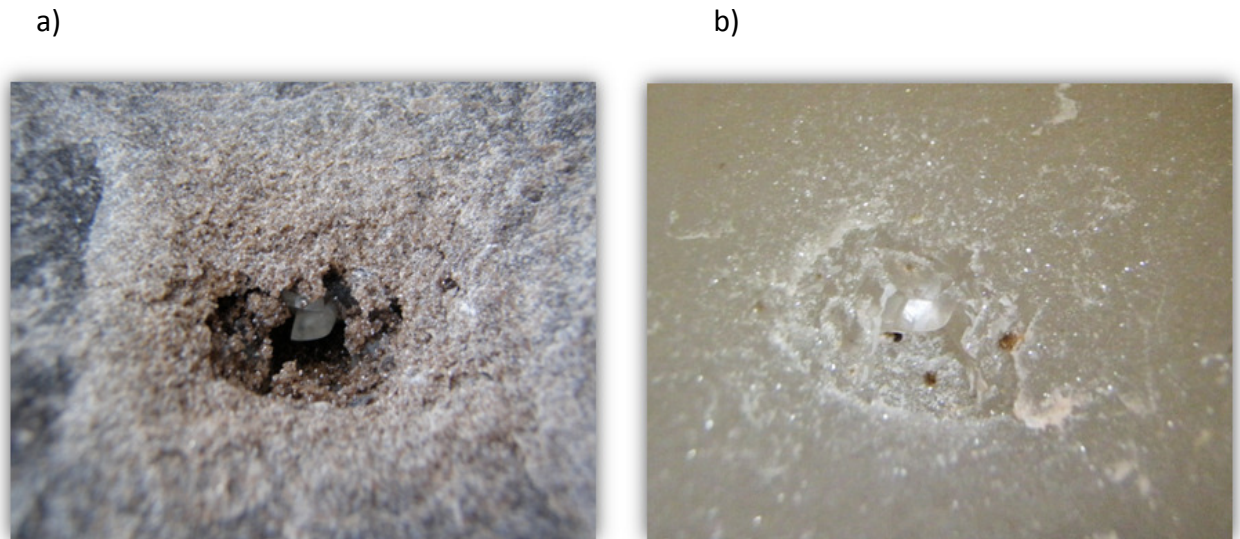


Figure 3 - 10: A comparison of the vugs in a) the natural dolomite fracture wall and b) the epoxy replica

Due to the shale-like texture of Fracture 2, there were 3 large chips of rock that broke off the Fracture. These pieces, shown in Figure 3-11, were too large to be negligible and therefore were collected and situated back in their original placement within the natural fracture. They were also moulded out of the epoxy and placed into the replicated fracture in order to make the replica as similar to the natural fracture as possible. The three rock chips that were moulded are all located along the longitudinal edge of the fracture starting at approximately 10 cm away from the influent edge.

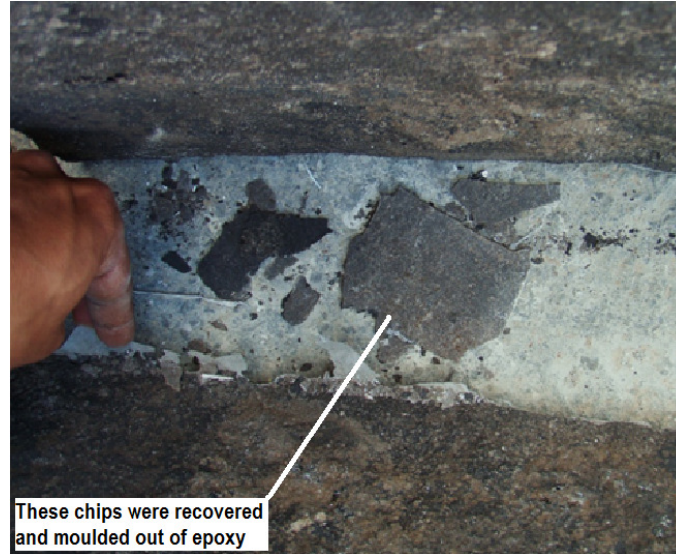


Figure 3 - 11: Showing the larger chips that occurred during the fracturing process

The list of relevant fractures, replicas and their dimensions, is included in Tables 2 and 3 in Section 4.1. From this point on, the terminology used to discuss the natural fractures and their replicates will be Fracture 1 (or 2) and Replica 1 (or 2), respectively.

3.3 Experimental Setup

Figure 3-12 a) and b) show the experimental set up for both the fractures and epoxy replicas, which are adapted from prior work by Zheng (2008), Sekerak (2004) and Dickson (2001). Flow cells were attached to the shorter edges of the samples, and the longer edges were sealed with silicone to create no flow boundaries. Once the epoxy fracture was sealed, it was sandwiched between two layers of plexiglass. The first layer consisted of a $\frac{1}{2}$ inch thick piece that was cut to the same dimensions as the fracture, and was used to help evenly distribute the loads that were added to compress the fracture. The next layer of plexiglass was $\frac{3}{4}$ of an inch thick and was cut to overhang the outer edges. Holes, spaced 7.5 cm apart, were drilled along the longer edges of this outer plexiglass. Threaded rod was then inserted into the holes and washers and bolts were used to apply pressure to the fracture. Three $\frac{3}{4}$ stainless steel bars were evenly spaced on each side of the fracture to ensure the fracture did not warp or buckle due to the load applied by tightening the bolts on the threaded rod. Both the steel bars and the plexiglass were slowly tightened ($\frac{1}{4}$ turn at a time), in attempt to match the aperture of the cast fracture to that of the natural rock fracture. The equivalent hydraulic aperture was used to compare the cast and natural fracture apertures.

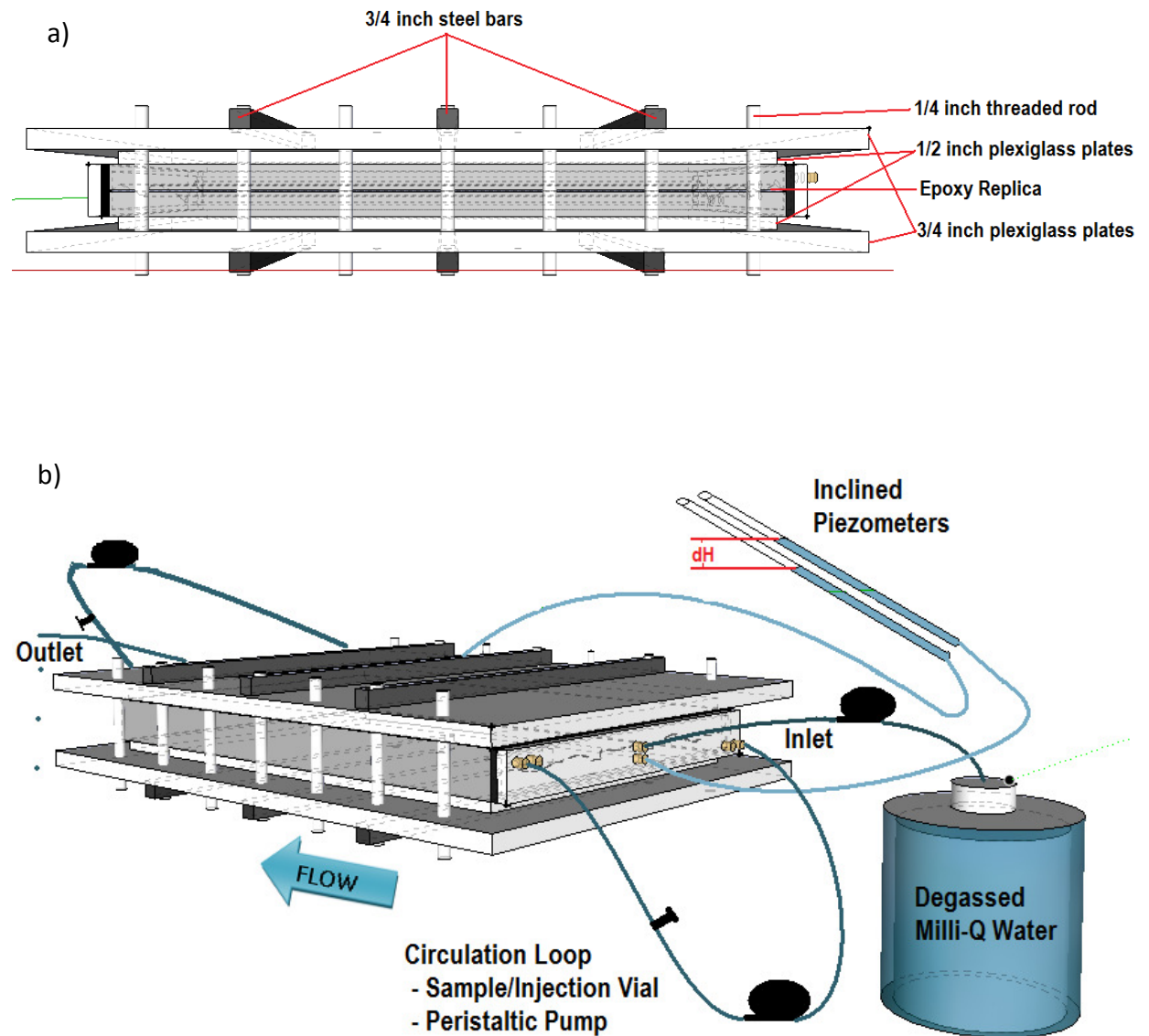


Figure 3 - 12: Experimental set-up a) section view, and b) three-dimensional view

A five mm thick rubber gasket was placed between each flow cell and the rock to prevent leaks, and silicone was used to attach and seal the flow cells on to the fracture.

Six 5 mm holes, or ports, were drilled in each end cap, and equipped with brass Swagelok fittings. Four of these six holes were used for water injection/withdrawal,

mixing, and measuring the head loss across the fracture. The remaining two holes were left capped, and were not used during these experiments.

The two ports located in the farthest diagonal corners of each flow cell were used for the recirculation system (Figures 3-12 and 3-13). This was accomplished by threading a Teflon tube, which was perforated every two-mm, through these ports. Masterflex pump tubing was attached to each end of the Teflon tubing to create a closed loop. A peristaltic pump was attached to the pump tubing, and used to recirculate the contents of the flow cell in order to create a uniform concentration. A custom made, six milliliter glass injection/withdrawal vial, equipped with a hole cap and septum, was placed in-line with the pump tubing in each recirculation system to enable the injection of tracer (e.g. *E. coli*, bromide).and the withdrawal of samples. Dye tests were performed in each recirculation system to ensure complete mixing of the flow cell by the circulation system. Concentrated dye was injected into the injection/withdrawal vial, and the pump on the recirculation system was turned up to full speed. The resulting colour in the flow cell was observed, and timed to determine the length of time required for complete mixing to occur. Figure 3-13 shows a photograph of a flow cell during a dye test.

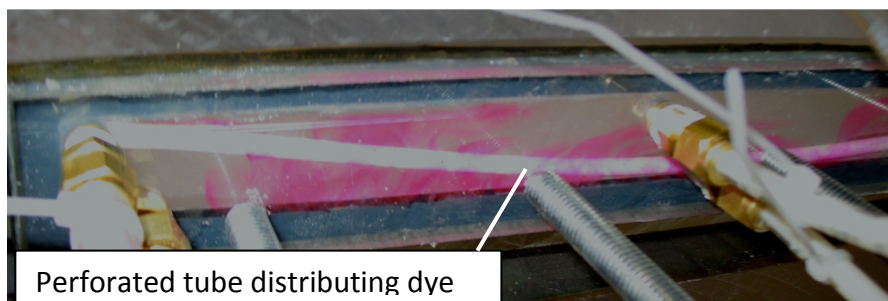


Figure 3 - 13: Flow cell during a mixing experiment

The hydraulic gradient loss was measured by attaching inclined piezometers to the upstream and downstream flow cells. Calipers were used to measure the difference in head between the upstream and downstream piezometers to ensure accurate measurement.

A hydraulic gradient was induced across the fracture using a peristaltic pump (*MasterFlex L/S 7523-70*), which pumped solution from a reservoir into the influent flow cell through one of the Swagelok ports.

In order to saturate the fracture with aqueous solution, it was first purged with carbon dioxide gas through the inlet flow cell. Carbon dioxide is much more soluble in water than air, and will therefore dissolve into an aqueous solution much more readily. After saturation of the fracture with carbon dioxide gas, a degassed aqueous solution, which changed depending on the experiment, was then pumped through the fracture.

Degassing was achieved by purging the solution with three times its volume of helium.

3.4 Aperture Field Characterization

The fractures were characterized using a combination of hydraulic and solute tracer tests, which provide three separate equivalent apertures: the cubic law aperture (hydraulic aperture) (b_h), the mass balance aperture (b_m), and the frictional loss aperture (b_f) as defined by Tsang (1992).

3.4.1 Hydraulic Tests

Hydraulic tests can be used to determine the equivalent hydraulic aperture through the cubic law. Hydraulic tests were completed by pumping the prepared solution through

the fracture under a range of flow rates, and measuring the resulting hydraulic head loss across the fracture. Every time the flow rate was changed, the hydraulic head was allowed to reach equilibrium prior to being measured. The flow rate vs. head loss was plotted to ensure that it remained within the linear range, which indicates laminar flow and therefore the validity of the cubic law. Hydraulic tests were repeated in triplicate.

3.4.2 Solute Tracer Tests

Solute tracer tests were completed to determine the mass balance and frictional loss apertures. Specific discharges of 5, 10, and 30 m/d were used in these experiments. Bromide was chosen as the conservative tracer, as it is easily quantifiable. 10 mg Br⁻/mL as NaBr stock solutions were made using sodium bromide and 18 mega ohm water. The required volume of 10 mg Br⁻/mL solution injected into the injection/withdrawal port in the upstream recirculation system was determined by calculating the mass of bromide required to achieve an initial concentration of 35 mg/L in the upstream flow cell. This calculation was based on the volume of the flow cell (including the recirculation loop) and the volume and concentration of the bromide stock injected into the injection/withdrawal port. The recirculation system was turned up to high for the requisite flow cell mixing time as determined by the dye tests. Following this, the feed pump was started to begin pumping the 18 mega ohm water through the fracture. Sampling intervals varied with each flow rate but a sample at time zero was always taken to determine the background concentration of bromide.

Approximately 2 mL samples were withdrawn from the downstream injection/withdrawal vial at each time interval using disposable syringes, which were then transferred into a glass HPLC vials. The samples were placed into a High-Performance Liquid Chromatograph (HPLC) (Varian ProStar 330) equipped with a conductivity detector to quantify the bromide. Fresh batches of eluent and regenerant solutions (recipes provided in reagents list) were prepared prior to each round of analyses, and the HPLC was given sufficient time to stabilize at a baseline between 14 – 16 μS . The HPLC was set to cover a sensitivity range of 40 μS .

Standards were prepared to cover concentrations ranging from 0 to 100 mg Br/L for calibration purposes according to the method described by Hautman *et al.* (1997). The HPLC was calibrated according to the method described by Hautman *et al.* Calibration curves with coefficients of determination (R^2) values of less than 0.995 were not accepted. Blank samples and test standards were inserted into each HPLC run for quality assurance/quality control (QA/QC) purposes according to the method described by Hautman *et al.* (1997).

3.5 *E. Coli* Tracer Tests

Once the aperture field characterization experiments were complete, tracer tests using *E. coli* were conducted at each specific discharge (5 m/d, 10 m/d and 30 m/d). The strain of *E. coli* chosen for these experiments was *E. coli* RS2G due to its non-pathogenic nature, resistance to two antibiotics (kanamycin and rifampicin, details provided in Section 3.6) and because it is tagged with a green fluorescent protein. The resistance to

the antibiotics was helpful in eliminating any contamination and therefore reduced error. The green fluorescent protein, excites optimally at a wave length 488 nm and also excites at 365 nm, which was important for the visualization tests performed with the *E. coli* (to be discussed further in Section 3.5.1). The *E. coli* RS2G was obtained from the Emelko Laboratory at the University of Waterloo who originally obtained it from Dr. Larry Halverson from the department of Agriculture and Biosystems Engineering at Iowa State University.

For the *E. coli* tracer tests, the fractures were set up and saturated in the same manner as described for the solute tests. The one major difference between the *E. coli* tests and the solute tests is that the fracture was saturated with degassed phosphate buffer solution (PBS), the recipe for which is provided in the reagent list. The experiments were completed using all three of the specific discharges as the solute tracer tests (5, 10 & 30 m/d). An *E. coli* tracer test was performed at each specific discharge with one duplicate test at the 30 m/d rate. Approximately 5 mL of *E. coli* stock was injected into the influent flow cell using a sterilized syringe. The concentration of the stock varied for each run and was therefore diluted and plated following the methods described in Section 3.5.2 in order to determine the initial concentration for each experiment. The initial concentration of the *E. coli* RS2GFP in the influent flow cell at the start of each experiment is included in Table 3-1. The *E. coli* solution was then allotted mixing time in order to achieve a uniform concentration prior to commencing the experiment by turning on the upstream pump to induce the flow of PBS through the fracture. Samples

were taken at various intervals chosen based upon the flow rate and the time elapsed since the start of the experiment.

Table 1: Showing the initial concentration of *E. coli* in the influent flow cell for each *E. coli* tracer test performed

	Specific Discharge			
	30 m/d	30 m/d	10 m/d	5 m/d
Replica 1	2.25E+07 CFU/mL	2.21E+08 CFU/mL	1.01E+08 CFU/mL	1.44E+09 CFU/mL
Replica 2	8.06E+08 CFU/mL	1.28E+09 CFU/mL	1.63E+09 CFU/mL	1.21E+09 CFU/mL
Fracture 1	9.85E+05 CFU/mL	3.17E+06 CFU/mL	9.60E+06 CFU/mL	1.10E+07 CFU/mL

3.5.1 *E. coli* Stock Preparation

Prior to preparing the *E. coli*, all items that were going to be used during each process of the preparation and enumeration were sterilized by autoclaving at 121°C for 20 minutes (*Hirayama Hiclave HV-50*). All items that were not autoclave safe were package sterile. The *E. coli* RS2G was prepared by pouring 4 mL of approximately 10^8 CFU/mL of a pre-prepared *E. coli* RS2G suspension into 200 mL of broth. It was then placed into the incubator for approximately 6 hours or until the optical density measured at 520 nm was between 0.5-0.8 to ensure optimal growth stage and to maintain consistency between experiments. The *E. coli* was then concentrated by centrifuging creating one stock solution with a concentration of approximately 10^{10} CFU/mL and another with a concentration of 10^8 CFU/mL. To centrifuge the *E. coli* a Beckman Coulter Allegra 25R centrifuge was used and set to spin at 5000 rpm for 10 minutes. The *E. coli* was rinsed twice with PBS before it was suspended in PBS. The high concentration was used for tests within the fracture casts in attempt to increase the signal emitted during the visualization tests.

3.5.2 *E. coli* RS2G Enumeration

E. coli samples extracted from the fracture outlet needed to be diluted to concentrations of 10^{-2} - 10^{-6} of their original concentration prior to being plated and counted. The samples were diluted into 1% PBS solution vials, which were autoclaved and cooled prior to use. A volume of 0.1 mL of each dilution was placed onto an agar plate (recipe provided in the reagent section) and spread evenly on the surface. Each dilution was plated in triplicate. This was done to ensure that there would be plates within the countable range of 10 – 300 (Emelko *et al.*, 2008). The plates were then given time to dry before being placed into the incubator for 24 hours at 37°C. Any plates showing evidence of contamination or with colony counts outside of the countable range were removed.

3.5.2 Visualization

The purpose of using the epoxy replicas was to visualize the transport of *E. coli* through the fracture to gain qualitative insight towards particulate transport in fractures. A CCD camera was employed to record the visualization experiments. As mentioned above, the *E. coli* RS2G is tagged with a green fluorescent protein that emits green wave length when excited. The GFP is optimally excited by a wavelength of 488 nm, which is a blue light wavelength. The GFP emits a wavelength of 510 nm. In order to optimally view the GFP, a fluorescent light source was used, and covered with a blue light filter (Visi-Blue filters, purchased from VWR) that was specifically designed for working with GFP. Once the GFP is excited with the blue light wave lengths, it emits a green light which is most intense at 510 nm. The CCD camera was equipped with a 510 nm +/- 10 nm bandpass

lens filter purchased from Delta Photonics. This will only allow wavelengths between 500-520 nm be captured, therefore increasing the sensitivity towards the GFP wavelengths. Also, to reduce noise signal, the entire setup was kept in a light blocking box. Figure 3-14 shows a schematic of the visualization setup.

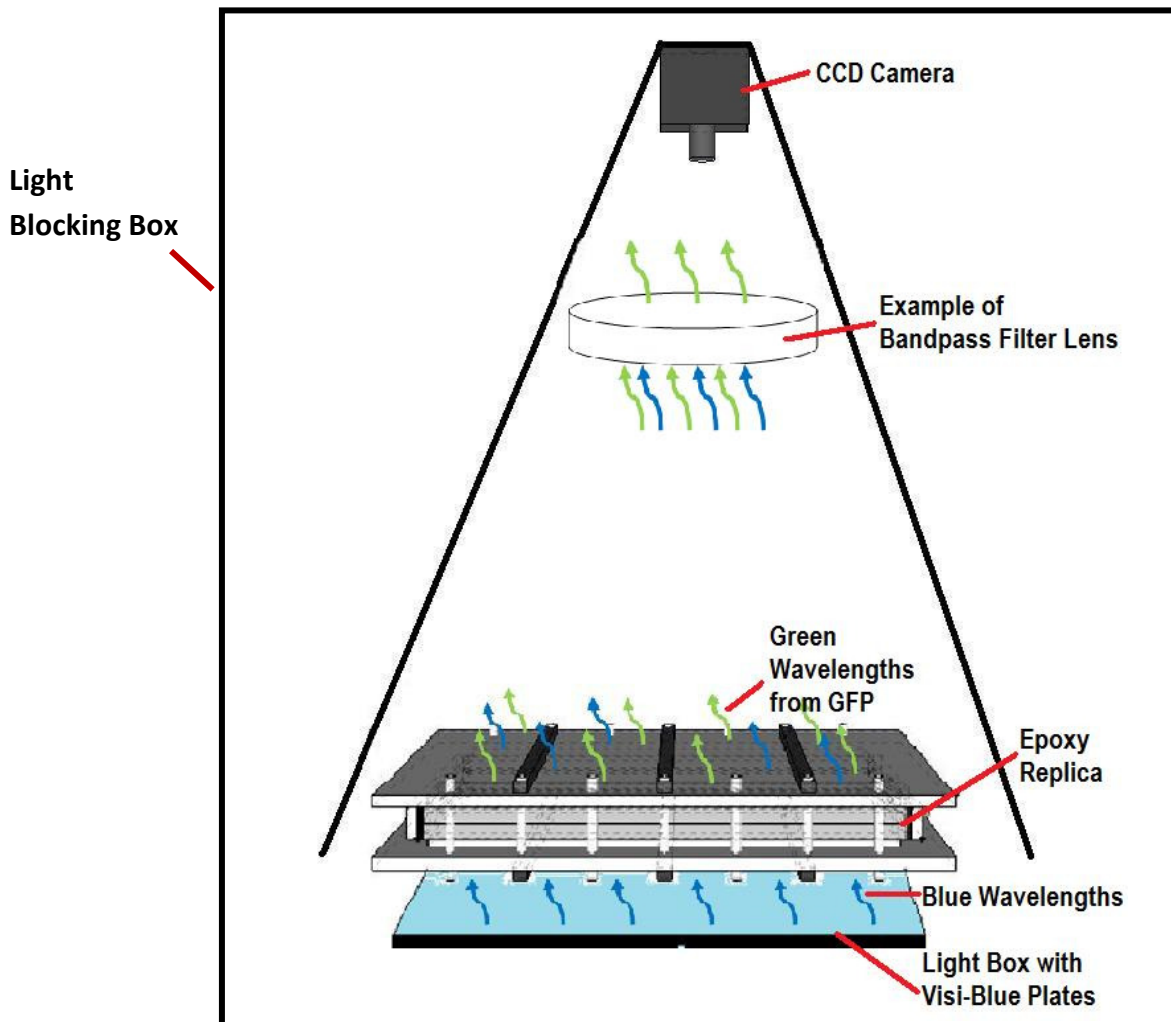


Figure 3 - 14: Showing theoretical setup for visualization tests. The E. coli become excited by blue light and emit green wavelengths and the camera lens filters out all light except for green.

3.6 Reagent List

Kanamycin

In 100 mL of Milli-Q Water:

- 1g of kanamycin

(must be filtered through a 0.22 μ m filter)

Stored in plastic bottles at -80 °C

Rifampicin

In 100 mL of Methanol:

- 0.1g of Rifampicin

Stored in an amber bottle at 4 °C

10% PBS Stock Solution

In 1 L of Milli-Q Water:

- Sodium Chloride (NaCl), 80.0g
- Potassium Chloride (KCl), 2.0g
- Sodium Phosphate (Na₂HPO₄), 14.4g
- Potassium Dihydrogen Phosphate (KH₂PO₄), 2.4g

The 10% solution was stored in plastic bottles and diluted to the 1% solution for all tests

Broth for E. coli RS2GFP

In 1 L of Milli-Q Water:

- HiVeg Hydrolysate (HIMEDIA RM030v-500G), 10g
- Yeast Extract (Bacto BD 212750), 5g
- Sodium Chloride (NaCl), 10g
- 10 mL Kanamycin solution
- 10 mL Rifampicin

(Broth is autoclaved and after the broth has cooled, the antibiotics are added)

Agar:

In 1 L of Milli-Q Water:

- HiVeg Hydrolysate, 10g
- Yeast Extract, 5g
- Sodium Chloride (NaCl), 10g
- Agar (Bishop AGR003.500), 15g
- 10 mL Kanamycin solution
- 10 mL Rifampicin

(Agar is autoclaved and after the broth has cooled slightly, the antibiotics are added. While the agar is still warm the agar is then poured into Fisher brand, 100 mm, sterilized petri dishes. The dishes are allowed to cool and solidify before being stored at 4°C. In order to avoid excess condensation, the plates are removed prior to plating bacteria and allowed to dry)

HPLC Solutions***0.3mM NaHCO₃ stock***

In 1 L of Milli-Q Water:

- Sodium Bicarbonate (NaHCO₃), 42 g

2.7mM Na₂CO₃ stock

In 1 L of Milli-Q Water

- Sodium Carbonate (Na₂CO₃), 106 g

HPLC Eluent

In 4 L of Milli-Q Water:

- 2.4 mL of Sodium Bicarbonate Stock Solution
- 21.6 mL of Sodium Carbonate Stock Solution

HPLC Regenerant

12.5mM H₂SO₄ Solution

In 4 L of Milli-Q Water

- 2.8 L of H₂SO₄

Chapter 4

4.1 Aperture Field Characterization

Flow and contaminant transport are highly dependent on the characteristics of the aperture field such as heterogeneity and equivalent aperture. Therefore, to gain understanding of the aperture field characteristics, hydraulic and tracer tests were conducted to determine three different equivalent apertures, all of which are sensitive to and describe different features within an aperture field. The apertures measured include the cubic law aperture (hydraulic aperture), the mass balance aperture and the frictional loss aperture, as defined by Tsang (1992).

4.1.1 Hydraulic Tests

Hydraulic tests were performed on each fracture and replicate in order to find the hydraulic aperture of each sample. Hydraulic tests were also very useful in determining the range of flows in which the flow regime is laminar, and therefore the range for which the cubic law applies, for each fracture and also reducing the hydrodynamic effects. To evaluate whether flow rates are within the laminar flow range, head loss across the aperture is plotted against the corresponding specific discharge, and the

results will produce a linear distribution in the laminar flow regime. The specific discharge v. headloss plots for Replica 1 and Replica 2 can be seen in Figure 4-1 and Figure 4-2, respectively. The hydraulic aperture (b_c) calculated as follows:

$$b_c = \sqrt[3]{\frac{12uQL}{\rho W(\Delta H)}} \quad (9)$$

where u ($M/L^2/T^2$) is the dynamic viscosity of the fluid, Q (L^3/T) is the flow rate, L (L) is the length of the fracture, ρ (M/L^3) is the density of the fluid, W (L) is the width of the fracture and ΔH (L) is the head loss at the corresponding flow rate.

Tests were performed on each fracture and replica within the range of 5-30 m/d. To determine the flow rates corresponding to these specific discharges in each fracture, the equation below was used:

$$Q = qb_c W \quad (10)$$

where q (L/T) is the specific discharge, and W (L) is the width of the fracture.

Reynold's number was an alternative way of confirming that the flow rates chosen were within the laminar regime. Reynold's number was calculated at each flow rate and values were consistently less than 1, indicating laminar flow in fractured media. The equation for Reynold's number is given by:

$$R_e = \frac{\rho qb_c}{u} \quad (11)$$

In order to create a more accurate level of comparison between Fracture 1 and Replica 1, Replica 1 was compressed by squeezing it between a combination of ¾ inch steel bars

and $\frac{3}{4}$ inch thick acrylic glass. This compression mimicked the compression the natural fracture was subject to due to the load of the rock. Replica 1 was compressed until the cubic law aperture of the replica was as close to the cubic law aperture of the natural fracture as possible. However, due to the elastic nature of the epoxy replicas, the aperture continued to decrease over time. Due to the changing aperture, a hydraulic test was completed before each tracer test to ensure that the proper flow rate was chosen to achieve the desired specific discharge, as it was important to keep the specific discharges consistent. Eventually, Replica 1 did arrive at a steady state condition when it reached a hydraulic aperture of 0.34 mm. Figure 4-1 shows a graph of the specific discharge versus head loss for Replica 1 on three separate dates. The results from April 4th, 2011 represent the time at which the hydraulic aperture reached its steady state hydraulic aperture of 0.34 mm. The tests from February 10th and March 4th show tests that resulted in hydraulic apertures of 0.54 mm and 0.42 mm, respectively. The results in Figure 4-1 show a linear relationship between specific discharge and head loss on each date, indicating that the specific discharge was within a linear range and therefore a laminar flow range. Additionally, Figure 4-1 demonstrates that the hydraulic aperture decreased over time due to the load applied.

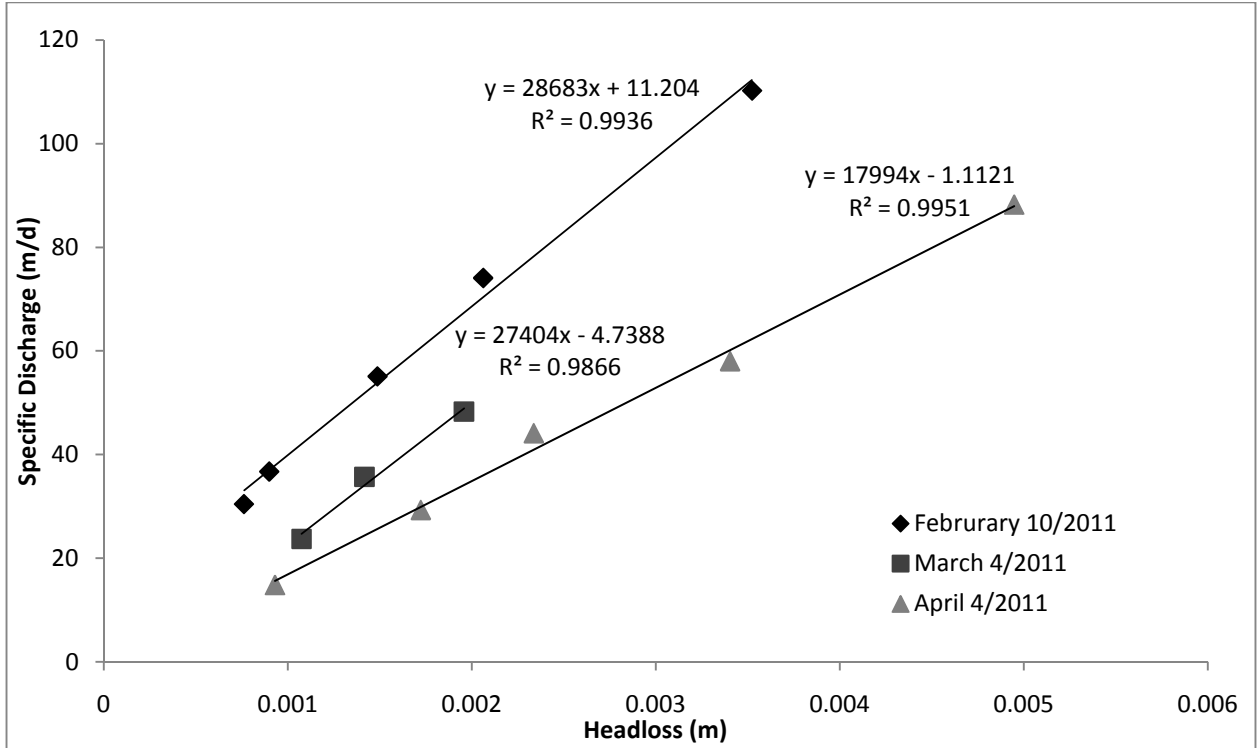


Figure 4 - 1: Hydraulic Test Results for Replica 1

Since the aperture of Replica 1 continually changed until reaching a steady aperture of 0.34 mm, some tracer tests were completed on Replica 1 before it reached the aperture width of 0.34 mm. Table 2 shows the list of the tests completed for the different measured hydraulic apertures.

Table 2: List of tracer tests performed on Replica 1 at varying hydraulic apertures

Date of Hydraulic Test	Aperture (mm)	List of tracer tests Performed during corresponding hydraulic aperture
February 10/2011	0.54	- Bromide: 30 m/d
March 4/2011	0.42	- Bromide: 30 m/d, 10 m/d
April 4/2011	0.34	- Bromide: 5 m/d - <i>E. coli</i> : 30 m/d, 30 m/d, 10 m/d, 5 m/d

Replica 2 was not compressed as significantly as Replica 1. This was because of the delicacy of the small, individual epoxy chips within the walls of Replica 2. Therefore, it was not possible to compare the results of Replica 2 with Fracture 2, as their apertures were too different. The cubic law aperture remained constant over time for Replica 2. However, Replica 2 did show a distinct transition between laminar and turbulent flow at a much lower flow rate than expected. Therefore, the flow rates employed for the remainder of the experiments in Replica 2 were all within the laminar range and Reynolds' number was calculated to ensure that the flow was laminar. It is unknown as to what caused the early transition from laminar to turbulent flow. However, it could be due to the chips within the fracture, which cause the flow to split into two separate flow paths, creating areas of turbulence around the edges of the rock chips. It may also be due to variability in the aperture field that are large enough for inertial forces to become important. The hydraulic test results for Replica 2 are shown in Figure 4-2. The linear region indicates laminar flow up to an approximate specific discharge of 35 m/d before entering the turbulent flow range.

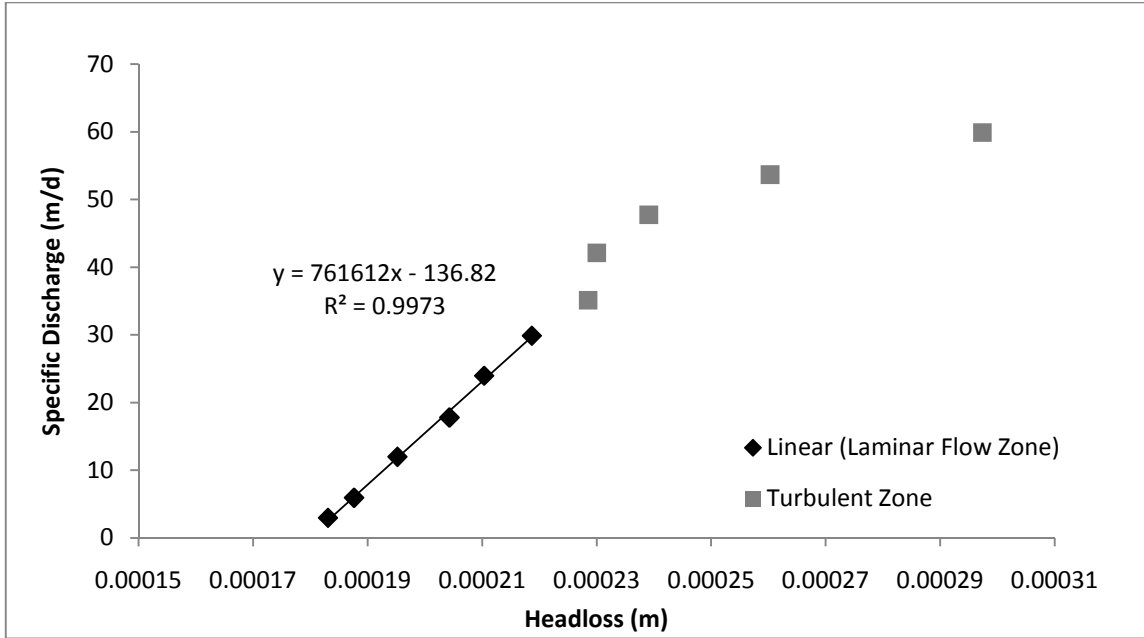


Figure 4 - 2 : Hydraulic Test Results for Replica 2

Table 4 includes the results from the hydraulic tests for both Replica 1 and Replica 2. It can be seen that Replica 2’s hydraulic aperture is constant, while that of Replica 1 is more dynamic due to the applied load. Table 3 shows the comparison of Fracture 1 and Replica 1. Due to the complicated nature of the hydraulic aperture for Replica 1, it is necessary to compare the size of their hydraulic apertures on a per test basis. Table 3 shows the summary of the difference and the fraction difference between the two apertures and shows that the final aperture difference between Fracture 1 and Replica 1 is relatively small.

Table 3: Hydraulic aperture comparison between Replica 1 and Fracture 1 for each tracer test (*averaged)

Tracer Tests for Replica 1	Hydraulic Aperture, Replica 1	Hydraulic Aperture, Fracture 1*	Difference (mm)	Fraction Difference
- Bromide: 30 m/d	0.54	0.29	0.25	1.86
- Bromide: 30 m/d, 10 m/d	0.42	0.29	0.13	1.45
- Bromide: 5 m/d - <i>E. coli</i> : 30 m/d, 30 m/d, 10 m/d, 5 m/d	0.345	0.29	0.055	1.19

Table 4: Summary of aperture characterization tests and results for Replica 1 and Replica 2

Fracture ID	Length	Width	Recirculation System Volume [m ³]		q_c	Q	u_c	u_m	u_f	Estimated Fracture Aperture Volume (mL)			Reynolds number
			Upstream	Downstream						m/d	mL/min	mm	
Replica 1	0.5	0.3	0.000119	0.0001505	30	3.58	0.54	0.700	0.450	64.8	83.76	54.24	1.87E-01
					30	3.53	0.42	0.775	0.270	50.52	93.12	32.28	1.46E-01
					10	1.46	0.42	0.810	0.180	50.52	97.08	21.6	4.85E-02
					5	0.72	0.34	0.870	0.195	41.16	104.64	23.28	1.98E-02
Replica 2	0.4	0.3	0.000115	0.000129	30	4.2	0.69	1.340	0.590	83.28	161.04	70.68	2.40E-01
					10	1.46	0.69	1.285	0.380	83.28	154.2	45.48	8.00E-02
					5	0.72	0.69	1.440	0.255	83.28	173.04	30.72	4.00E-02

Table 5: Summary of aperture characterization tests and results for Replica 1 and Fracture 1

Fracture ID	Length	Width	Recirculation System Volume [m ³]		q_c	Q	u_c	u_m	u_f	Estimated Fracture Aperture Volume (mL)			Reynolds number
			Upstream	Downstream						m/d	mL/min	mm	
Replica 1	0.5	0.3	0.000119	0.0001505	30	3.58	0.540	0.700	0.450	81.0	104.7	67.8	1.87E-01
					30	3.53	0.420	0.775	0.270	63.2	116.4	40.4	1.46E-01
					10	1.46	0.420	0.810	0.180	63.2	121.4	27.0	4.85E-02
					5	0.72	0.345	0.870	0.195	51.5	130.8	29.1	1.98E-02
Fracture 1	0.49	0.31	0.00022156	0.0002156	30	1.668	0.300	1.575	0.135	44.6	236.3	20.4	2.76E-07
					10	0.556	0.285	5.675	0.060	42.6	851.0	9.1	8.79E-08
					5	0.28	0.285	2.110	0.10	42.6	316.4	14.9	4.40E-08

4.1.2 Solute Tracer Tests

Before completing the tracer tests, it was necessary to determine the amount of time required for complete mixing of the inlet flow cell. This was done by injecting a dye into the flow cell. The pump must be turned on and then the time it takes the dye to completely mix within the flow cell is recorded. The results can be seen in Table 6. Initial concentrations of bromide for the tracer tests were kept consistent at a starting concentration of 35 mg/L in the inlet flow cell.

Table 6: Flow Cell Mixing Times

	Volume of inlet flow cell (mL)	Volume of outlet flow cell (mL)	Volume of 10mgBr/L injected (mL)	Measured mixing time of inlet flow cell
Fracture A (Esther)	119	150.5	0.416	5 minutes
Fracture B (Otis)	111.5	129	0.39	2 minutes

To analyze the results of the tracer tests, the measured values must be manipulated in order to find the actual concentration of bromide exiting the fracture, as the samples, or measured values, represent the concentration in the recirculation system on the downstream side of the fracture. However, the concentration exiting the fracture is diluted by the solution in the downstream flow cell, when it enters the flow cell. The effluent flow cell was modeled using a continuous flow stirred tank reactor (CFSTR), as shown in figure 4-3, and a mass balance approach was employed to determine the actual concentration exiting the fracture, $C_{eff-frac}$, from the measured concentration.

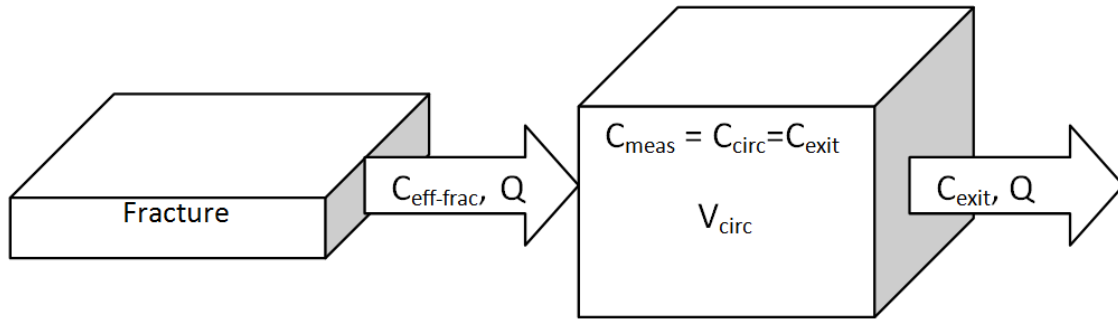


Figure 4 - 3: Mass balance approach used to back calculate the actual concentration exiting the fracture

Equation 12a shows the differential equation resulting from the mass balance, and equation 12b shows how the derivatives in 12a were approximated.

$$C_{eff-frac}(t) = \frac{V_{circ}}{Q} * \frac{\partial C_{meas}}{\partial t} + C_{meas}(t) \quad (12a)$$

$$\approx C_{eff-frac}(t) = \frac{V_{circ}}{Q} * \frac{C_{meas}^t - C_{meas}^{t-1}}{\Delta t} + C_{meas}(t) \quad (12b)$$

All analyses from this point will be conducted using only the actual fracture effluent concentration. Solute tracer tests were performed at specific discharges of 5, 10 and 30 m/d to determine the mass balance and frictional loss apertures. The mass balance aperture is based on the laws of the conservation of mass, and therefore most closely represents the arithmetic mean aperture. This approach is most sensitive to the larger aperture regions as this is where the majority of mass is stored. The mass balance aperture (b_m) was calculated as follows (Tsang, 1992):

$$b_m = \frac{Qt_m}{LW} \quad (13)$$

where t_m (T) is the mean residence time of the tracer, and is calculated using equation 15.

The second equivalent tracer aperture is the frictional loss aperture. Like the mass balance aperture, it also uses the mean residence time; however it also considers the head loss over the entire length of the fracture. Head loss is due to friction, which can be attributed to the smaller aperture regions. Therefore the frictional loss aperture is more sensitive to these areas. The frictional loss aperture (b_f) can be calculated as follows (Tsang, 1992):

$$b_f = L \left(\sqrt{\frac{12u}{\rho t_m (\Delta H)}} \right) \quad (14)$$

The mean residence time was calculated using the modified moment method (Fahim & Wakao, 1982) as follows:

$$t_m = \frac{\sum C_{eff-frac}^t * t_t * \Delta t_t}{\sum C_{eff-frac}^t * \Delta t_t} \quad (15)$$

The variance of the back-calculated concentration was also calculated for each time step as follows (Fahim & Wakao, 1982):

$$Var = \frac{C_{eff-frac}^t (t_{avg}^n - t_m) * \Delta t_n}{C_{eff-frac}^n * \Delta t} \quad (16)$$

Table 4 shows the equivalent apertures calculated from the hydraulic and tracer tests. Replica 1 has a smaller hydraulic aperture than Replica 2. Once Replica 1's aperture had settled to 345 μm Replica 2's aperture of 695 μm was practically double Replica 1's aperture. Consistently

throughout the tests, a trend of $b_m > b_h > b_f$. This trend was expected and has been seen in previous research. Table 5 shows the results of both Fracture 1 and Replica 1 to compare their values. Fracture 1 had a slightly lower hydraulic head of 285-300 μm than Replica 1's final hydraulic head. Although Fracture 1 also followed the trend of $b_m > b_h > b_f$, it showed a significantly differences between the mass balance, frictional loss and hydraulic apertures. Table 6b shows the fraction differences between the equivalent apertures for each fracture.

Table 6 b: Fraction difference between the cubic law aperture and the mass balance and frictional loss aperture

	Average u_m/u_c	Average u_f/u_c
Replica 1	1.9	0.62
Fracture 1	10.9	0.34
Replica 2	2.0	0.59

A typical breakthrough curve from a bromide tracer test is shown in Figure 4-4, which shows the measured concentration, the back calculated (actual) concentration, and the variance of the back-calculated concentration as a function of time for the bromide tracer test conducted at 30 m/d in Replica 1. Figure 4-4 shows that the back-calculated concentration data had a much higher peak value than the measured concentration data. Additionally, the back-calculated curve is not as smooth as the measured curve. This was expected due to the fact that the back-calculated concentrations are computed using the derivative of the measured concentrations. Therefore, any irregularity in the measured concentration curve is amplified through the calculation of the derivative. As the breakthrough curve begins to tail, the variance begins to increase significantly. Therefore, the equivalent aperture calculations based on the bromide breakthrough curves did not employ data beyond the point where the variance started

to rise. These observations were typical of all bromide tracer tests. The breakthrough curves for the remainder of the bromide tracer tests conducted are included in Appendix A.

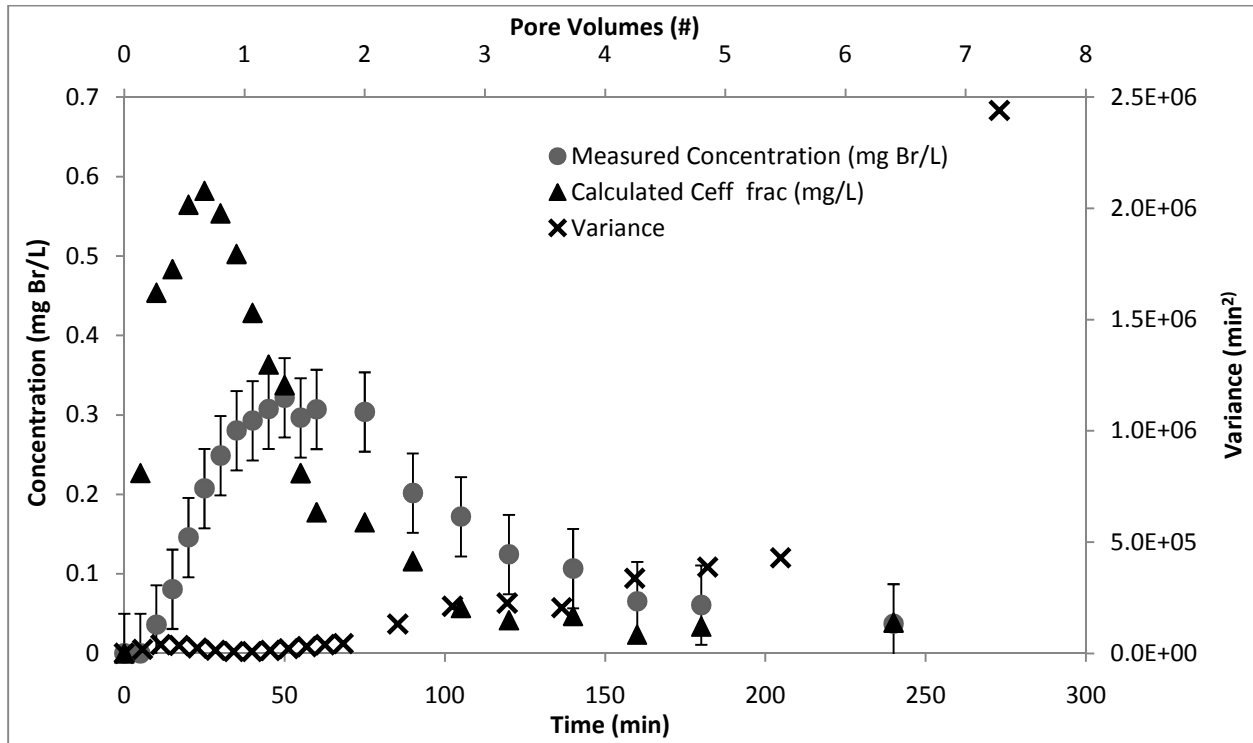


Figure 4 - 4: Typical Solute Breakthrough Curve: Replica 1, 30 m/d. Error bars represent the standard error based on the calibration curve.

The fraction of bromide mass recovered was determined by integrating the breakthrough curve and comparing it with the initial mass of bromide injected into the fracture. However, in conducting this mass balance, it was important to be aware that the input was not a true pulse input. Although a pulse of bromide was injected into the influent flow cell, it was flushed through gradually with the bromide-free feed water. Therefore, the input bromide function actually decayed exponentially, and the actual mass input was calculated as follows:

$$C_{in}(t) = \frac{M_{Br}}{V_{recirc}} * e^{\left(\frac{-Qt}{V_{recirc}}\right)} \quad (17)$$

A summary of residence times, peak concentrations and percent bromide recoveries for each bromide tracer test conducted is presented in Table 7.

Table 7: Summary of bromide tracer test results.

Fracture ID	qc	Q	Mean Residence Time	Peak Measured Concentration	Peak Calculated Concentration	Percent Recovery
	m/d	mL/min	min	C/C _o	C/C _o	
Replica 1	30	3.58	30	0.487	0.988	109.00%
	30	3.53	33	0.331	0.583	109.00%
	10	1.46	138	0.414	0.740	96.25%
	5	0.72	297	0.431	0.986	105.50%
Replica 2	30	4.2	38.3	0.223	0.315	105.20%
	10	1.46	105.6	0.212	0.291	97.91%
	5	0.72	240.3	0.363	0.611	96.25%

The percent recoveries for the bromide tracer tests are high and are comparable to one another. Some percent recoveries are higher than 100% due to the error associated with the back calculation of the effluent concentration. There does not seem to be any major trend in percent recoveries between the two replicas and their hydraulic aperture. However, Replica 2 consistently shows significantly lower peak concentrations than Replica 1. This is likely due to the fact that Replica 1 has a larger equivalent aperture, and therefore the bromide is diluted more than it is in Replica 2.

4.2 *E. coli* RS2G Tracer Tests

Tracer tests were performed using *E. coli* RS2G at specific discharges of 5, 10, and 30 m/d, the same three specific discharges as bromide tracer tests in order to compare these tests directly.

All samples that were within an acceptable countable range were used to plot the

breakthrough curve. Since all the samples were taken from the circulation system which dilutes the fracture effluent, it was necessary to back calculate from the measured concentration using equation 12b.

Figure 4-5 shows the measured concentration, back-calculated concentration, and the variance of the back-calculated concentration as a function of both time and pore volumes flushed for Replica 1 at a flow rate of 30 m/d. The error bars represent the average percent deviation over the course of the entire experiment calculated as follows:

$$Average\ Percent\ Deviation = \sum \frac{(standard\ deviation)_t}{(mean)_t} \tag{18}$$

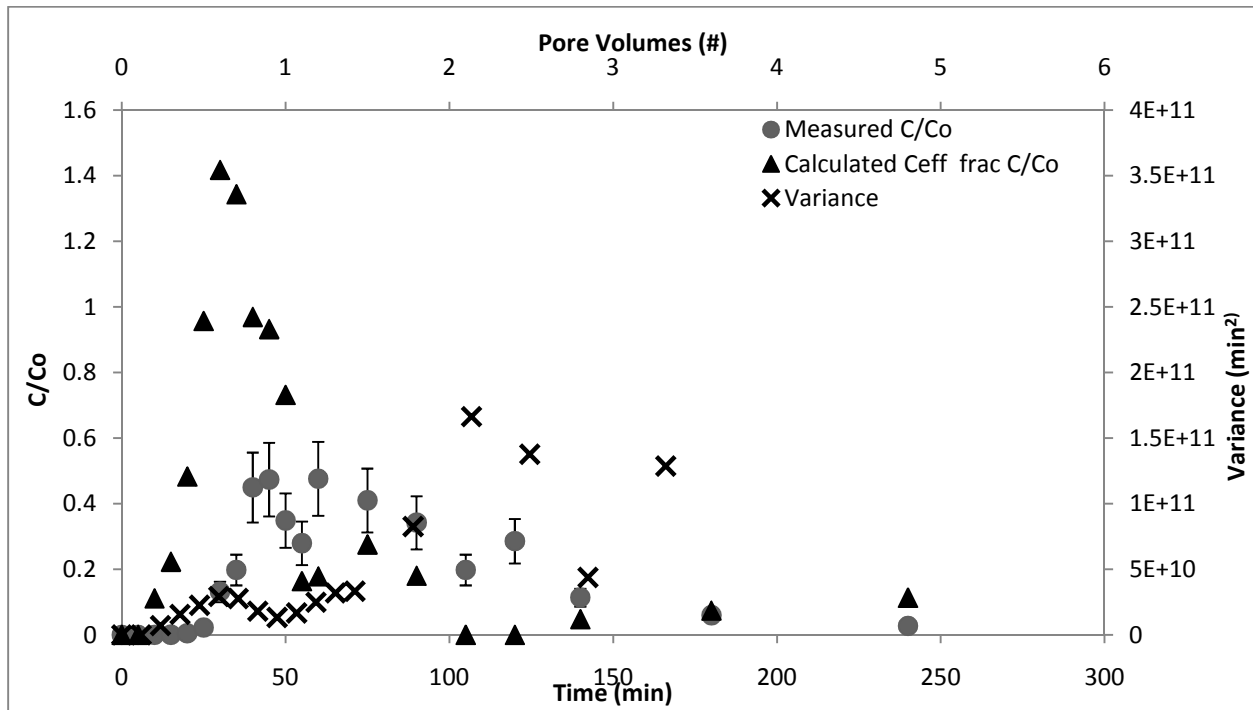


Figure 4 - 5: E. coli breakthrough curve from Replica 1, 30 m/d. Error bars represent the average percent deviation.

This graph shows that the normalized back-calculated concentrations exceed one, which is obviously not possible. However, as indicated previously, the back-calculated are calculated

using the derivative of the measured values, and therefore any irregularities in the measured curve are amplified. The increase in variance that coincides with the peak also indicates the increase error in these calculated values. The general shape and characteristics of Figure 4-5 are typical of all *E. coli* tracer tests conducted in this research. Appendix B includes graphs of the remaining *E. coli* tracer tests.

Comparison of Replica 1 and Replica 2

Table 8 summarizes the peak concentrations and percent of *E. coli* RS2G recoveries for all *E. coli* tracer tests, and does not reveal any obvious relationship between specific discharge and recovery rate or specific discharge and peak concentration. However, a comparison of the recovery rates between Replica 1 and Replica 2 shows that there is consistently less recovery of *E. coli* in Replica 2. Replica 2 also consistently elutes smaller effluent peak concentrations. This observation is consistent with the bromide tracer test results, in which the peak bromide concentration was also smaller in Replica 2 than Replica 1 in all experiments.

Table 8: Summary of *E. coli* tracer test results

Fracture ID	qc	Q	Mean Residence Time	Peak Measured Concentration	Peak Calculated Concentration	Percent Recovery
	m/d	mL/min				
Replica 1	30	2.2	41	0.48	1.42	76.67%
	30	2.2	31	0.84	2.11	79.83%
	10	0.77	115	0.43	1.20	62.35%
	5	0.4	161	0.60	1.38	71.00%
Replica 2	30	4.2	35.5	0.14	0.20	23.11%
	30	4.2	33	0.51	0.53	50.72%
	10	1.47	110.5	0.57	0.89	54.72%
	5	0.723	193.03	0.58	0.68	40.70%

In fractures with larger apertures (i.e. Replica 2), constituents (e.g., *E. coli*) may be more diluted than in smaller-aperture fractures (i.e. Replica 1), particularly if channeling is not a major factor. Additionally, due to the fact that Replica 2 likely had a turbulent flow zone at even the lowest specific velocities, due to the presence of the fracture chips, mixing zones within or around the rock chips were likely present. The presence of the rock chips could also explain the lower percent recovery. Theoretically, contact with the fracture walls should decrease with increasing aperture size as diffusion (Brownian motion) is not sufficient to cause particles closer to the centre of a larger aperture to contact the fracture wall. However, if the presence of the rock chips did create turbulence, this may have generated increased *E. coli* contact with the replica walls in Replica 2, which would have resulted in increased retention of *E. coli*. This also explains why this trend of lower recovery in Replica 2 was not observed during the bromide test, as bromide is a conservative tracer and would not be retained through attachment to surfaces.

Table 9: Showing the differences in mean residence time of Bromide and *E. coli* (*averaged)

Fracture ID	qc	Mean Residence Time (Bromide)	Mean Residence Time (<i>E. coli</i>)	Difference in Time (Bromide - <i>E. coli</i>)	Fraction Difference
	m/d	min	min	min	
Replica 1	30	31.5*	36*	-4.5	1.14
	10	138	115	23	0.83
	5	297	161	136	0.54
Replica 2	30	38.3*	34.3*	4	0.90
	10	105.6	110.5	-4.9	1.04
	5	240.3	193.03	47.27	0.80

An additional major difference between the bromide and *E. coli* tracer tests are the mean residence times. Although the results are relatively consistent at the highest specific discharge, 30 m/d, the mean residence time of the *E. coli* generally decreases at the specific discharges of 10 m/d and 5 m/d. Table 9 shows the time differences between the mean residence times for the bromide and the *E. coli* tracer tests, as well as the fraction difference. Replica 1 shows higher fraction differences than Replica 2, indicating that aperture size plays a direct role in differential transport. These early arrival and shorter mean residence times provide confirmation to those theories discussed in Chapter 2, specifically size exclusion. Size exclusion is the theory that colloids will not enter aperture regions that are smaller than a certain size which is often related to the size of the colloid. This means that in general, colloids will stay in larger aperture, higher velocity areas within the aperture field. The earlier mean residence times of the *E. coli* in the smaller aperture replica indicates that there were fewer flow pathways available that *E. coli* could enter, leaving it to travel the higher velocity pathways. Charge exclusion also played a role but will be discussed in the next section during the comparison of Fracture 1 and Replica 1.

Comparison of Fracture 1 and Replica 1

Although there are some significant differences between the natural fracture and its replica, it can be assumed that the geometry of the two fractures is approximately the same and because of this, the preferential pathways will also be the same. Furthermore, because it is a direct comparison of two fractures with the same geometry, many of the hydrodynamic influences will be similar. A great deal of valuable information can be gained not only from the similarities between the two fractures but also from the isolation of the differences between the two

fractures. In other words, it is possible to make conclusions about the influence of factors such as charge and matrix flow by looking at the differences in the results and tracer test curves. Even if care is taken to fabricate the moulds as best as possible, and effort is made to match the hydraulic aperture of the epoxy fracture to the rock fracture, rock fractures and their epoxy replicates will not behave in exactly the same manner due to their different surface properties. The zeta potential is a useful surrogate measure of charge, which plays an important role in retention. The zeta potential of both the rock and the epoxy was measured in the PBS solution. Table 10 reports the zeta potentials for the matrix materials employed in these experiments, together with that of the *E. coli* RS2GFP, and shows that the epoxy replica has a higher zeta potential than the natural fracture. This is significant because the *E. coli* tests were done using PBS. Since the *E. coli* has a high zeta potential as well, that means the epoxy fracture, the natural rock fracture and the *E. coli* all have a negative charges. This results in repulsion forces between the *E. coli* and the matrix, with the larger repulsion forces occurring in the experiments conducted in the epoxy replica fractures, as that matrix had a larger negative charge. The larger negative matrix charge associated with the epoxy fractures would be expected to result in smaller retention times due to charge exclusion. Tables 11 and 12 show that this was observed in terms of retention time, and therefore it can be concluded that charge exclusion was a dominant mechanism in these experiments.

Table 10: Zeta Potential of Dolostone, Epoxy and *E. coli* (*grown in nutrient rich media. (Soni et al., (2008)))

	Zeta Potential (mV)	Standard Error
Dolostone in 1% PBS Solution	-7.47	.36
Epoxy in 1% PBS	-24.64	1.16
<i>E. coli GFP*</i>	-45.9	0.6

There are also large repulsion forces in between the natural rock fracture and the *E. coli* and they would need to be overcome in order for collisions to occur between the *E. coli* and the fracture wall, which is the first step of the attachment process. Therefore, if attachment is a significant retention mechanism in these experiments, it would be expected that more attachment would occur in the natural rock fracture due to the lower repulsion force that needs to be overcome for attachment to occur. Even so, the difference in zeta potential is not likely the only factor contributing to such a low *E. coli* recovery. It is highly likely that the retention, partially due to repulsive forces in the natural fracture is increased due to the presence of dead-end fractures. When the rock was first saturated with dye, several little pink spots appeared on the outside of the fracture. This indicated that several secondary fractures existed in the matrix, with very low flow properties. The entire outside of the natural rock fracture was then covered with epoxy to prevent any flow from occurring in these fractures. Even so, there is still an increased opportunity for retention in the natural rock fracture if contaminants are able to enter these secondary fractures due to diffusion, and accumulate there due to the lack of flow in these dead end fractures. These secondary dead end fractures may also contribute to the lower percent recovery of Bromide in the natural fracture than in the replica. Therefore we can assume that both attachment and dead end fractures are highly influential on the retention of both *E. coli* and bromide. Bromide recoveries also show that there is more retention of bromide in the natural fracture at higher specific velocities. This suggests that the preferential flow path expanded during these high velocities and in turn, caused more solute to enter smaller aperture regions where diffusion into the matrix or the secondary dead end fractures is more likely. There was no trend in the retention of bromide

within the epoxy fracture which further confirms the theory that the dead end fractures did play an important role in both solute and colloid recovery.

Figure 4-6 shows a sample of the measured and back-calculated bromide concentration profiles from Fracture 1 and Replica 1 at 30 m/d plotted as a function of pore volumes flushed.

The remaining Fracture 1 and Replica 1 bromide concentration profiles are included in Appendix C.

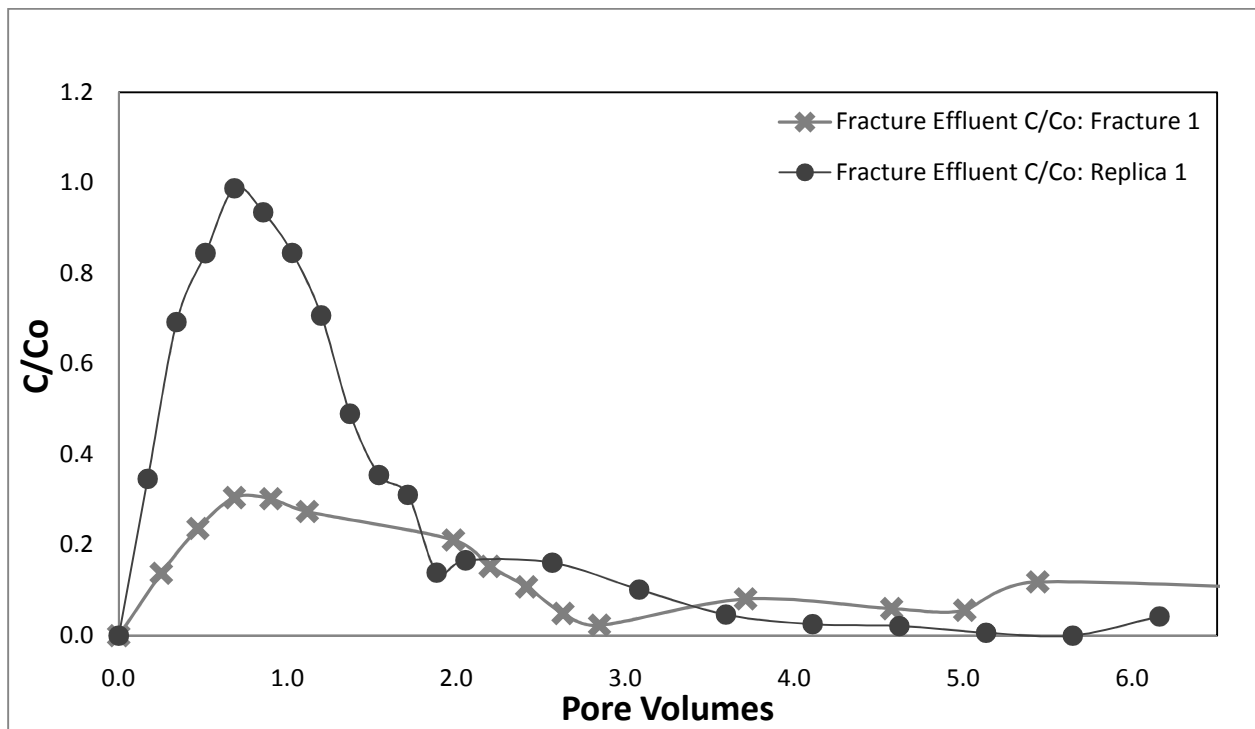


Figure 4 - 6: Comparing the bromide tracer test results from Fracture 1 and Replica 1.

Figure 4-6 clearly demonstrates the similarities and differences between the two fractures. In both the measured and calculated curves, the epoxy replica has higher peaks.

Table 11: Summary of Bromide Tracer Tests comparing Replica 1 and Fracture 1

Fracture ID	qc	Q	Mean Residence Time	Peak Measured Concentration	Peak Calculated Concentration	Percent Recovery
	m/d	mL/min	min	C/Co	C/Co	
Replica 1	30	3.58	30	0.49	0.99	109.00%
	30	3.53	33	0.33	0.58	109.00%
	10	1.46	138	0.41	0.74	96.25%
	5	0.72	297	0.43	0.99	105.50%
Fracture 1	30	1.668	513	0.24	0.3	81.02%
	30	1.668	304	0.25	0.34	91.41%
	10	0.556	1021	0.21	0.31	86.63%
	5	0.28	5458	0.32	0.36	101.44%

Table 12: Summary of E. coli Tracer Tests comparing Replica 1 and Fracture 1 (*manually estimated from the tracer curves)

Fracture ID	qc	Q	Mean Residence Time	Peak Measured Concentration	Peak Calculated Concentration	Percent Recovery
	m/d	mL/min	min	C/Co	C/Co	
Replica 1	30	3.58	41	0.48	1.42	76.67%
	30	3.53	31	0.84	2.11	79.83%
	10	1.46	115	0.43	1.2	62.35%
	5	0.72	161	0.6	1.38	71.00%
Fracture 1	30	1.668	149	0.0052	0.0652	14.63%
	30	1.668	130*	0.004	0.0588	8.02%
	10	0.556	390	0.126	0.178	35.71%
	5	0.28	650*	0.0529	0.0883	6.89%

Figure 4-7 shows the percent recovery of *E. coli* vs. specific velocity for each fracture and replica. It can be seen that Replica 1 and Fracture 1 do not follow the same trend. Replica 1 exhibits the most recovery at both the highest and lowest velocities, whereas Fracture 1

displays the opposite trend. Fracture 1 also displayed lower retention of bromide at higher velocities. It was speculated that less bromide and *E. coli* were recovered at higher velocities due to the possible increase in size of the preferential flow path, causing more *E. coli* or bromide to enter low flow zones and in turn, causing more diffusion into dead end pathways. At higher velocities there is a higher potential for collision with the fracture wall which could result in attachment due to turbulence. However, the hydraulic test and Reynold's number both suggest that turbulence is not a probable cause. A lower retention at the lowest velocity is to be expected due to increased time for collision into the fracture walls due to diffusion or sedimentation. The *E. coli* recovery results from Replica 1 suggest that charge did indeed play an important role in the transport of *E. coli* through the epoxy replica. For instance, at the lowest velocity, where diffusion would play a dominant role in retention by collision or diffusion into low flow zones, the repellent forces would deter the colloid. Furthermore, at the high specific discharge, where the preferential flow path may widen into smaller aperture regions and low flow zones, the repellent charge would also discourage colloid transport into these zones. Therefore, it can be determined that the dominant transport and retention mechanisms within the natural fracture are not the same as those in the epoxy fracture.

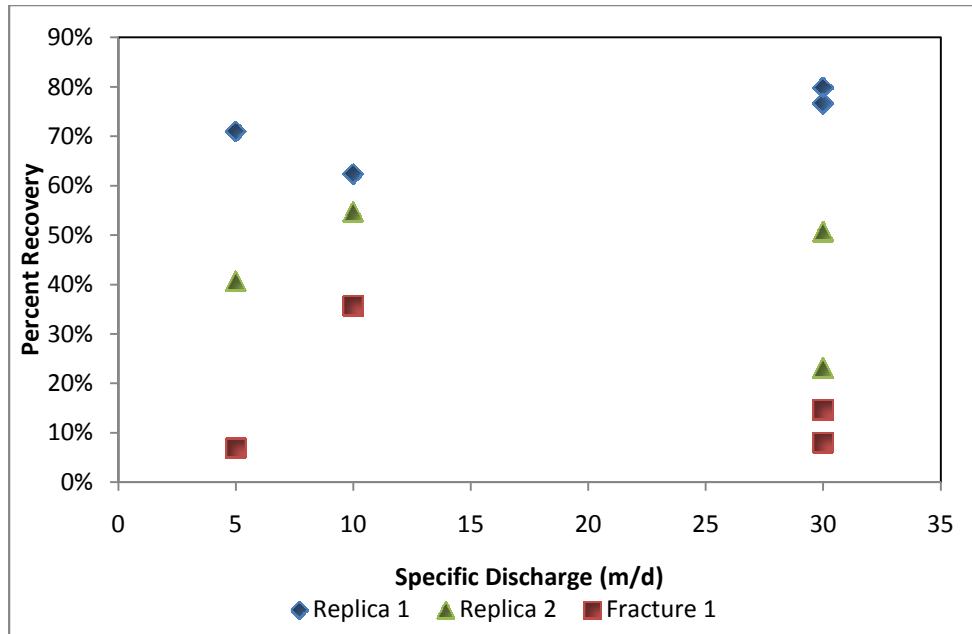


Figure 4 - 7: Percent recovery vs. specific discharge for each fracture

Since bromide is a conservative tracer, it was expected that it would behave differently in each fracture in comparison to *E. coli*. Figure 4-8 shows a typical comparison of *E. coli* tracer tests conducted at 30 m/d in both Fracture 1 and Replica 1. The remainder of the *E. coli* comparison graphs are included in Appendix C. Figure 4-7 demonstrates that the *E. coli* is transported differently than the bromide. The most significant difference is the how much smaller the peak measured and calculated relative concentrations are in the rock fracture in comparison to the concentrations in the epoxy fracture.

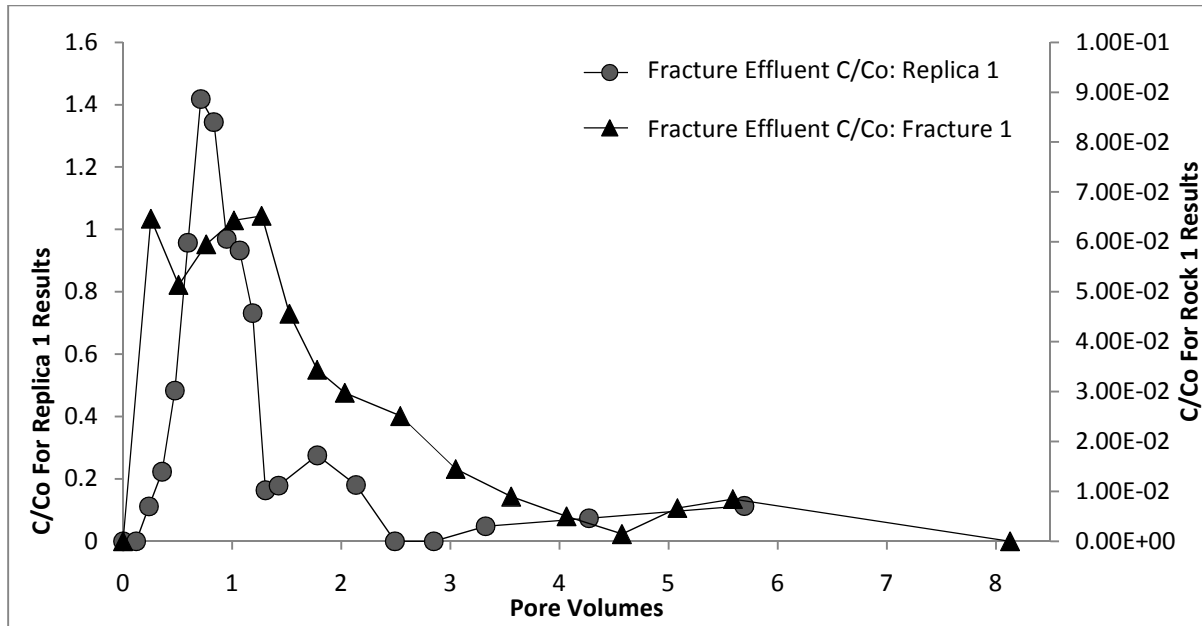


Figure 4 - 8: Comparing the *E. coli* tracer test results of Fracture 1 and Replica 1. The error represents the average percent deviation.

The peak concentrations occur slightly earlier than the bromide peak concentrations, as shown in Table 11 and 12. Table 13 shows the comparison of the arrival times of bromide and *E. coli* through both Fracture 1 and Replica 1 and Replica 2. All three fractures display shorter arrival times for the solute at a specific discharge of 30 m/d. As the specific velocity decreases, so does the fraction difference between the peak arrival times. This suggests that differential transport is governed in part by the specific discharge, since this trend is seen in both the natural fracture as well as the replica. Replica 1 exhibits significantly lower arrival times of *E. coli* at all specific discharges. This indicates that charge exclusion plays a more significant role in differential transport than size exclusion due to the similarities in aperture field and the differences in electric charge. However, Replica 1 also displays more differential transport than Replica 2, showing that size exclusion does still play an important role. Therefore differential transport is governed by charge exclusion, size exclusion and specific velocity.

Table 13: Comparing the arrival times of bromide and *E. coli* in both Fracture 1 and Replica 1 (* averaged)

Specific Velocity (m/d)	Fracture 1		Fraction Difference	Replica 1		Fraction Difference	Replica 2		Fraction Difference
	Bromide	<i>E. coli</i>		Bromide	<i>E. coli</i>		Bromide	<i>E. coli</i>	
30*	45	60	1.3	5	7.5	1.5	5	10	2
10	150	180	1.2	20	15	0.75	20	15	0.75
5	300	240	0.8	120	60	0.5	90	60	0.67

4.2.1 Visualization

Visualization tests were conducted at each specific discharge during the *E. coli* tests in Replica 2. Several challenges were encountered during the visualization tests due to increasing the signal to noise ratio enough so that the *E. coli* was visible.

In order to track the movement of *E. coli* through the replica, the difference between the fracture at time zero and at each subsequent time interval was taken and then processed using Matlab. The code used for the image processing is included in Appendix D. Image processing conducted on these photos generated a significant amount of error, however, they are still extremely useful for qualitative purposes.

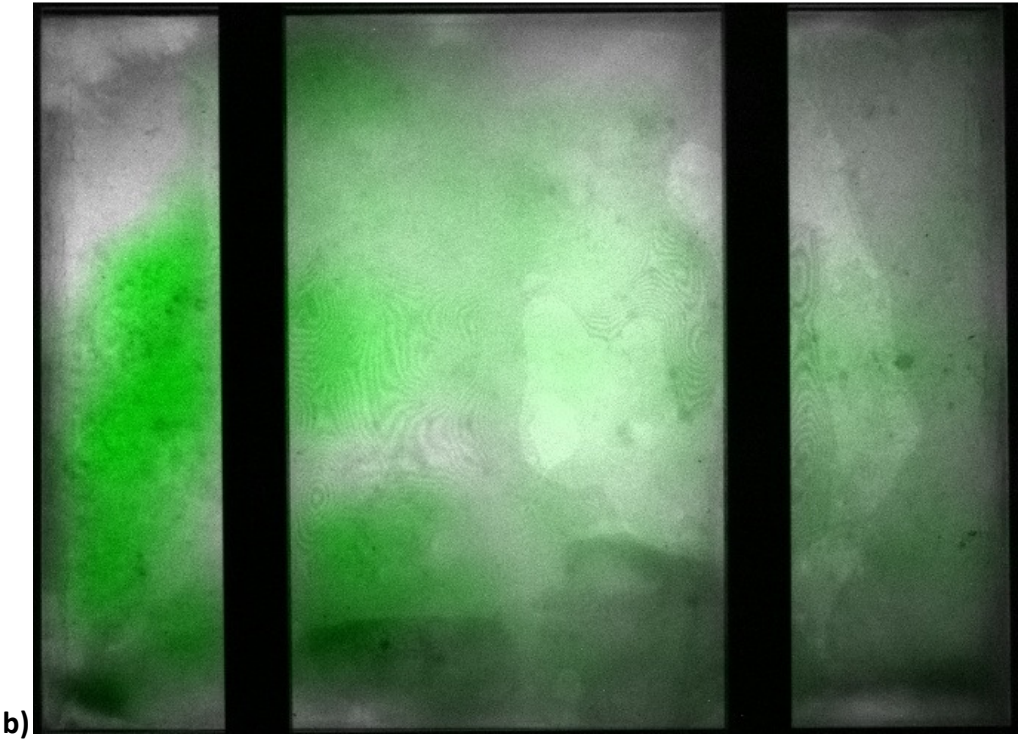
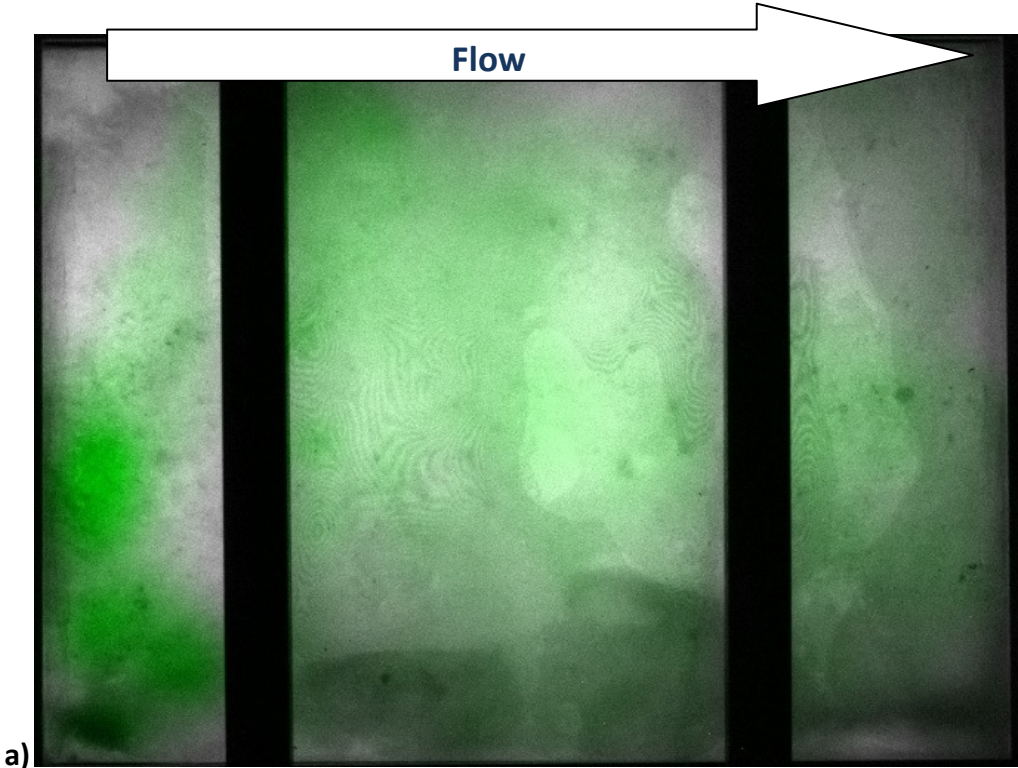
One factor that was adjusted in order to increase the signal that had considerable effect on the results was the concentration of *E. coli* that was injected into the fracture. It was hypothesized that placing a greater concentration of *E. coli* into the fracture would increase the amount of signal the *E. coli* were emitting. However, after analyzing the results, it was found that the

increased *E. coli* concentration actually caused a “cloud” or “shadow” within the replica.

Although this was not the desired effect, it actually produced the best results and the remaining tests were done using this setup.

Another factor that increased the amount of noise significantly was the clarity of the replicas themselves. As mentioned earlier, during the curing stages of the epoxy moulding, tiny air bubbles would undissolve from the epoxy solution and attach to the surface of the silicone mould. This created fracture replicas that were not appropriate for use due to the fact that the surface properties of the rock were not effectively captured in the replica. For this reason, a small amount of defoamer was added to the epoxy mix before curing in order to decrease the amount of dissolved gasses within the mix. The defoamer effectively reduced the bubbles but also caused cloudiness within the epoxy moulds. It was not expected that this would have a great effect on the visualization tests. However, when the same tests were completed on a replicated fracture that was moulded prior using a discontinued epoxy that was significantly clearer, the signal to noise ratio was greatly reduced and the processed images turned out significantly clearer.

The results of a test performed on Replica 2 at 10 m/d can be seen in Figure 4-9.



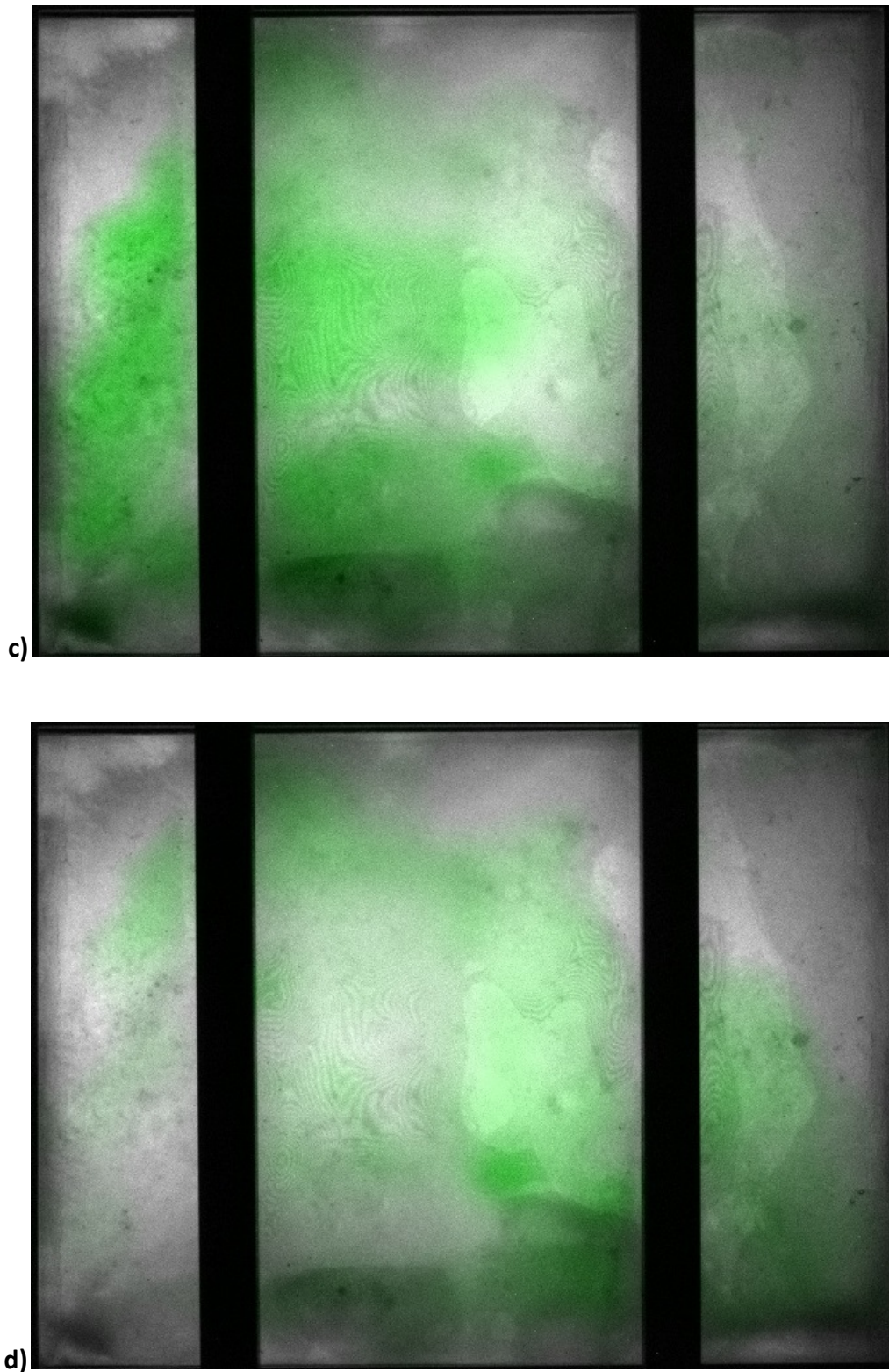


Figure 4 - 9: Visualization results at a) 0.25 Pore Volume Flushes b) 0.5 Pore Volume Flushes c) 0.75 Pore Volume Flushes d) 2.0 Pore Volume Flushes

Although the visualization experiments were not entirely successful, there are still some qualitative results to be drawn from these photos. There are two main preferential flow paths in the fracture. One being almost down the center of the fracture and the other being along the edge of the fracture where the epoxy chips are placed. This gives some insight and confirms that there is significant flow in the rock chip section located on the lower longitudinal edge approximate 10 cm away from the inlet edge. There are also areas where there is little to no visible colloid transport within the fracture.

Chapter 5

5.1 Conclusions

The goal of this research was to further the mechanistic understanding of biocolloid transport in saturated fractures through laboratory-scale physical model experiments. Specifically, the effect fracture matrix properties as well as the fracture aperture size and variability on the transport and retention of *E. coli* were investigated. Visualization experiments were conducted to gain qualitative data from the transport pathways. The following conclusions were drawn from the results of this research:

- The hydraulic tests produced a linear relationship between specific discharge and head loss for all specific discharges within the range of our tracer test specific discharges. This linear trend is consistent with previous research. However, Replica 2 did show a transition into the turbulent range at a much lower specific discharge than expected, indicating that the addition of rock chips, which effectively simulate fracture joints, may induce turbulence.
- The bromide tracer tests resulted in a frictional loss aperture that was smaller than the hydraulic aperture and a mass balance aperture that was larger than the hydraulic aperture. This is consistent with previous research, and indicates that the aperture field is variable.
- The percent recovery of bromide showed no trend and remained consistent in the range of 100% for all three specific discharges in both Replica 1 and Replica 2. This indicated that the retention of solutes in the synthetic fractures was negligible. Conversely,

Fracture 1 experienced less retention than Replica 1 in all experiments except for one. This indicates that the retention of solutes in the natural fracture is due to the matrix, and is most likely due to secondary fractures within the matrix rather than matrix porosity.

- The percent recovery and the peak concentrations of *E. coli* in Replica 1 were consistently larger than the percent recovery and peak concentrations in Replica 2. Replica 2 has a significantly larger aperture than Replica 1 and is also more variable. This indicates that aperture field plays an important role in colloid transport. Since, all else being equal, larger recoveries would actually be expected due to less attachment in larger apertures, this result suggests that aperture field variability has more of an effect on colloid recovery than aperture size in the range of apertures employed in these experiments.
- Percent recoveries of *E. coli* within the synthetic fractures showed inconsistent results when compared to specific discharge. This is likely due to the difference in aperture size and variability of the two synthetic replicas, as all other variables are equal. Replica 2 also could possibly experience some irregular flow patterns due to the three rock chips approximately 10 cm from the influent edge, which may have also contributed to this phenomenon. The turbulence would have aided in transporting colloids through the energy barrier for collisions to occur with the aperture wall, resulting in subsequent attachment.
- Percent recoveries of *E. coli* in Replica 1 were significantly higher than in Fracture 1. This indicates that the matrix properties play a major role in colloid transport. Especially if the matrix has dead end zones where solutes and colloids can diffuse into and then become retained in the no flow zone.

Peak concentrations of *E. coli* in Replica 1 were significantly higher than in Fracture 1. This indicates that matrix and material properties, specifically the presence of dead end zones, play a major role in colloid transport.

- The visualization experiments demonstrated that preferential pathways were evident within a discrete, laboratory scale fracture.
- Differential transport was evident in both the Natural Fracture as well as the Synthetic Fractures. However, differential transport was significantly more prominent in the synthetic fractures. This suggests that charge exclusion plays a more significant role in differential transport and early arrival times of colloids than size exclusion.
- Differential transport also became more significant as specific velocity decreased, indicating that the percent difference between the arrival time of solutes and colloids will increase as your specific velocity decreases.

5.1 Recommendations

Although analyzing transport characteristics through the evaluation of breakthrough curves is important, it is also necessary to improve our conceptual mechanistic understanding by observing specific retention mechanisms within a fracture. This would be possible through refining the visualization technique to increase the signal to noise ratio.

It is also necessary to evaluate the transport of different types of microorganisms through different types of natural fractures. This will provide information on the effect of microorganism size and surface properties, as well as the effect of matrix properties.

Furthermore, field testing must be conducted in order to assess the applicability of the lab results to large-scale scenarios. By continuing the study of microorganism and colloid transport within the subsurface, it will be possible to improve the understanding, increase the reliability of models, and justify the modification and creation of new guidelines or policies for groundwater management strategies.

References

- Abu-Lail, N. I., & Camesano, T. A. (2003). Role of Lipopolysaccharides in the Adhesion, Retention, and Transport of *Escherichia coli* JM109. *Environmental Science Technology*, *37*, 2173-2183.
- Aris, R. (1956). On the Dispersion of a Solute in a Fluid Flowing through a Tube. *Proc. R. Soc. Lond.*, *235*, 67-77.
- Berkowitz, B. (2002). Characterizing flow and transport in fractured geological media: A review. *Advances in Water Resources*, *25*, 861–884.
- Bonnet, E., Bour, O., Odling, N. E., Davy, P., Main, I., Cowie, P., et al. (2001). Scaling of Fracture Systems in Geological Media. *Reviews of Geophysics*, *39* (3), 347–383.
- Bradford, S. A., Simunek, J., Bettahar, M., Genuchten, M. T., & Yates, S. R. (2003). Modeling Colloid Attachment, Straining, and Exclusion in Saturated Porous Media. *Environmental Science Technology*, *37*, 2242-2250.
- Bradford, S. A., Simunek, J., Bettahar, M., Genuchten, M. T., & Yates, S. R. (2006). Significance of straining in colloid deposition: Evidence and implications. *Water Resources Research*, *42*.
- Brunton, F. (2011). *25. Project Unit 08-004. Update of Revisions to the Early Silurian Stratigraphy of the Niagara Escarpment: Integration of Sequence Stratigraphy, Sedimentology and Hydrogeology to Delineate Hydrogeologic Units*. Ontario: Ontario Geological Survey, Sedimentary Geoscience Section.
- Chrysikopoulos, C. V., & Abdel-Salam, A. (1997). Modeling Colloid Transport and Deposition in Saturated Fractures. *Colloids and Surfaces: Physicochemical and Engineering Aspects*, *121*, 189-202.
- Corapcioglu, M. Y., & Haridas, A. (1984). Transport and fate of microorganisms in porous media: A theoretical investigation. *Journal of Hydrology*, *72* (1-2), 149-169.
- Cumbie, D., & McKay, L. (1998). Influence of diameter on particle transport in a fractured shale saprolite. *Journal of Contaminant Hydrology*, *37*, 139-157.
- Detwiler, R. L., Rajaram, H., & Glass, R. J. (2000). Solute transport in variable-aperture fractures: An investigation of the relative importance of Taylor dispersion and macrodispersion. *Water Resources Research*, *36* (7), 1611-1625.
- Ewing, R. P., & Jaynes, D. B. (1995). Issues in Single-Fracture Transport Modeling: Scales, Algorithms, and Grid Types. *Water Resources Research*, *31* (2), 303-312.

Fahim, M., & Wakao, N. (1982). Parameter estimation from tracer response measurements. *The Chemical Engineering Journal* , 1-8.

Fetter, C. W. (1999). *Contaminant Hydrology*. Waveland Press, Inc.

Foppen, J., & Schijven, J. (2006). Evaluation of data from the literature on the transport and survival of *Escherichia coli* and thermotolerant coliforms in aquifers under saturated conditions. *Water Research* , 40, 401-426.

Gerba, C. P., Melnick, J. L., & Wallis, C. (1975). Fate of Wastewater Bacteria and Viruses in Soil. *Journal of the Irrigation and Drainage Division* , 101 (3), 154-174.

Ginn, T. R., Wood, B. D., Nelson, K. E., Scheibe, T. D., Murphy, E. M., & Clement, T. P. (2002). Processes in microbial transport in the natural subsurface. *Advances in Water Resources* , 25, 1017–1042.

Grisak, G. E., & Pickens, J. F. (1980). Solute transport through fractured media: 1. The effect of matrix diffusion. *Water Resources Research* , 16 (4), 719-730.

Harvey, R. (1997). *Manual of Environmental Microbiology, 2nd Edition*, pp. 753-776 (Hurst, C.J., Knudsen, G.R., McInerney, M.J., Stetzenback, L.D., Crawford, R.L., eds.). Washington, DC: ASM Press.

Hautman, D., Munch, D., & J., a. P. (1997). *Method 300.1, determination of inorganic anions in drinking water by ion chromatography*.

Haznedaroglu, B., Bolsterb, C., & Walkera, S. (2008). The role of starvation on *Escherichia coli* adhesion and transport in saturated porous media. *Water Research* , 42, 1547 – 1554.

J. Bodin, F. D. (2003). Solute transport in a single fracture with negligible matrix permeability:. *Hydrogeology Journal* , 11, 418–433.

James, S. C., & Chrysikopoulos, C. V. (2003). Effective velocity and effective dispersion coefficient for finite-sized particles flowing in a uniform fracture. *Journal of Colloid and Interface Science* , 263, 288–295.

Jardine, P. M., Sanford, W. E., Gwo, J. P., Reedy, O. C., Hicks, D. S., Riggs, J. S., et al. (1999). Quantifying diffusive mass transfer in fractured shale bedrock. *Water Resources Research* , 35 (7), 2015-2030.

Johnson, P. R., & Elimelech, M. (1995). Dynamics of Colloid Deposition in Porous Media: Blocking Based on Random Sequential Adsorption. *Langmuir* , 11 (3), 801–812.

Litton, G. M., & Olson, T. M. (1996). Particle Size Effects on Colloid Deposition Kinetics: Evidence of secondary minimum deposition. *Colloids and Surfaces*, 107, 273-283.

Maloszewski, P., & Zuber, A. (1993). Tracer experiments in fractured rocks: Matrix diffusion and the validity of models. *Water Resources Research*, 29 (8), 2723-2735.

McKay, L. D., & Driesse, S. G. (2004). Epi-Fluorescence micromorphology of saprolite reveals evidence for colloid retention in microscale pore systems. *Geoderma*, 121, 143-152.

McKay, L., Sanford, W., & Strong, J. (2000). Field Scale Migration of Colloidal Tracers in a Fractured Shale Saprolite. *Ground Water*, 38 (1), 139-147.

Middleton, G. V. (2003). Encyclopedia of sediments and sedimentary rocks.

Myers, D. (1999). *Surfaces, Interfaces, and Colloids: Principles and Applications, Second Edition*. John Wiley & Sons, Inc.

Ontario Geological Survey. (2010). *Lithologies of Southern Ontario*.

Passmore, J. M., Rudolph, D. L., Mesquita, M. M., Cey, E. E., & Emelko, M. B. (2010). The utility of microspheres as surrogates for the transport of E. coli RS2g in partially saturated agricultural soil. *Water Research*, 44, 1235 – 1245.

Ross, N., Villemur, R., Desche, L., & Samson, R. (2001). Clogging of a Limestone Fracture by Stimulating Groundwater Microbes. *Water Research*, 35 (8), 2029–2037.

Roux, S., Plouraboué, F., & Hulin, J.-P. (1998). Tracer Dispersion in Rough Open Cracks. *Transport in Porous Media*, 32 (1), 97-116.

Sen, T. K., & Khilar, K. C. (2006). Review on subsurface colloids and colloid-associated contaminant transport in saturated porous media. *Advances in Colloid and Interface Science*, 119, 71-96.

Sirivithayapakorn, S., & Keller, A. (2003). Transport of colloids in saturated porous media: A pore-scale observation of the size exclusion effect and colloid acceleration. *Water Resources Research*, 39 (4).

Soni, K. A., Balasubramanian, A. K., Beskok, A., & Pillai, S. D. (2008). Zeta Potential of Selected Bacteria in Drinking Water When Dead, Starved, or Exposed to Minimal and Rich Culture Media. *Current Microbiology*, 56 (1), 93-97.

Taylor, S. G. (1953). Dispersion of Soluble Matter in Solvent Flowing Slowly through a Tube. *Proceedings of the Royal Society of London*, 219 (1137), 186-203.

Taylor, S. W., & Jaffé, P. R. (1990). Biofilm Growth and the Related Changes in the Physical Properties of a Porous Medium 1. Experimental Investigation. *Water Resources Research* , 26 (9), 2153-2159.

Torkzaban, S., Tazehkand, S. S., Walker, S. L., & Bradford, S. A. (2008). Transport and fate of bacteria in porous media: Coupled effects of chemical conditions and porespace geometry. *Water Resources Research* , 44 (3).

Tsang, Y. W. (1992). Usage of "Equivalent Apertures" for Rock Fractures as Derived From Hydraulic and Tracer Tests. *Water Resources Research* , 28 (5), 1451-1455.

Tsang, Y. W., & Tsang, C. F. (1987). Channel model of flow through fractured media. *Water Resources Research* , 23 (3), 467-479.

Yang, H.-H., Morrow, J. B., Grasso, D., Vinopal, R. T., & Smets, B. F. (2006). Intestinal versus External Growth Conditions Change the Surficial Properties in a Collection of Environmental *Escherichia coli* Isolates. *Environmental Science Technology* , 40, 6976-6982.

Yao, K.-M., Habibian, M. T., & O'Melia, C. R. (1971). Water and Waste Water Filtration: Concepts and Applications. *Current Research* , 5 (11), 1105-1112.

Yates, M. V., & Ouyang, Y. (1992). VIRTUS, a Model of Virus Transport in Unsaturated Soils. *Applied Environmental Microbiology* , 59 (5), 1609-1616.

Zvikelsky, O., & Weisbrod, N. (2006). Impact of particle size on colloid transport in discrete fractures. *Water Resources Research* , 42.

Appendix A

Bromide Tracer Tests - Replica 1

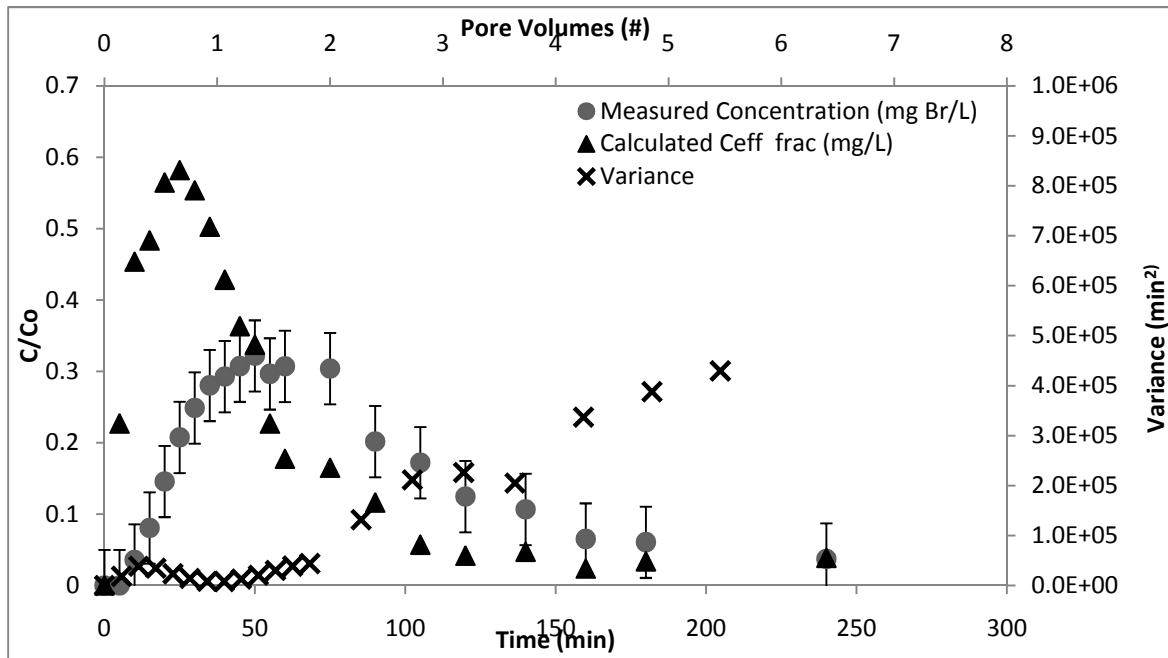


Figure: Bromide Tracer Test at Specific Discharge = 30 m/d - Replica 1

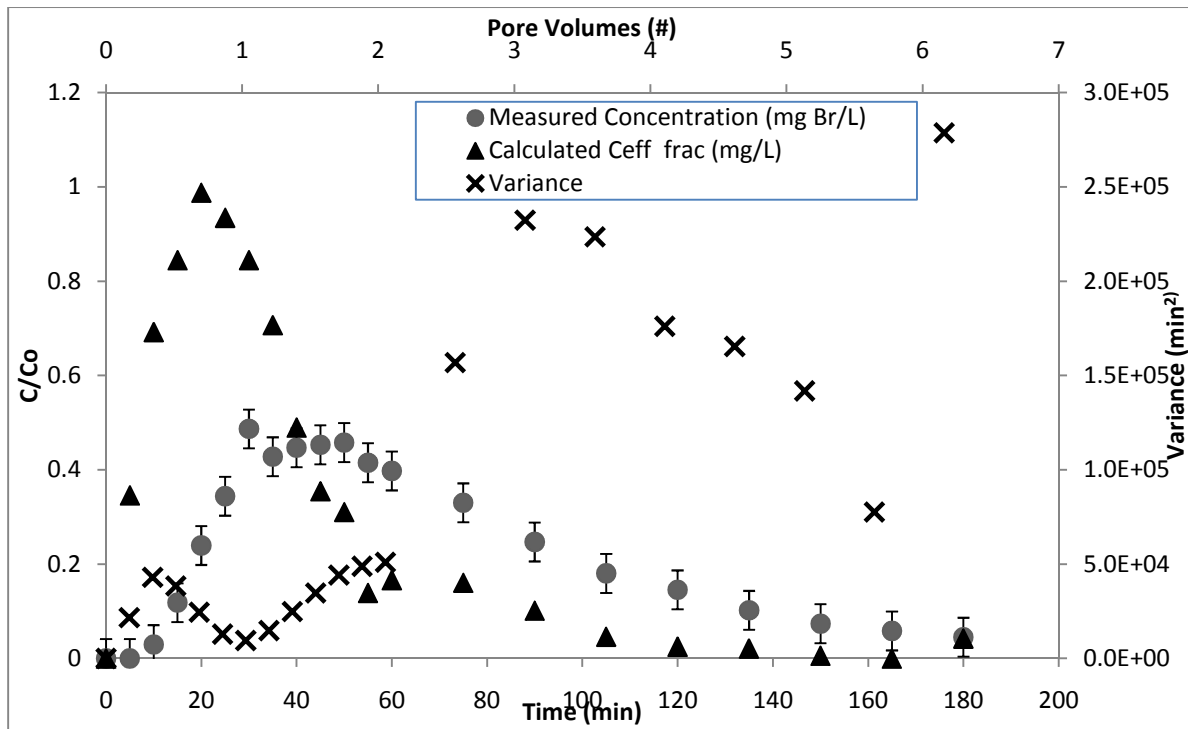


Figure 2: Bromide Tracer Test at Specific Discharge = 30 m/d (Trial 2) - Replica 1

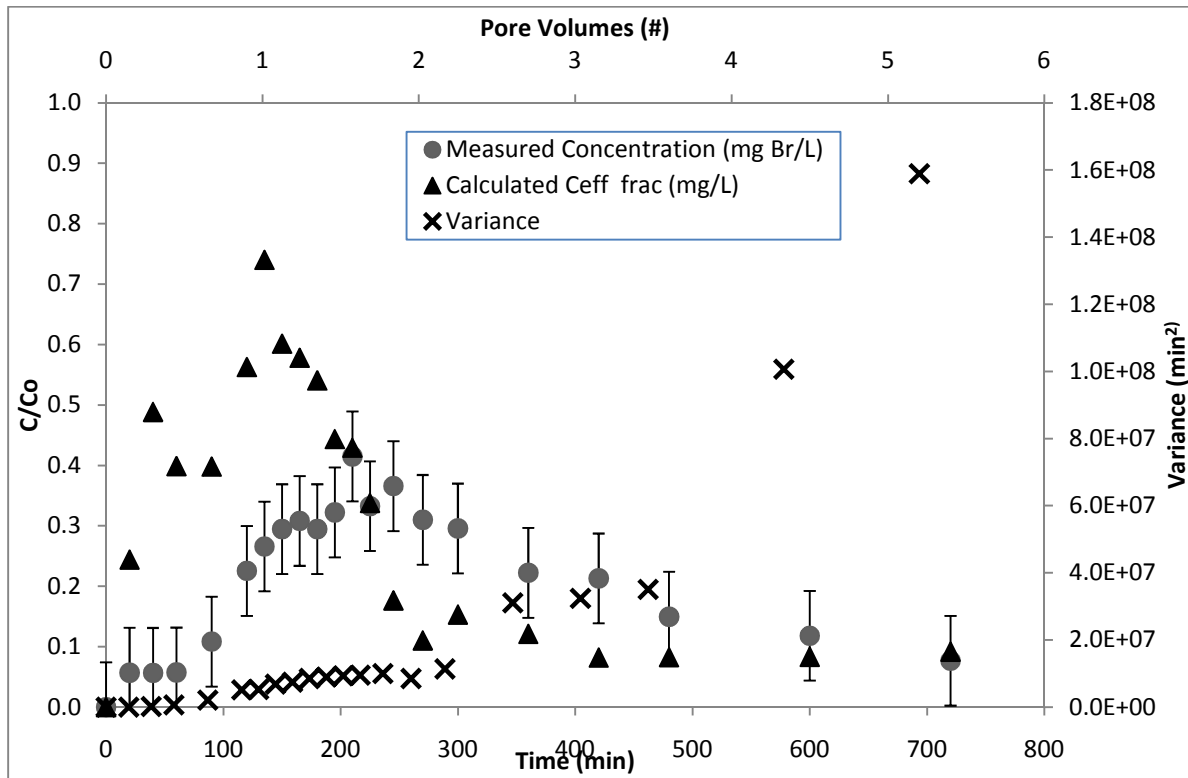


Figure 3: Bromide Tracer Test at specific discharge = 10 m/d - Replica 1

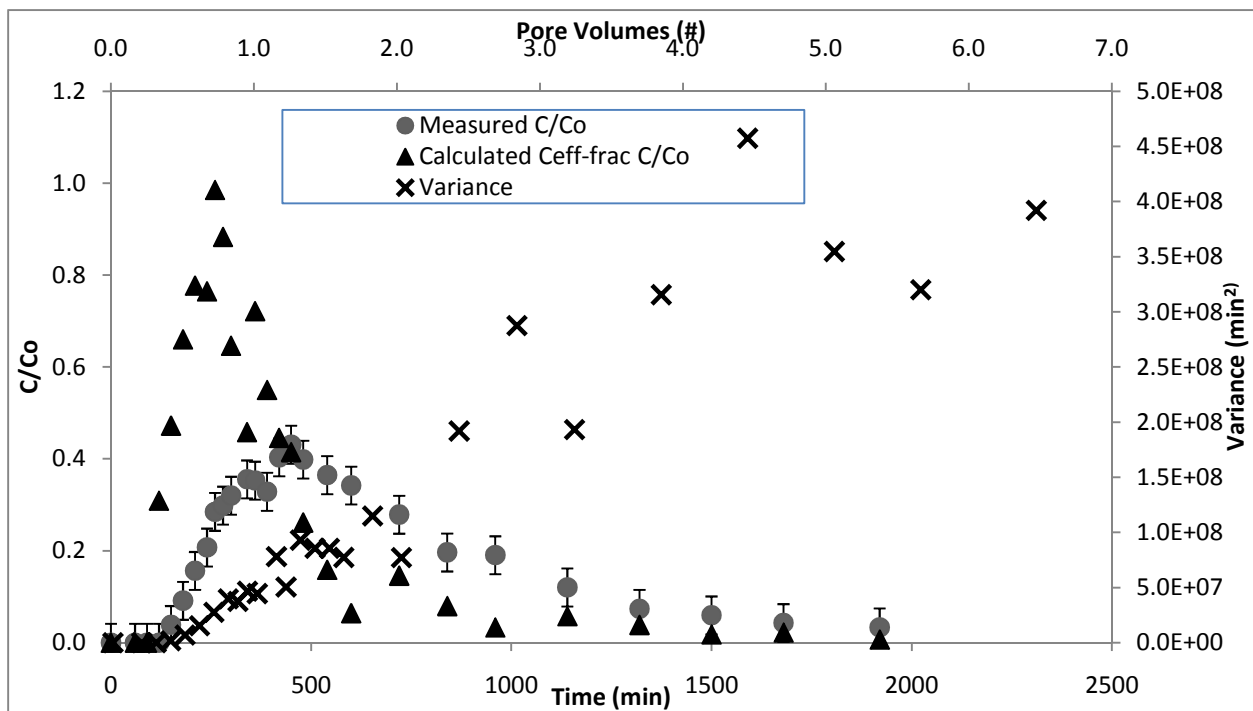


Figure 4: Bromide Tracer Test at specific discharge = 5 m/d - Replica 1

Bromide Tracer Tests - Replica 2

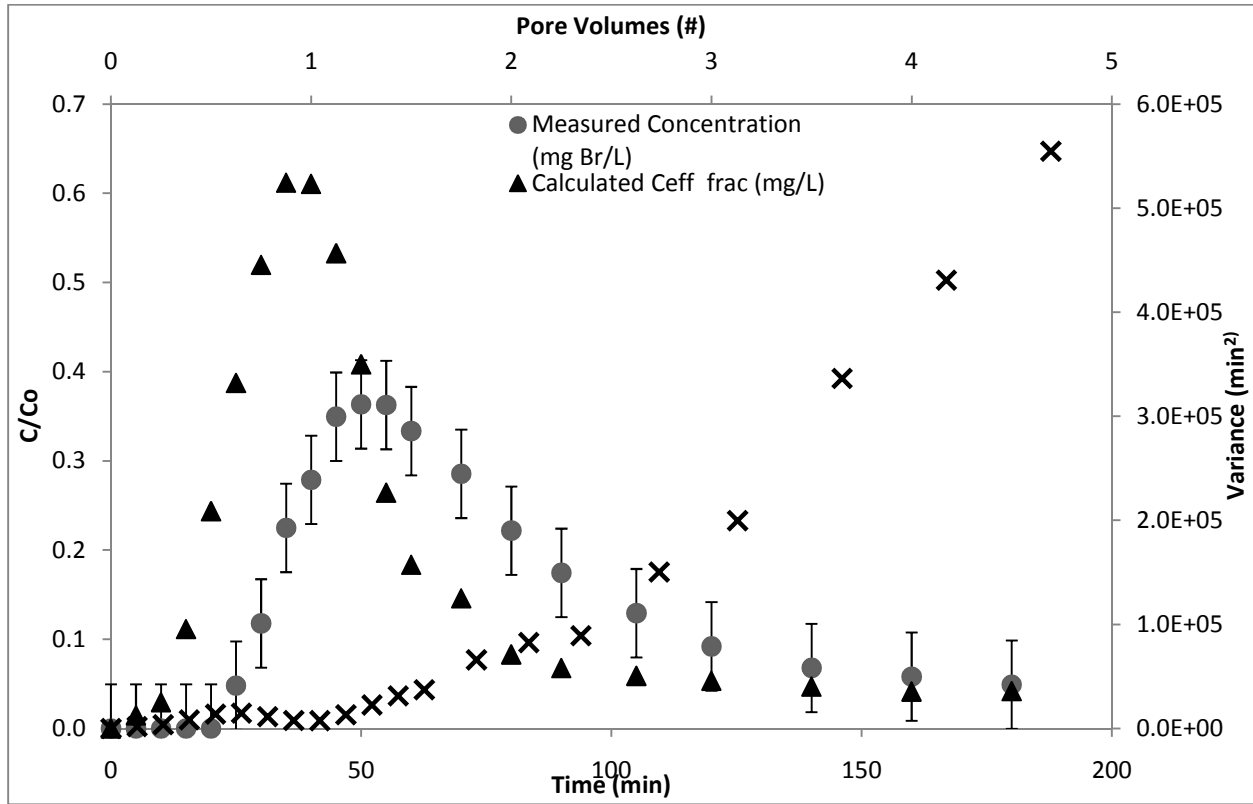


Figure 5: Bromide Tracer Test at Specific Discharge = 30 m/d - Replica 2

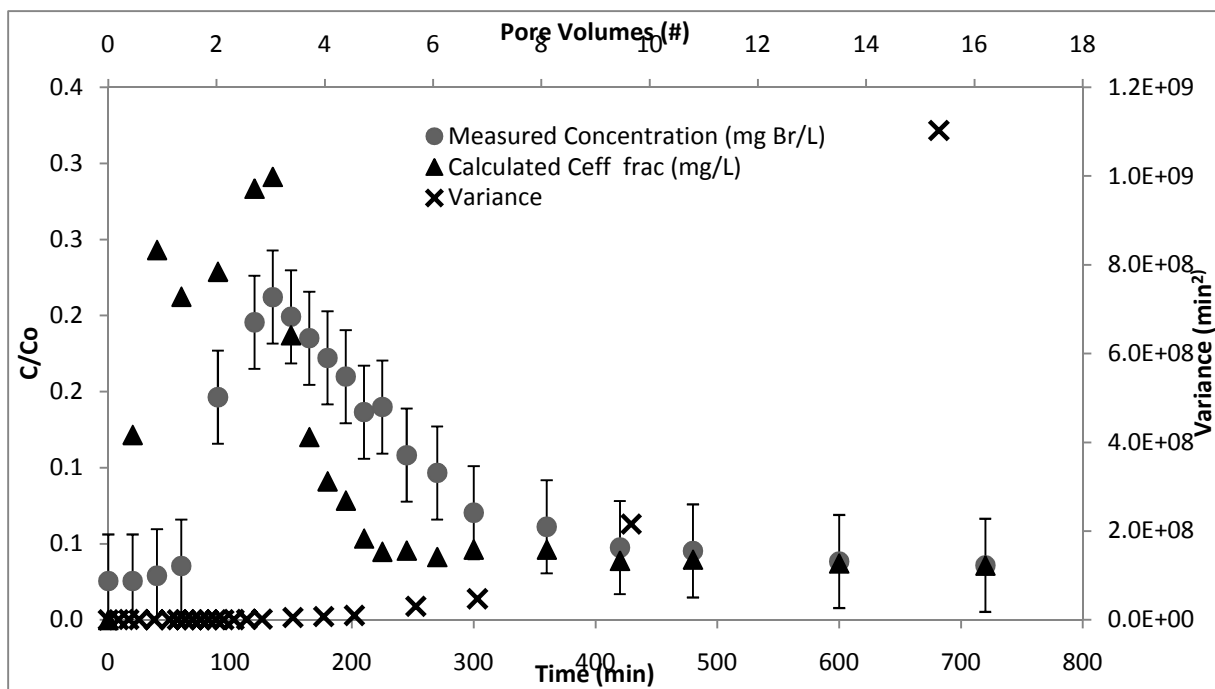


Figure 6: Bromide Tracer Test at Specific Discharge = 10 m/d -- Replica 2

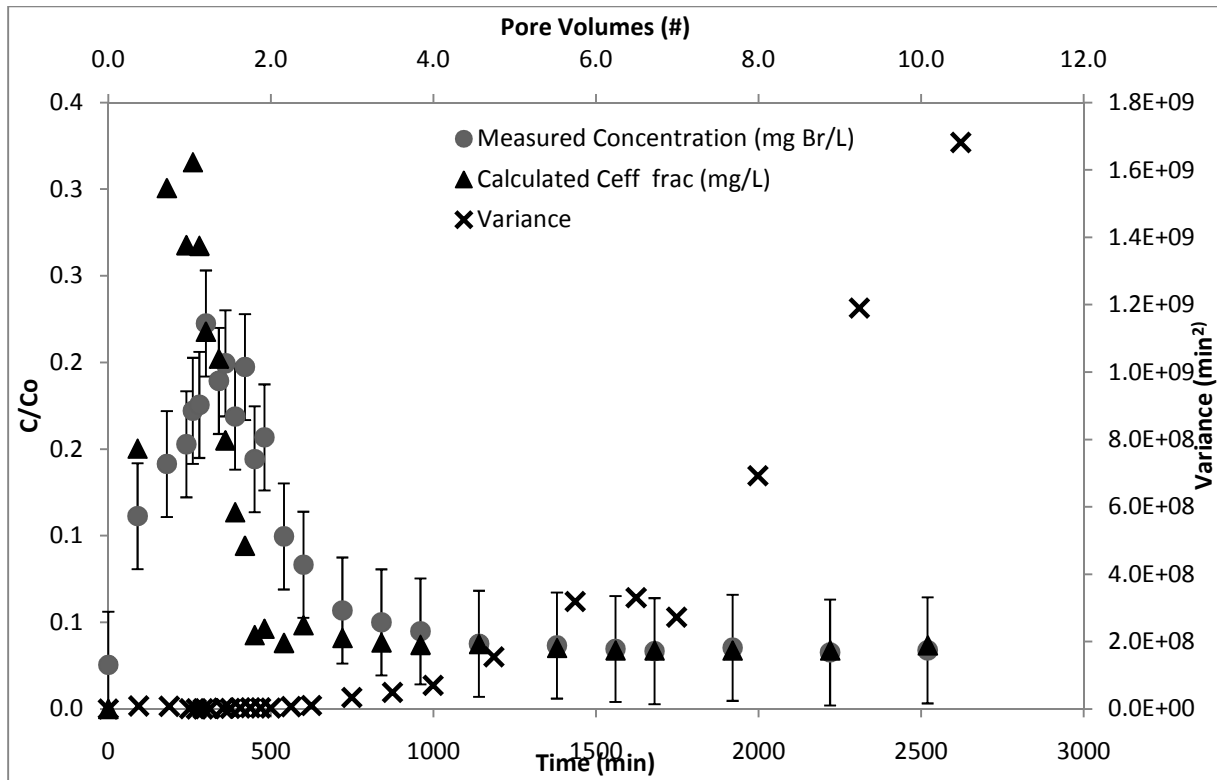


Figure 7: Bromide Tracer Test at Specific Discharge = 5 m/d -- Replica 2

Appendix B

E. coli RS2G Tracer Tests – Replica 1

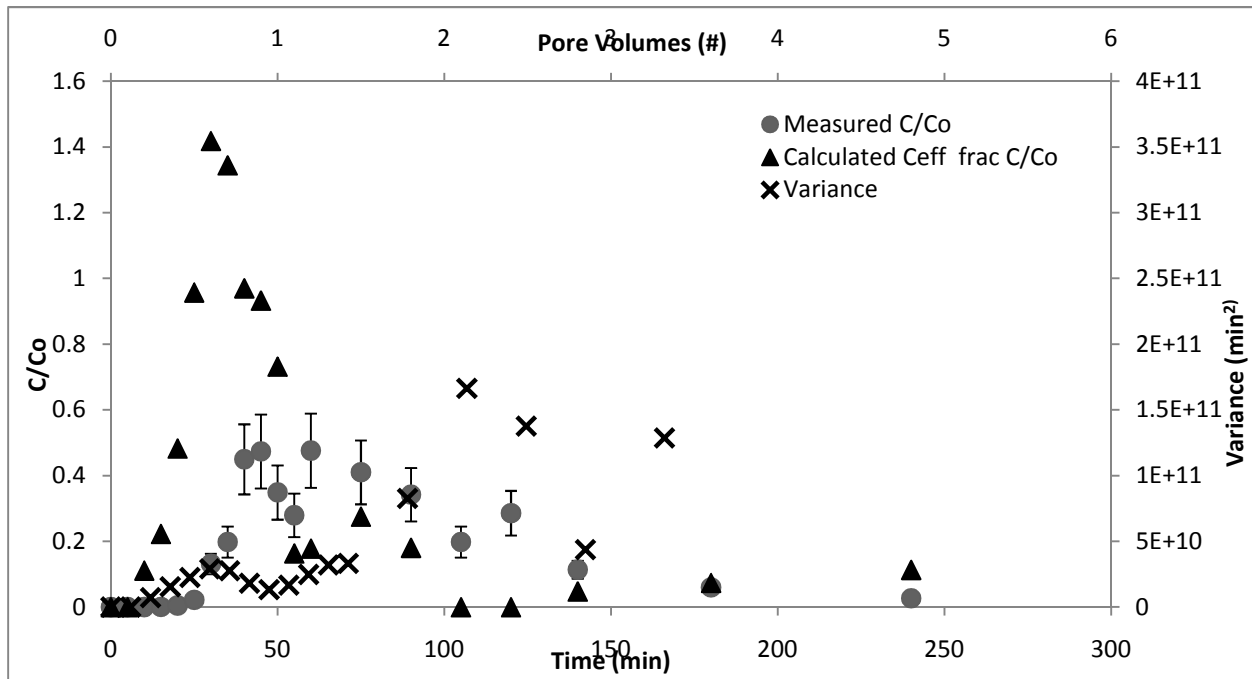


Figure 8: *E. coli* Tracer Test at Specific Discharge = 30 m/d – Replica 1

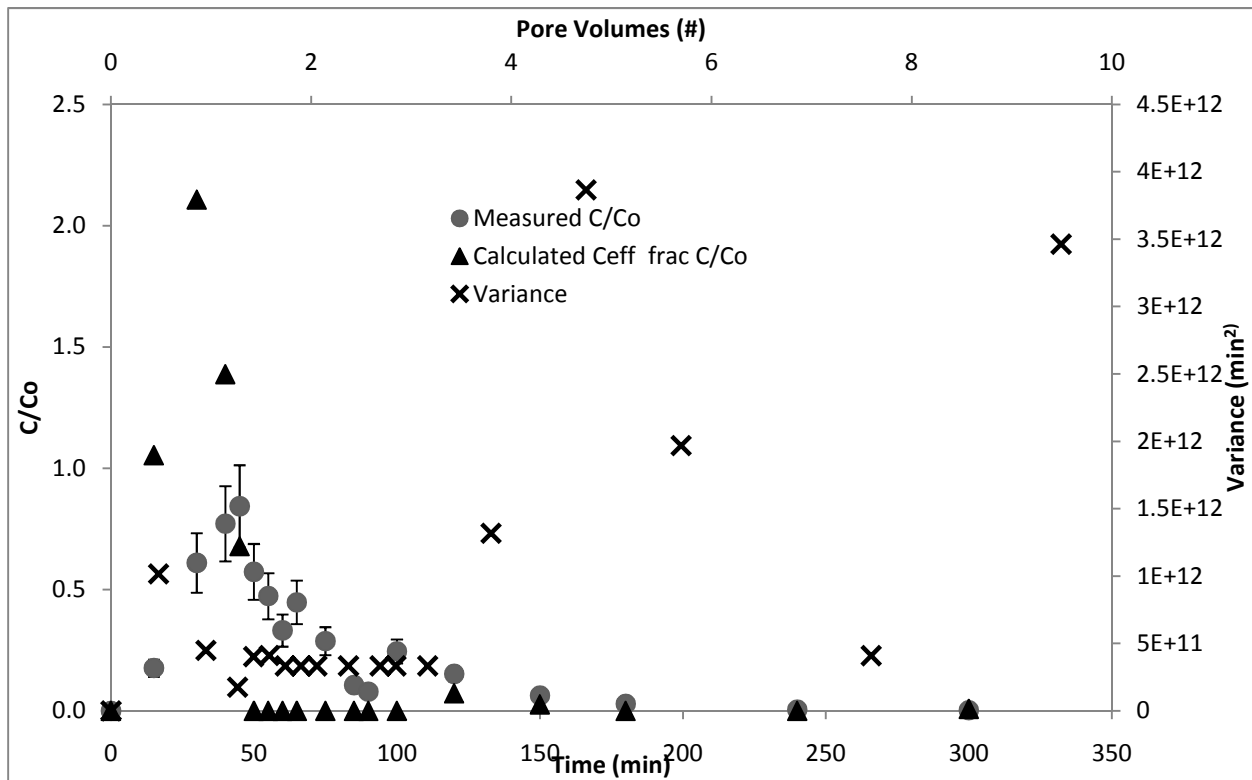


Figure 9: *E. coli* Tracer Test at Specific Discharge = 30 m/d - Trial 2 – Replica 1

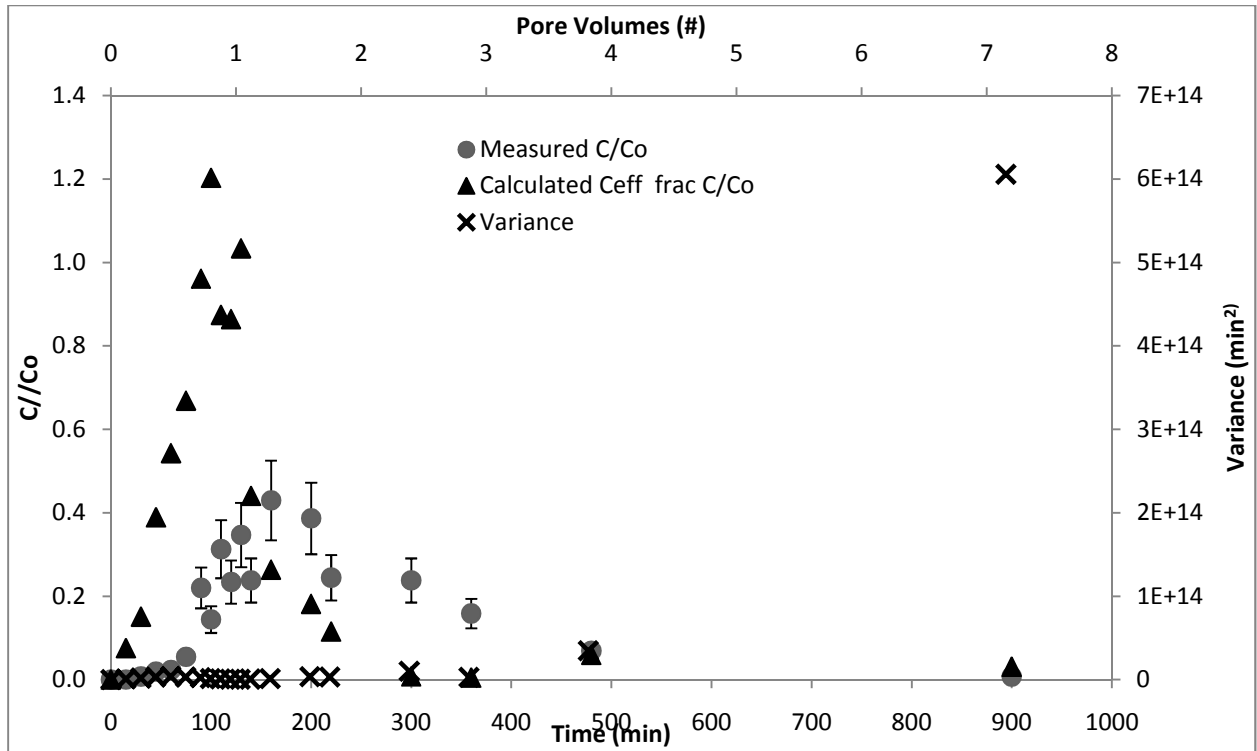


Figure 10: *E. coli* Tracer Test at Specific Discharge = 10 m/d – Replica 1

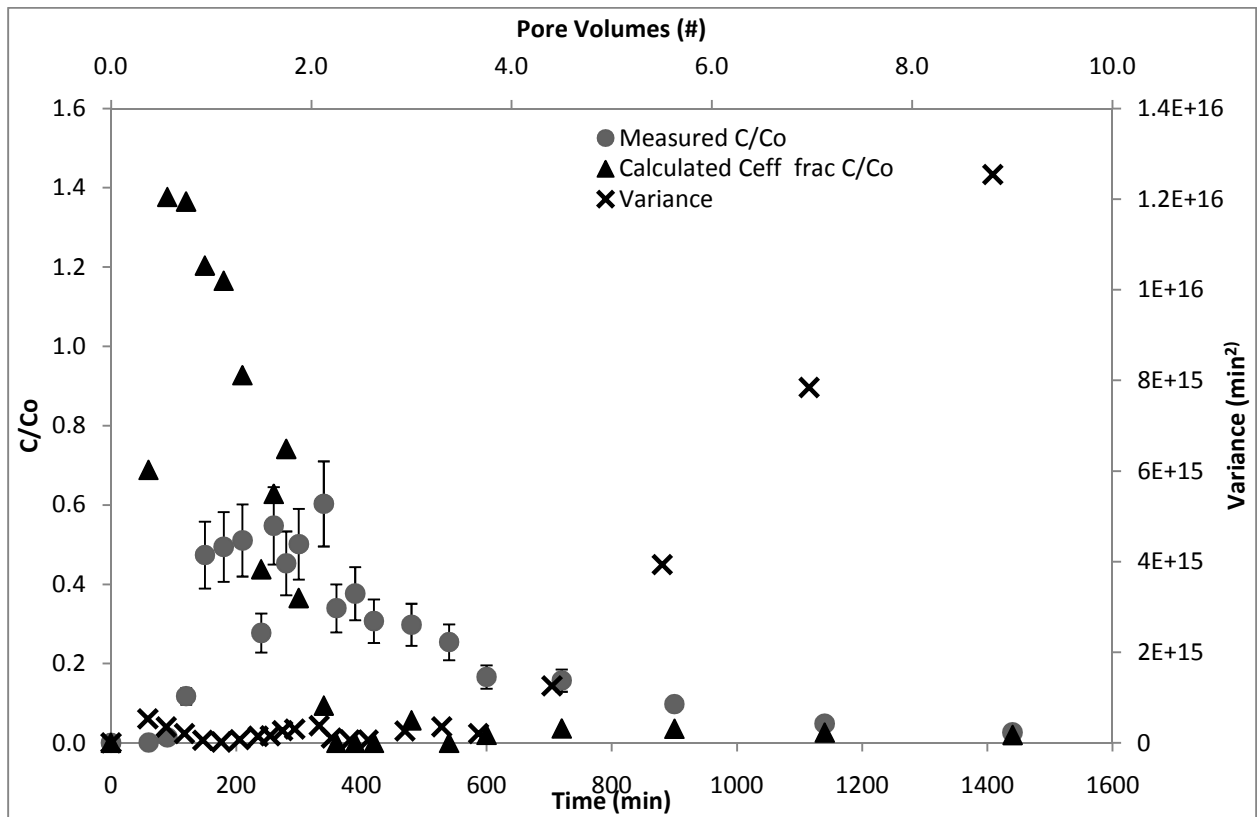


Figure 11: *E. coli* Tracer Test at Specific Discharge = 5 m/d – Replica 1

E. Coli RS2G Tracer Tests – Replica 2

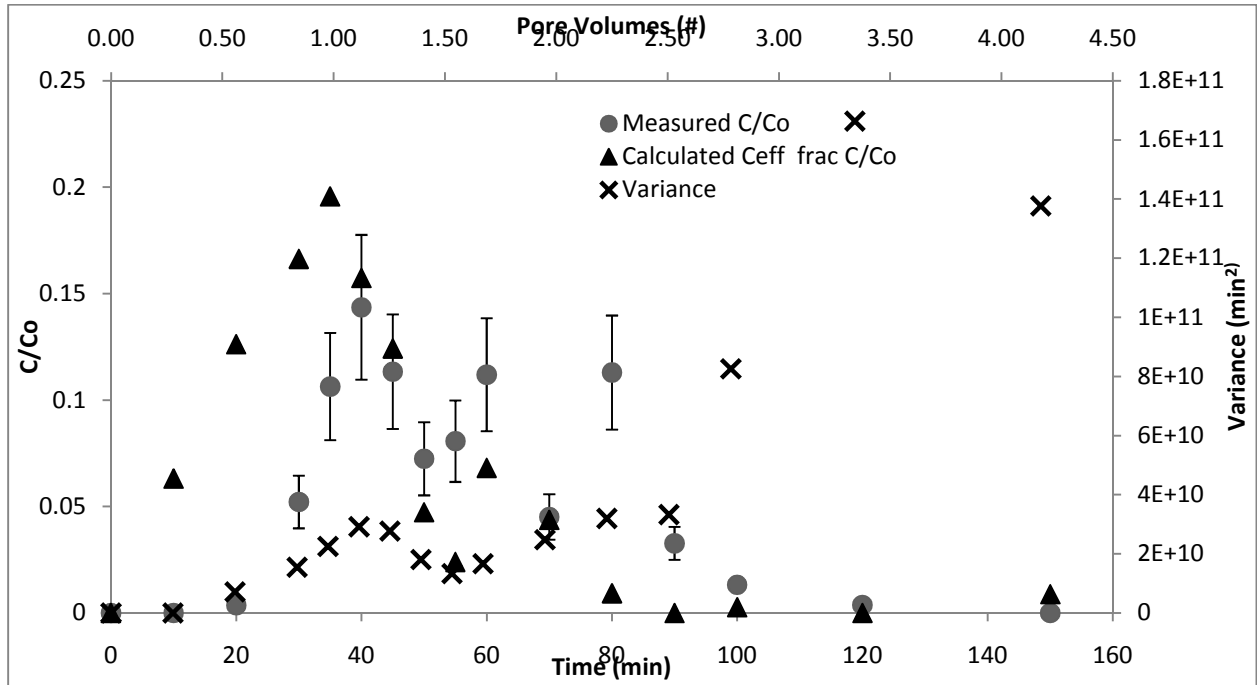


Figure 12: *E. coli* Tracer Test at Specific Discharge = 30 m/d – Replica 2

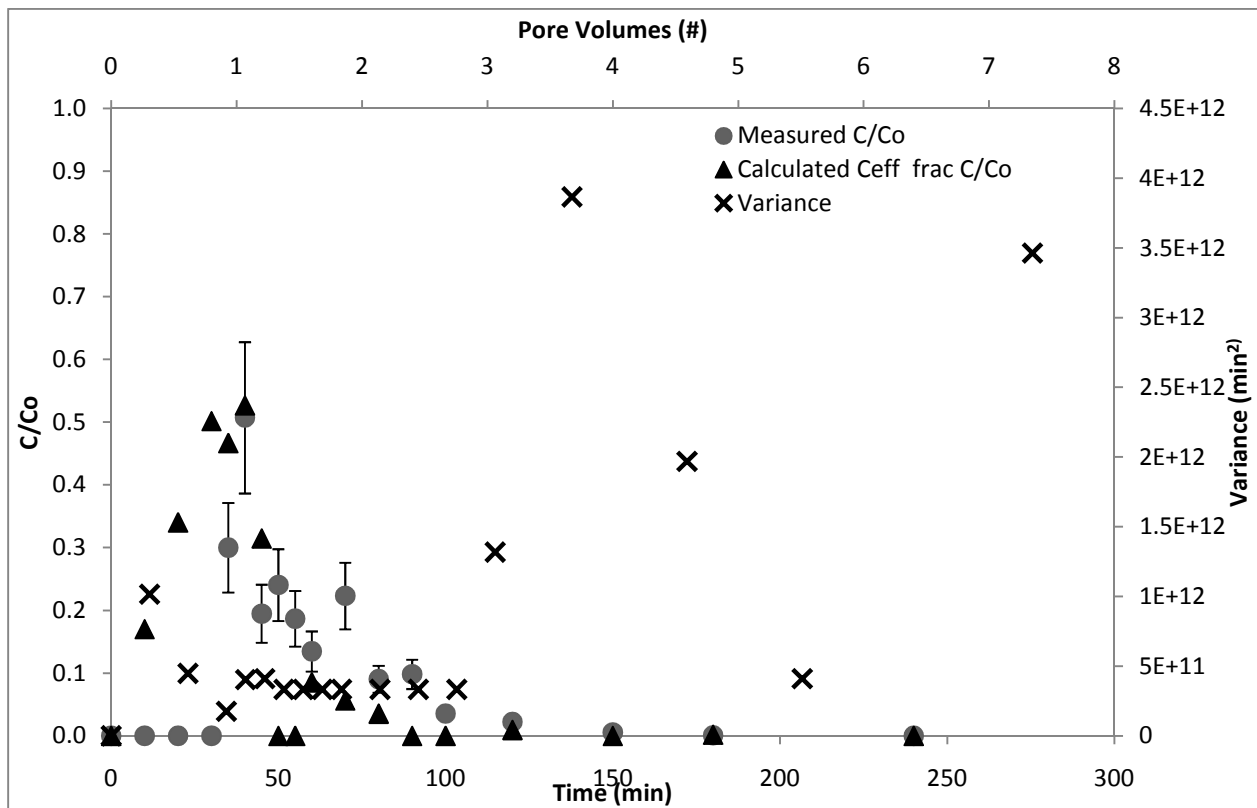


Figure 13: *E. coli* Tracer Test at Specific Discharge = 30 m/d - Trial 2 – Replica 2

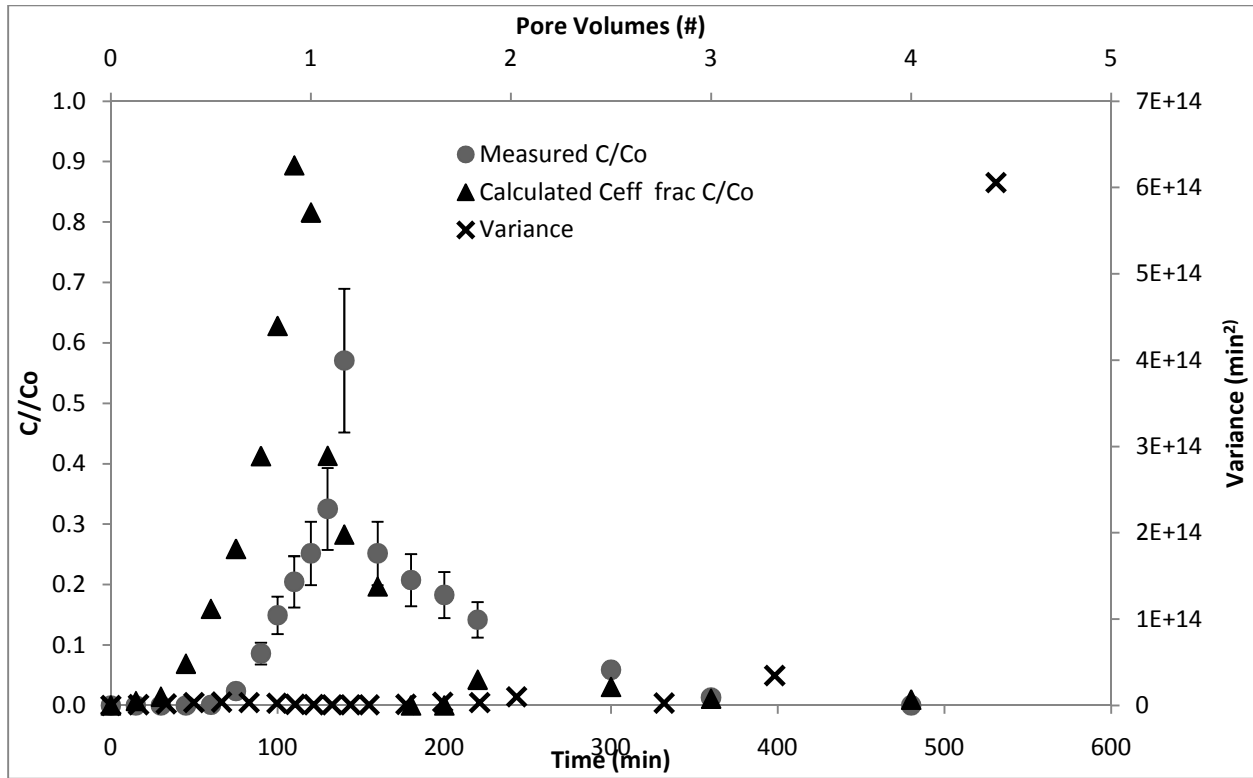


Figure 14: *E. coli* Tracer Test at Specific Discharge = 10 m/d – Replica 2

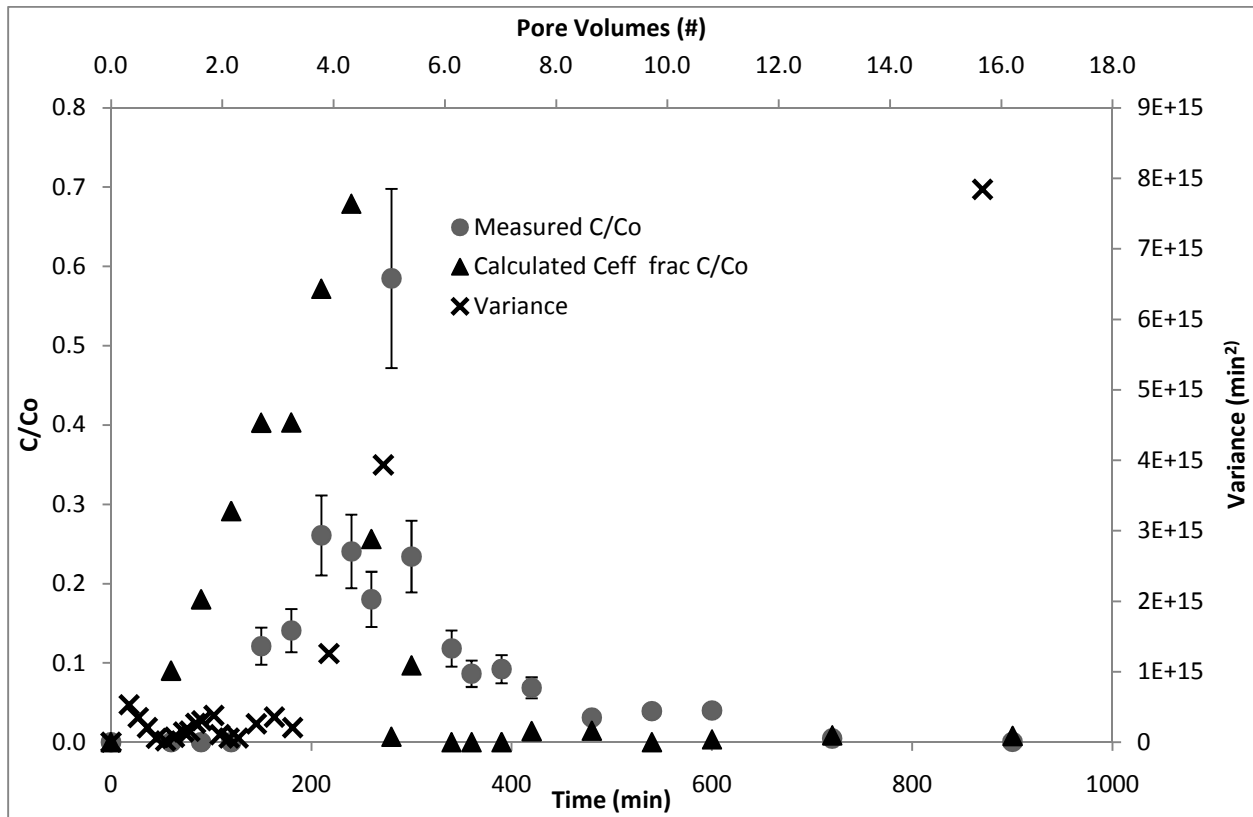


Figure 15: *E. coli* Tracer Test at Specific Discharge = 5 m/d – Replica 2

Appendix C

Bromide Tracer Tests: Rock vs Replica

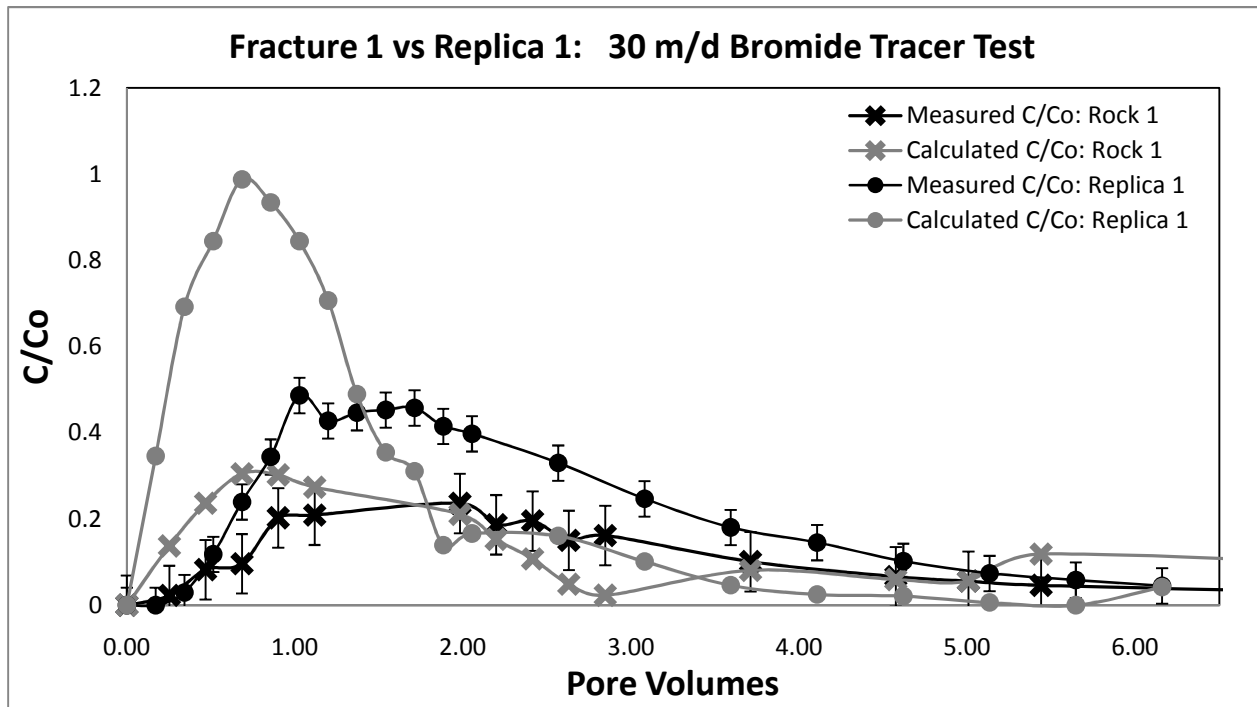


Figure 16: Bromide Tracer Test at Specific Discharge = 30 m/d

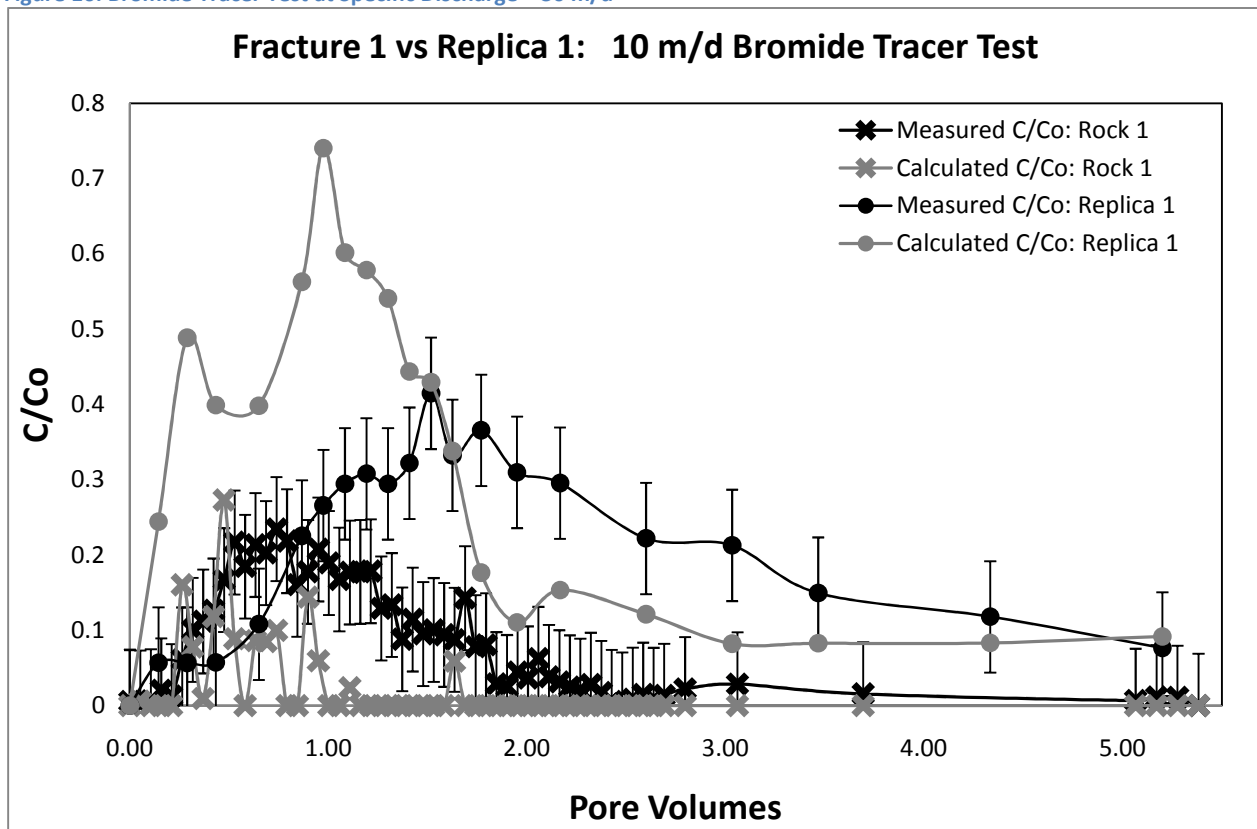


Figure 17: Bromide Tracer Test at Specific Discharge = 10 m/d

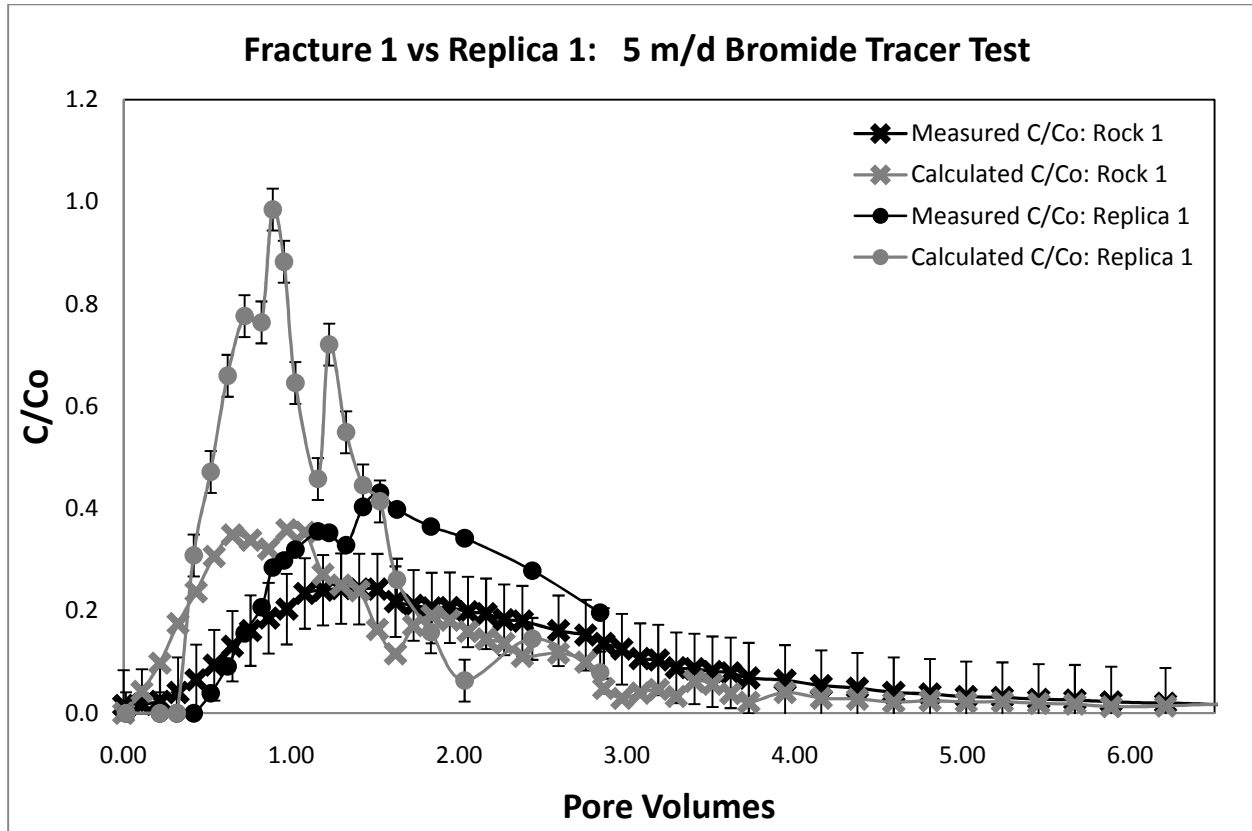


Figure 18: Bromide Tracer Test at Specific Discharge = 5 m/d

Rock 1 vs Replica 1: *E. coli* RS2G Tracer Test Results

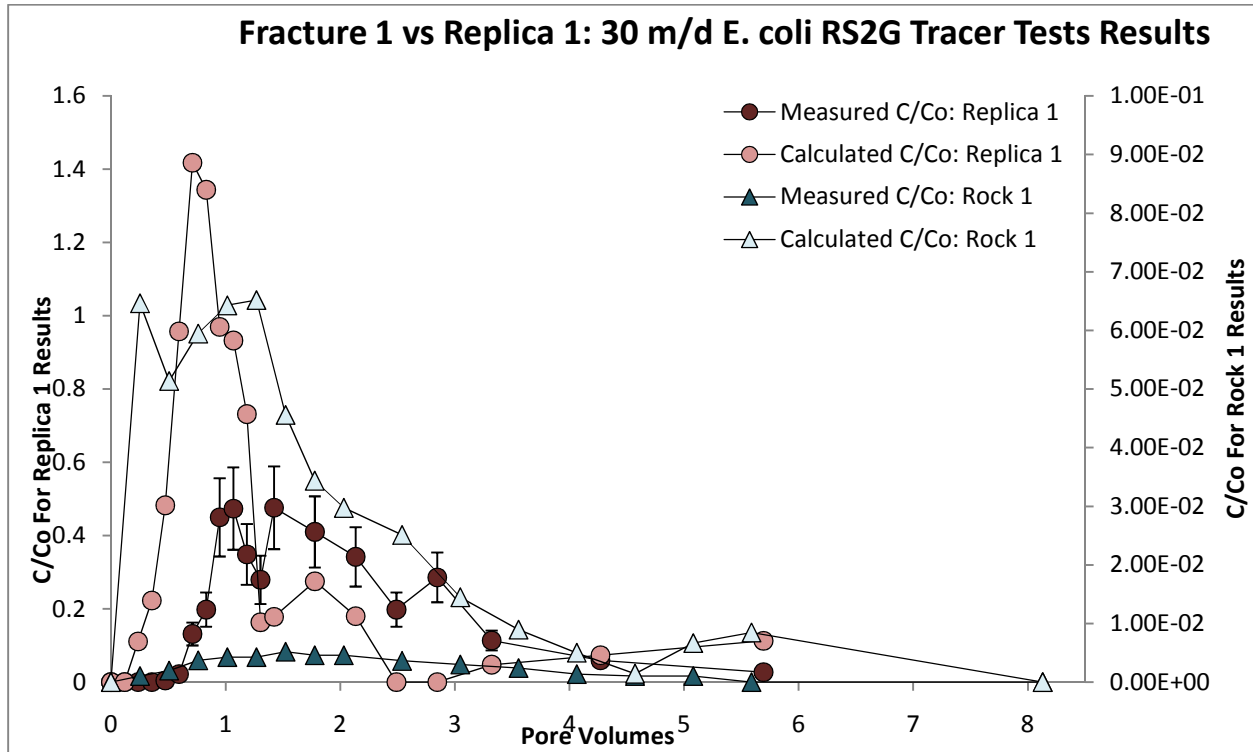


Figure 19: *E. coli* Tracer Test at Specific Discharge = 30 m/d

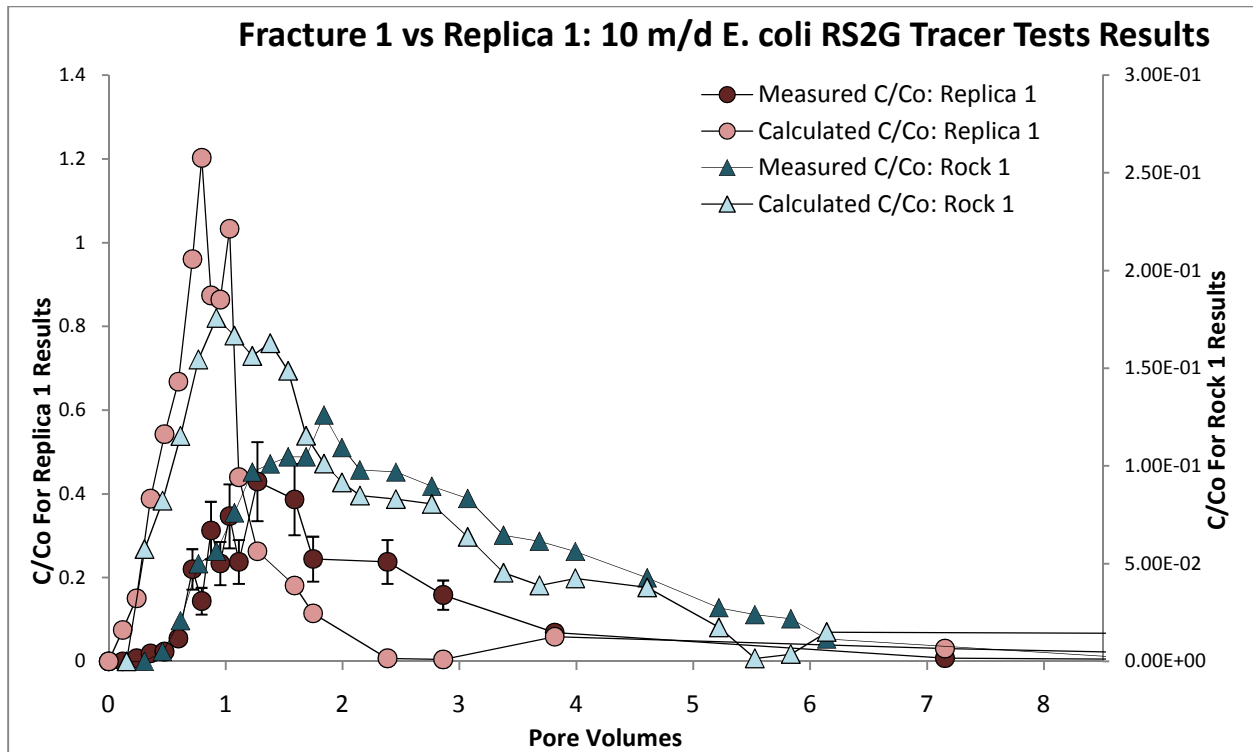
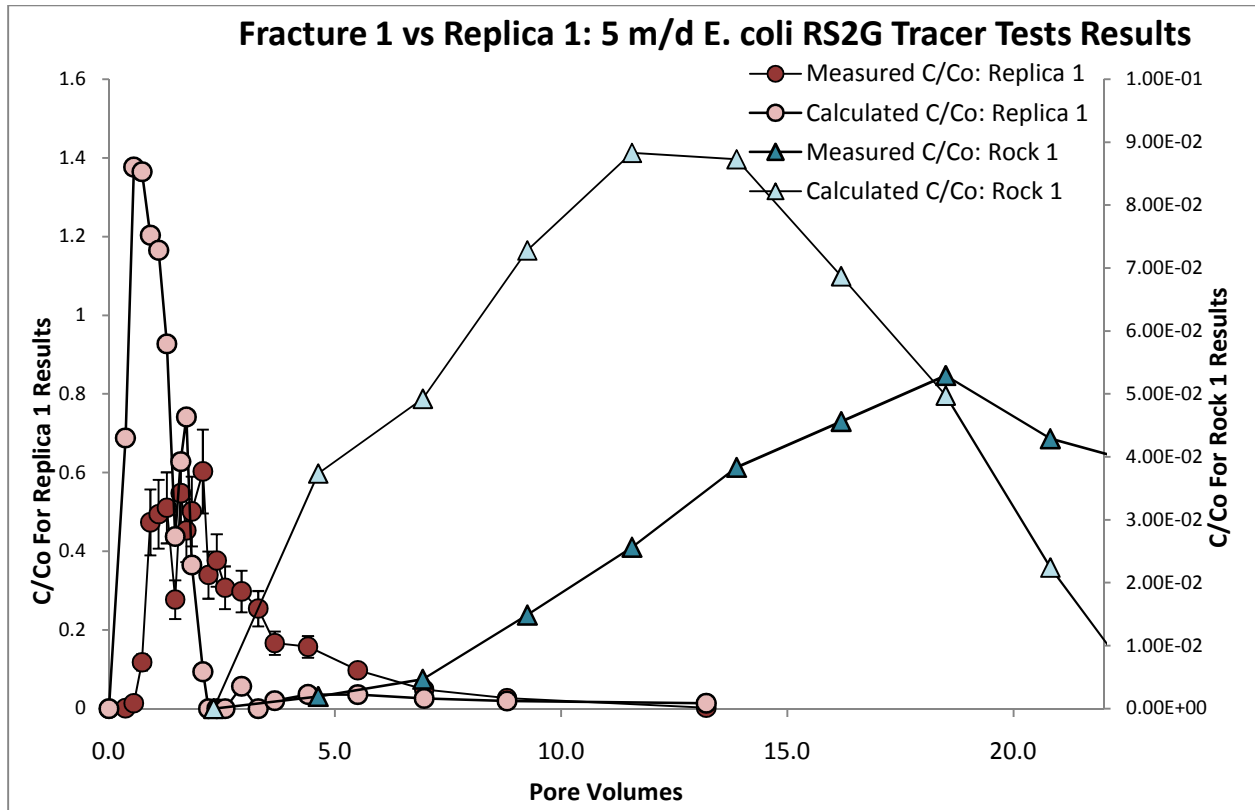


Figure 20: *E. coli* Tracer Test at Specific Discharge = 10 m/d



Appendix D

Matlab Code for Image Processing

```

folder = 'Aug 24 Replica 2 30md/';
out = '5/';
lowpass = fspecial('gaussian', 30, 5);

yrange = 68:988;
xrange = 20:1257;

mkdir('.', out);

test_images = dir([folder '*.tif']);
frame_range = 1:40;

ydown = round(length(yrange) * 0.2);
xdown = round(length(xrange) * 0.2);

img=zeros(length(test_images), ydown, xdown);

for i=1:length(test_images)
    p = im2double(imread([test_folder test_images(i).name]));
    p = p(yrange, xrange);
    p = imresize(p, [ydown xdown], 'lanczos2');
    img(i, :, :) = p;
end
background_range = 61:length(test_images);
background = zeros(ydown, xdown);

for i = background_range
    background = background + squeeze(img(i, :, :));
end
background = background / length(background_range);

low_high = stretchlim(background);

%for i = 20:20
for i = 1:60
    diff = background - squeeze(sum(img(i + (0:1), :, :))) / 2;
    diff = imfilter(diff, lowpass);
    diff(find(diff < 0)) = 0;

    orig = im2double(imread([test_folder test_images(i).name]));
    orig = orig(yrange, xrange);
    orig = imadjust(orig, low_high);
    orig = repmat(orig, [1 1 3]);

    diff = imresize(diff, [length(yrange) length(xrange)]);
    diff = diff * 15000;
    diff = repmat(diff, [1 1 3]);
    diff(:, :, 2) = 0;

    %    imshow(orig - diff);
    imwrite(orig - diff, [out 'out_' sprintf('%03d', i) '.jpg'], 'Quality',
92);
end

```